Eugenia Solano-Castiella: In Vivo Anatomical Segmentation of the Human Amygdala and Parcellation of Emotional Processing. Leipzig: Max Planck Institute for Human Cognitive and Brain Sciences, 2011 (MPI Series in Human Cognitive and Brain Sciences; 135)

In vivo anatomical segmentation of the human amygdala and
parcellation of emotional processing

In vivo anatomical segmentation of the human amygdala and
parcellation of emotional processing

Der Fakultät für Biowissenschaften, Pharmazie und Psychologie
der Universität Leipzig
genehmigte

D I S S E R T A T I O N

zur Erlangung des akademischen Grades

doctor rerum naturalium
(Dr. rer. nat.)

vorgelegt von

Eugenia Solano-Castiella, M.A.

geboren am 29. Dezember 1981 in Bilbao, Spain

Dekan: Prof. Dr. Matthias Müller

Gutachter: Prof. Dr. Robert Turner

                Prof. Dr. Angela D. Friederici

Leipzig, den 11.08.2011

To my mentor Prof. Robert Turner who taught me everything about neurophysics.

To my family who taught me everything else:
To my grandmother Maria Gloria Castiella Acha, my grandmother, for her modern mind.
To my father, Eugenio Solano, for his sensitivity.
To my sister Begoña Solano for her support during critical situations and for her creativity.
To my sister Maria Solano for fantastic intellectual conversations.
To my sister Teresa Solano, for being a solid family bond, for her tireless listening, humility, optimism and generosity.
To my brother Carlos Solano, for his incredible trust, practical mind and creativity.

To my great friends and colleagues having big brains and big hearts Robert Trampel, Bibek Dhital and Markus Streicher for all their support, advice, guidance, care and sense of humor.

To Felix von Zwehl, for the wholehearted support, generosity and sense of humor.

This thesis is especially dedicated to my mother, Marian Castiella, who is the biggest fan of all her children and has managed to understand them individually. None of us would be who we are now without your wholehearted support. Thank you.

Acknowledgments

contribution during the different projects. Both scientists helped me have a better understanding of MRI and the different MR sequences used.

Bibliographic details

Eugenia Solano-Castiella

***In vivo* anatomical segmentation of the human amygdala and parcellation of emotional processing**

Fakultät für Biowissenschaften, Pharmazie und Psychologie

Universität Leipzig

Dissertation

112 pages, 191 references 37 figures, 3 tables

The goal of this thesis is to parcellate the human amygdala *in vivo* and correlate its subregions with their functional properties. Since the amygdala is involved in a range of emotions, their anatomical specificity within the amygdala has become a target of functional imaging. Diffusion tensor imaging (DTI) was used to robustly segment this grey matter area, enabling the consequent creation of probabilistic maps. Polarized light imaging validated the DTI results *ex vivo,* demonstrating similar regional orientations as those obtained with DTI. DTI of non-myelinated structures is atypical. Therefore, DTI of non-myelinated fetal brain was performed to confirm that anisotropic water diffusion can take place in brain areas even in the absence of myelin. These three studies have revealed intrinsic tissue properties within the amygdala and have been able to provide, for the first time *in vivo*, a segmentation of amygdala subregions. Using the high signal to noise ratio offered by ultra-high field MRI at 7 Tesla, the combination of two conventional anatomical MR contrasts enabled additional robust probabilistic maps of the amygdala to be formed. Finally, this work explored the distribution of emotional functions within the amygdala with the aide of the connectivity-based segmentations and the structural-based segmentations. This last work directly correlated function with its anatomical substrate. In conclusion, this thesis provides the first probabilistic maps of the amygdala *in vivo*, and has identified different emotional valences related to the probabilistic maps achieved.

Contents

Preface

The limbic system in the human brain is characterized for its role as the "emotional brain". The human emotions constitute, to a great extent, what we are or, in other words, the idea of ourselves. Emotions represent our personality to a great extent. Therefore, researchers persist in trying to gain better understanding of the limbic system and the emotions through the assignation or relation of its components with specific roles. Each one of the structures that form the limbic system can have more than a single role. For this reason, in recent years, emphasis has been placed on finding out exactly where a particular brain response takes place.

The amygdala is a highly relevant structure for the limbic system. The primary focus of this thesis will be the amygdaloid body and its components. This structure is involved in both positive and negative emotions to a great degree, and therefore represents a key target in the research of emotions.

Regarding the anatomy of the amygdala, the most widely used general description of this structure's subdivisions arose in the 1920's from *ex vivo* samples. More than half a century later, research exploring the anatomy of the amygdala is still in constant development, and as yet there are no established methods for parcellating the amygdala *in vivo*. The need for an *in vivo* amygdala parcellation has become more and more evident. This would help to elucidate more on the relationship between functional specificity and its anatomical substrate. Unfortunately, the complicated localization and the tissue properties of the amygdala generally hinder the task of making an accurate non-invasive study of this structure. However, considering the tremendous technological advances in imaging techniques in the last decade, an improvement of the hundred-year-old parcellation of the human amygdala is the goal of this study.

Non-invasive techniques such as magnetic resonance imaging (MRI) performed at an ultra-high field strength of 7 Tesla could become the tool for this task. However, MRI at 7 Tesla is still in his early stages. Consequently, the optimization of existing techniques as well as the development of new approaches for MR acquisition and analysis are necessary. Therefore, the present work applies the latest MR imaging techniques to examine the human amygdala *in vivo*.

The first chapters present an overview of the anatomical features of the amygdala as well as the principles of the MR imaging techniques employed. The choice of the MR protocols applied and their potential benefits for the investigation of the amygdala are explained in detail. Next, the tissue properties of the amygdala and how they manifest themselves in the different imaging experiments are discussed. This involves the structural details found with MRI, together with the resulting diffusion features. Finally, a functional study will attempt to correlate anatomy and function within this area.

The ultimate aim of this thesis is the *in vivo* segmentation of the amygdala using structural, diffusion-weighted and functional MRI techniques. Dealing with MRI issues as befits this area, with the limitations that relate to this tissue, have fortunately provided outstanding results. The outcome of this project is intended to provide new insights into the understanding of human emotion through the precise functional localization of specific emotions within the amygdala and the understanding of the anatomy of this structure from a new perspective.

I

Theoretical background

Chapter 1

The amygdala: Anatomy, connectivity and function

The amygdala is a small grey matter area located within the temporal lobe in the mid-brain. This structure was first identified as the amygdaloid complex by Burdach in 1819, although this first discovery did not include the whole complex as it is known today (Burdach, 1826; Sah, Faber, Lopez De Armentia, & Power, 2003). Further knowledge was provided by with the anatomist Johnston, who in 1923 recognized basolateral, centromedial and cortical divisions, which remained one of the main classifications of the components of this volume (Johnston, 1923). Later studies have subdivided the amygdala into many different regions, transforming this structure into a fairly complex region (Alheid, de Olmos, & Beltramino, 1995; de Olmos, 2004; Price, Russchen, & Amaral, 1987).

It was not until the studies of Klüver and Bucy that the amygdala was assigned as an essential component for processing emotions and the resulting human behaviour (Klüver & Bucy, 1937). The visceral brain created by MacLean in 1949 (known today as the limbic system) included the amygdaloid complex as one additional structure involved in these forebrain circuits (MacLean, 1949).

1.1 Anatomy

The amygdala is located deep within the temporal lobe beside the sinus sphenoidalis. The reported size of this structure varies across studies depending on the specific techniques used and the inclusion or exclusion of certain nuclei. One widely accepted description has been given by Amunts et al. as a result of the histological study of 10 human cadaver brains (Amunts, et al., 2005). Their study took several factors into consideration for a better quantification, following the equation:

$$V = s \times T \times x \times y \times \sum A_i \times F \tag{1.1}$$

Where V is the volume of the cortical region (mm³), s the distance between two measured amygdala sections, T the thickness of a histological section (0.020 mm), x and y are the width and height of a pixel (0.02116 mm²), $\sum A_i$ is the sum of areas across sections and F constitutes the individual

shrinkage factor. Following this equation, the left amygdala showed an average volume of 1536 ± 286 mm³ and the total right amygdala, 1506 ± 272 mm³.

Surrounding structures are used to define boundaries to delineate the amygdala. Guided by the 2 mm thick anatomical sections of human cadaver brains shown in the Duvernoy atlas (Duvernoy, 1999) it can be seen:

Coronal limits from rostral to caudal sections are defined by the gyrus ambiens, lateral ventricle, entorhinal area, semilunar gyrus, anterior perforated substance, and hippocampal formation. The sagittal boundaries are shown, from lateral to medial, by the peduncle of the lentiform nucleus, hippocampus, anterior commissure, temporal gyrus, and optic tract. Finally, boundaries in the axial plane from ventral to dorsal are given by the hippocampus, parahippocampal gyrus, piriform lobe, entorhinal area, gyrus ambiens, temporal horn of the lateral ventricle, and semilunar gyrus.

As previously mentioned, the most accepted subdivision of the amygdala was provided by Johnston's studies. These three main subdivisions have been also reported on human fetal brain (Humphrey, 1968). This study differentiated cell masses (corticomedial, anterior and basolateral) on a 10 mm sized embryo size. Additionally, developing fibres running in diverse directions were observed on a 13 mm sized embryo.

Although this segmentation is widely accepted, histological studies have, in addition, identified multiple subdivisions as well as one additional major nucleus – the extended amygdala (Table 1.1) (Alheid, et al., 1995; Brockhaus, 1938; de Olmos, 2004; Sah, et al., 2003).

BASOLATERAL	CORTICAL GROUP	CENTROMEDIAL	EXTENDED AMYGDALA
Lateral nucleus ➤ Smaller celled dorsolateral Sub. ➤ Larger celled ventrolateral Sub.	**Bed nucleus of the accessory olfactory tract**	**Central nucleus** ➤ Capsular Sub. ➤ Lateral Sub. ➤ Intermediate Sub.	**Sublenticular portion substantia innominata**
Basolateral nucleus ➤ Rostral magnocellular Sub. ➤ Caudal Intermediate ➤ Parvicellular Sub.	**Nucleus of lateral olfactory tract**	**Centro medial** ➤ Rostral ➤ Central ➤ Caudal	**Intersitial nucleus of the posterior limb of the anterior commissure**
Accessory basal nucleus ➤ Magnocellular Sub. ➤ Intermediate Sub. ➤ Parvidellular Sub.	**Anterior and posterior cortical nucleus**	**Bed nucleus of stria terminalis**	
	Peryamygdaloid cortex ➤ Periamygdaloid cortex ➤ Medial division		

Table 1.1. Amygdaloid divisions and subnuclei by Sah, McDonald and Price (A. J. McDonald, 1998; Price, et al., 1987; Sah, et al., 2003).

1.2. Connectivity

Extensive connections between amygdaloid nuclei and the rest of the brain have been observed in several studies. After injecting anterograde or retrograde tracers in animal experiments, different groups have shown micro-afferences and efferences at a subnuclear level (Ghashghaei & Barbas, 2002; A. J. McDonald, 1987, 1998; A. J. McDonald & Mascagni, 1997; Pitkänen, 2000; Pitkänen, Savander, & LeDoux, 1997). This great specificity also appears to be involved in all sensory systems loops – olfactory, somatosensory, gustatory, visual and auditory systems (Bordi & LeDoux, 1994; Campeau & Davis, 1995; J. E. LeDoux, Farb, & Ruggiero, 1990; A. J. McDonald, 1998; Nakashima, et al., 2000; Price, et al., 1987; Sah, et al., 2003; Shi & Cassell, 1998; Shin, Tsvetkov, & Bolshakov, 2006). Furthermore, the amygdala participation in a particular system related to autonomic responses and pain (Bernard, Peschanski, & Besson, 1989; Gaykema, Chen, & Goehler, 2007) includes projections from the brain stem. Similarly, there are multiple apparent efferences arising from particular nuclei within the amygdala. These projections include intra-amygdala connections as well as both cortical and subcortical regions (Dong, Petrovich, & Swanson, 2001; Floresco, St Onge, Ghods-Sharifi, & Winstanley, 2008; Gallagher & Holland, 1994; Ghods-Sharifi, St Onge, & Floresco, 2009; A. J. McDonald, 1991; A. J. McDonald & Jackson, 1987).

The amygdalar diversity, as a connectivity model, suggests that an appropriate use of imaging techniques (e.g., diffusion tensor imaging) may allow the *in vivo* visualization of some pathways. For a summary example of specific connections see Figure 1.1.
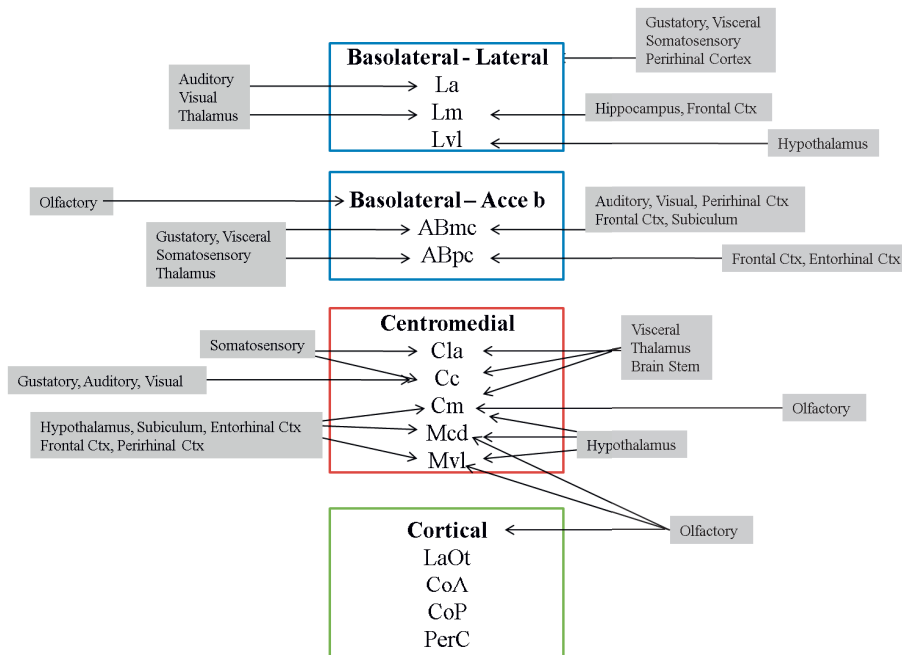
Figure 1.1. Specific connection at a subnuclear level based on Sah et al. (Sah, et al., 2003). Some of the subdivisions of the three main groups (Basolateral, Central, Cortical) are involved in sensory pathways. The lateral and accessory basal nuclei from the basolateral complex are labelled in blue. The lateral divisions shown are lateral *La*, latero-medial *Lm*, latero-ventral *Lvl*. In the accessory basal division, the parvicellular subdivision *ABpc* and magnocellular subdivision *ABmc* are located. The centromedial group labelled in red is composed of a central and a medial part. The central part is divided into the centro-lateral *Cla*, capsular *Cc* and centro-medial division *Cm*. The medial part contains a caudal *Mcd* and a ventral region *Mvl*. The last group at the bottom labelled in green, constitutes the cortical group. This group shows major input from the olfactory system to the nucleus of lateral olfactory tract *LaOt*, anterior and posterior cortical nucleus (*CoA* and *CoP*, respectively) and the periamygdaloid cortex *PerC*. This figure reveals great amygdaloid diversity in a connectivity model.

1.3 Function

Over the last few years, an increasing number of functional studies have identified the human amygdala's involvement in a wide variety of functions (Ball, et al., 2009; Hamann, 2009; Schirmer, et al., 2008; Vuilleumier, 2009). After Klüver and Bucy's initial results in the macaque brain, and the

later inclusion into the limbic system by McLean during the early 1950s, it appears that the amygdala has a crucial role in the processing of emotions (Klüver & Bucy, 1937; MacLean, 1949).

In order to classify the possible emotions processed in this region, it is first necessary to categorize the different human emotions. However, in spite of the vast amount of neuropsychological, philosophical and physiological research on this topic, an ultimate classification of all the emotional states, its intensities, connotations, merges or even individual appreciation of the emotion itself is still complex.

Initial studies on macaque lobotomy of the temporal brain region, established the amygdaloid complex as a region responsible for fear and anger processing (Clugnet & LeDoux, 1990; Fendt & Fanselow, 1999; Klüver & Bucy, 1937; Weiskrantz, 1956). The extensively studied fear circuitry appears to have explicit allocations. For instance, lesions at the basolateral complex affect on different manners the feeling of fear. Similarly, the central nucleus projects to areas mediating autonomic responses. In this regard, damage located at this nucleus affects the expression of fear (Butler, et al., 2007; Campeau & Davis, 1995; Killcross, Robbins, & Everitt, 1997; J.E. LeDoux, 2000; Rabinak & Maren, 2008; Young & Leaton, 1996).

The involvement of the amygdala in several emotional and mental disorders aroused scientific attention to this structure's functional role (Anderson & Phelps, 2000; Aylward, et al., 1999; Boccardi, et al., 2002; Burnett, Reutens, & Wood, 2010; Douaud, et al., 2006; García-Martí, et al., 2008; Hayman, Rexer, Pavol, Strite, & Meyers, 1998; J.E. LeDoux, 2000; Elizabeth A. Phelps, LaBar, & Spencer, 1997; Sachdev, Chen, Joscelyne, Wen, & Brodaty, 2007; Shayegan & Stahl, 2005; Wiest, Lehner-Baumgartner, & Baumgartner, 2006). The increased interest in the amygdaloid complex, combined with the improved experimental tools, have identified the involvement of this structure in a broad variety of emotions besides the already known fear and anger. The use of intra-craneal stimulation on epilepsy patients at the amygdala, the intake of certain substances, stimulating music or even simple positive anticipation measured using fMRI, have revealed that the amygdala is also related with positive emotional responses (Ball, et al., 2009; Blood & Zatorre, 2001; Breiter & Rosen, 1999; Lanteaume, et al., 2007; Sharot, Riccardi, Raio, & Phelps, 2007).

The following study bases the complex system of emotion, on a widely accepted assumption of the conception of basic emotions – The Ekman's six (P. Ekman, 1977). These consist of sadness, happiness, anger, fear, surprise and disgust. This study is grounded on the simplicity of Ekman's model in order to focus on the functional distribution given in the amygdala rather than the research of emotions itself. This intends to avoid the multiple emotional connotations and, as a result, interpretations.

Based on this variability, research has attempted to assign specificity within the amygdala regarding the emotional spectrum from positive to negative valence. In 2007 and 2009, Ball et al. presented a compilation of recent fMRI studies in which amygdalar involvement was reported. The relationship between emotions and structure was established by identifying the centroid points of the activations caused by a specific emotion to a particular segment (Ball, et al., 2009; Ball, et al., 2007). In order to classify these activations, the study made use of an statistical parametric mapping (SPM) mask generated by Amunts and colleagues (Amunts, et al., 2005). This mask computed using cytoarchitectonic data (see above), was later interpolated to MR resolution (a translation in y and z plane by 4 and 5 mm, respectively). The resulting probabilistic map has successfully assisted the *in vivo* functional localization within the amygdala (Aylward, et al., 1999).

The useful segmentation and classification mentioned above are a major step to understand the amygdala and its function. However, considering partial volume effects arising from the interpolation of cytoarchitectonic data into MRI resolution, both segmentation and resolution need further improvement.

Chapter 2

Magnetic resonance imaging (MRI) principles

The effect of nuclear magnetic resonance (NMR) was discovered independently by Felix Bloch and Edward Purcell in the 1940s. It took more than 30 years to develop magnetic resonance imaging (MRI) based on NMR by Paul Lauterbur and Peter Mansfield. The groundbreaking work of all four researchers was rewarded with a Nobel Prize.

MRI is a non-invasive imaging technique, which makes use of magnetic fields to obtain images from the inside of the body with an excellent soft-tissue contrast. The strength of the magnetic field is measured in Tesla (T).

Since the 1980s, MRI has evolved into a routinely used imaging technique for clinical diagnosis and intervention (Bizzi, et al., 1996; Goldman, Pohost, Ingwall, & Fossel, 1980; Raslan, et al., 2009). The clinical magnetic field strength varies from 0.5 T to 3 T. In research, the field strength used for human imaging reaches 9.4 T. Currently, 11.7 T systems are been developed.

2. 1. The static magnetic field (B_0) and the spin

When a tissue sample (e.g., a human body) is placed in a static magnetic field **B**$_0$, all nuclear spins of certain atoms orient themselves parallel or anti-parallel to the magnetic field. In conventional MRI, mostly bound hydrogen atoms in water molecules are used for imaging. The spin is a quantum-mechanical property of the nucleus of an atom. However, it can be considered, for simplicity, as a small magnet.

Only atoms with a non-zero spin are sensitive to NMR, such as phosphorus (^{32}Ph), sodium (^{14}Na) or, most important for MRI, hydrogen (^1H). The sensitivity of a certain method for MRI depends on the natural abundance (the abundance ratio of an isotope in a naturally occurring terrestrial sample), the biological abundance (the fraction of one atom in a biological tissue sample) and the gyromagnetic ratio (a fundamental physical constant) of the nucleus under investigation. In biological tissue like

the human body, Hydrogen (^1H) nuclei are perfect candidates for MRI. ^1H has the greatest natural (99.985 %) as well as biological abundance (63 %) in human tissue and a high gyromagnetic ratio (γ = 42.58 MHz/T). The gyromagnetic ratio not only determines the sensitivity of a certain nucleus, but also the frequency at which the associated spin precesses around the main magnetic field. This frequency is called the Larmor frequency ($\boldsymbol{\omega}_0$) and is proportional to the magnetic field strength ($\mathbf{B}_0$) with γ as proportionality factor:

$$\boldsymbol{\omega}_0 = \gamma \mathbf{B}_0 \qquad\qquad (2.1)$$

2. 2. Time dependent magnetic field in MRI (B_1) and precession

In an MRI experiment, we do not consider only a single spin, but a group of spins, also called a spin ensemble, which builds up a macroscopic magnetization represented by the vector $\mathbf{M}$. In an equilibrium state this vector represents the net magnetization $\mathbf{M}_0$ oriented along the direction of the main field $\mathbf{B}_0$. In order to receive an MRI signal, this magnetization has to be transferred from its equilibrium state into a plane perpendicular to the main magnetic field called the transverse plane. To achieve this, a temporally varying magnetic field ($\mathbf{B}_1$) is applied perpendicular to the main magnetic field with the use of a radiofrequency (RF) coil. If the $\mathbf{B}_1$ field is applied at the Larmor frequency $\boldsymbol{\omega}_0$, $\mathbf{M}$ is "tipped" away from the main magnetic field towards the transverse plane. This is called excitation. In a coordinate system rotating with $\boldsymbol{\omega}_0$, $\mathbf{M}$ forms an angle with $\mathbf{B}_0$ which is called the flip angle α. If α reaches 90°, $\mathbf{M}$ lies completely in the transverse plane. Besides this special case, the magnetization vector has always two orthogonal components: a longitudinal component M_L or M_z, which remains parallel to $\mathbf{B}_0$ and a transverse component M_T or M_{xy}, which is perpendicular to the main magnetic field. After application of the RF pulse, the spin system returns to its equilibrium state by building up the longitudinal magnetization at a certain time constant T_1. This is called the longitudinal or T_1 relaxation. In general, much faster than the T_1 relaxation, the transverse magnetization and, hence, the detectable MR signal, decays with a specific time constant T_2. This is because the precessing spins lose their phase coherence. This effect is named transversal or T_2 relaxation. The reason for this loss of phase coherence is due to subtle variations in the main magnetic field caused by interactions among the spins, resulting in different Larmor frequencies. If one also considers inhomogeneities of the main magnetic field as a source of dephasing, then this

relaxation process is called T_2* relaxation. In general, the T_1 relaxation corresponds to a recovery of $\mathbf{M}_L$ and the T_2 and T_2* relaxation to a decay of $\mathbf{M}_T$.

Because of their different biological and chemical properties, various tissue types have different relaxation times. Therefore, a variety of contrasts can be achieved by weighting the MR signal for the T_1, T_2 or T_2* relaxation, each containing different information about the tissue. In Fig. 1.1, different MR contrasts are shown in a human brain at approximately the same slice position. A T_1 weighted image shows a bright ring of subcutaneous fat and dark cerebro-spinal fluid (CSF). Since grey matter has lower signal intensity than white matter, a sharp grey matter / white matter boundary can be observed. T_2 weighting results in a bright CSF and a darker fat signal. The contrast between grey and white matter is reversed compared to a T_1 weighted image. Finally, T_2* weighting shows a similar but weak grey-white matter contrast as T_2 but is more sensitive to vascular structures (Fig. 2.1).

| | | |
| T1 | T2 | T2* |
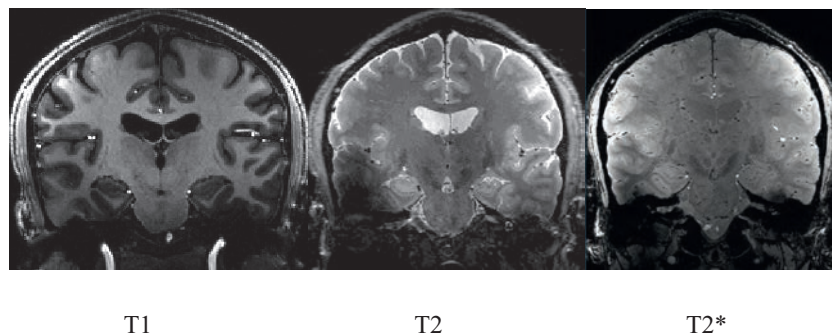
Figure 2.1. Coronal view of human brain data acquired at 7 T. a) T1-weighted magnetization-prepared rapid acquisition with gradient echo (MP-RAGE) sequence (TR/TE = 3000/2.5 ms, flip angle = 6º, voxel size (0.8 mm)³ (Mugler & Brookeman, 1990). b) T2-weighted turbo spin echo (TSE) sequence (TR/TE = 14540/25 ms, refocusing flip angle = 180º, voxel size (0.5 mm)³ (Hennig, Nauerth, & Friedburg, 1986). c) T2*-weighted fast low angle shot (FLASH) sequence (TR/TE = 43/21.4 ms, flip angle = 13º, voxel size 0.5 x 0.5 x 0.6 mm) (Frahm, Haase, & Matthaei, 1986). T1 contrast presents the grey matter darker and the white matter lighter while T2 and T2* show the opposite while T2* being particularly sensitive to veins (courtesy of Drs Robert Trampel and Andreas Schäfer, MPI Leipzig).

As myelin is the major determinant of tissue contrast in the human brain, MR images correspond to details seen in cadaver sections that have been stained for myelin.

2. 3. From frequencies to images

The spatial encoding relies on the careful application of magnetic field gradients. We have seen that the Larmor-frequency depends upon the magnetic field strength (see Eq. 2.1). The application of a magnetic field gradient creates a spatial varying magnetic field strength and therefore the resonance frequency is spatially dependent. An RF excitation pulse has always a certain frequency bandwidth. Together with a slice selective gradient applied G_s, exists a spatial region in which the resonance constraint is fulfilled. Due to this, the MR signal comes from a well defined region along the slice encoding gradient direction. For the remaining dimensions, two more gradients are employed, the phase-encoding gradient G_θ and the frequency-encoding gradient G_f. While G_f creates a certain frequency range along its direction, G_θ achieves the spatial encoding along the remaining axis by creating different stages of dephasing. Hence, the phase-encoding gradient has to be applied several times each with different amplitudes. After the application of the gradients, the signal is acquired using an RF coil. This whole cycle constitutes the repetition time (TR) (Fig. 2.2).

If one applies another RF pulse between excitation and acquisition, it is possible to account for the loss in phase coherence caused by magnetic field inhomogeneities. As a result, the spins refocus after what is called the echo time (TE) (Fig. 2.2). Spin Echo (SE) is the most common sequence used in MRI. The use of a 90° RF pulse deflects the longitudinal magnetization **Mz** into the transverse plane starting the dephasing of the transverse magnetization **Mxy**. The following 180° refocusing pulse rotates the magnetization by 180° leading to a refocusing of the spins. This generates spin echoes while regaining coherence (Carr & Purcell, 1954; Hahn, 1950).

Other commonly used sequence is Gradient Echo (GRE). In this sequence, no 180° pulse is used for refocusing of the spins but the application of a certain gradient scheme leads to a so called gradient echo (Frahm et al., 1986a). The excitation pulse is not necessarily a 90° pulse but lies between 0-90°. T2* is the characteristic contrast associated with this sequence (see Fig. 2.3). With short TRs, after a

certain number of alpha pulses, the z-magnetization cannot fully recover and cannot be reduced due to the following pulses resulting in equilibrium.
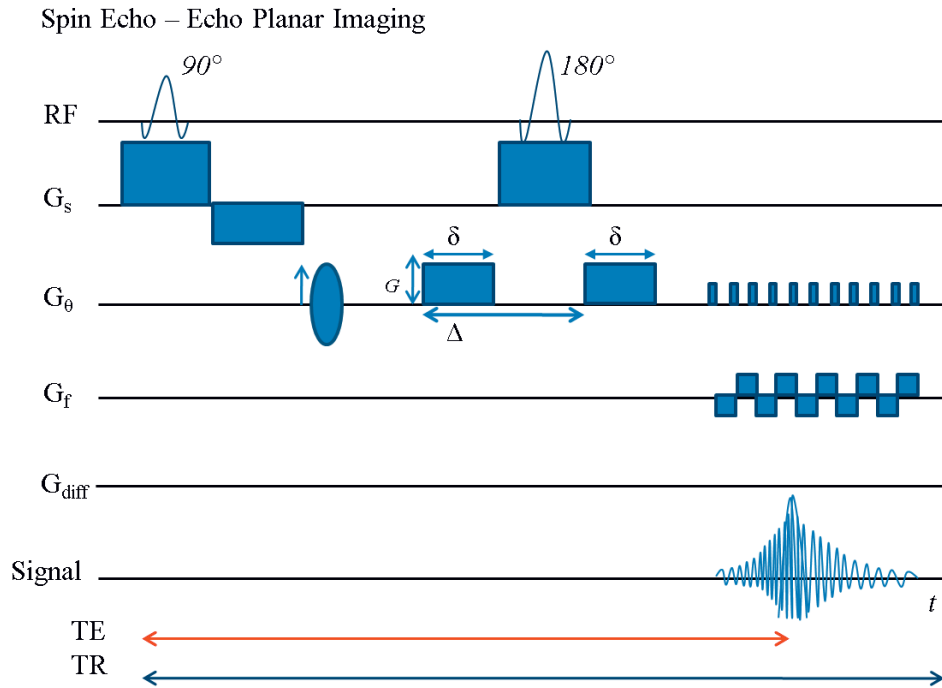

Figure 2.2. Schematic of a typical Spin-Echo (SE) MRI experiment.
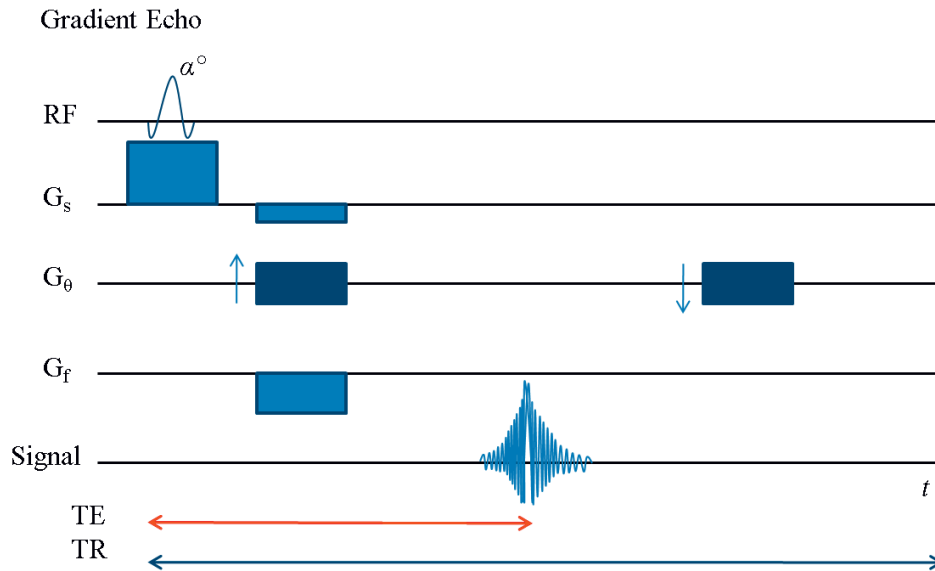
Gradient Echo

Figure 2.3. Schematic of a typical Gradient-Echo (GE) MRI experiment.

In order to describe the conversion of the signal acquired into an image, the concept of k-space is used. Here, k-space contains the spatial frequency information of an object, which is acquired during the MR experiment. The coverage of k-space is thereby determined by the phase and the frequency encoding gradients.

The translation of k-space data into an image is done by the mathematical concept of Fourier transform (FT). FT converts functions from the time domain to the frequency domain, separating the frequency components of a signal. The transformation is performed in a vertical and horizontal direction. As a result, the spatial information of an acquired MR data set is obtained from its representation in k-space and, finally, an image of the scanned object can be reconstructed.

Once the data is transformed, the coordinates used to describe a spatial position in the image of a human brain are xyz, which follow the Talairach system (Talairach & Tournoux, 1988). The three main image planes are called the axial (xy), coronal (xz), and sagittal (yz) planes (see Fig. 2.4). Each point in the data set is called a voxel (3D representation of a pixel).
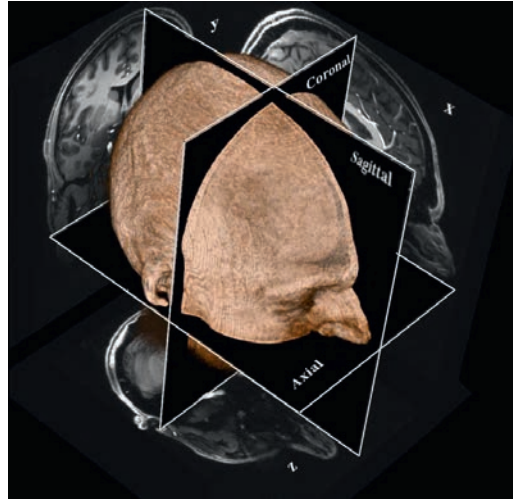
Figure 2.4. The three main imaging planes in MRI – axial, sagittal and coronal.

2. 4. Ultra-high field strength (7 Tesla)

The signal-to-noise ratio (SNR) of the MR signal increases approximately linearly with the strength of the main magnetic field $\mathbf{B}_0$ (Collins & Smith, 2001; Triantafyllou, et al., 2005).

Hence, a high field strength of 7 T increases the sensitivity of MRI more than two-fold compared to a more conventional field strength of 3 T providing detailed images comparable to histological sections (Fig. 2.5). Besides the clear advantage of a higher SNR, higher field strengths also lead to an increase in T_1 and a decrease in T_2 and T_2*, which can be advantageous or disadvantageous depending on the application. However, two main limitations also need to be mentioned. First, inhomogeneities in the irradiated RF field are more pronounced at higher field strengths resulting in artificial intensity variations in the acquired MR image (Van de Moortele, et al., 2005). The second limitation is related to the specific absorption rate (SAR). The SAR describes the absorption of the RF power per unit of mass on biological tissue, and must be limited in order to avoid heating of the tissue under investigation. Moreover, this issue becomes more severe at higher fields, leading to either prolonged scan times or smaller scan coverage.
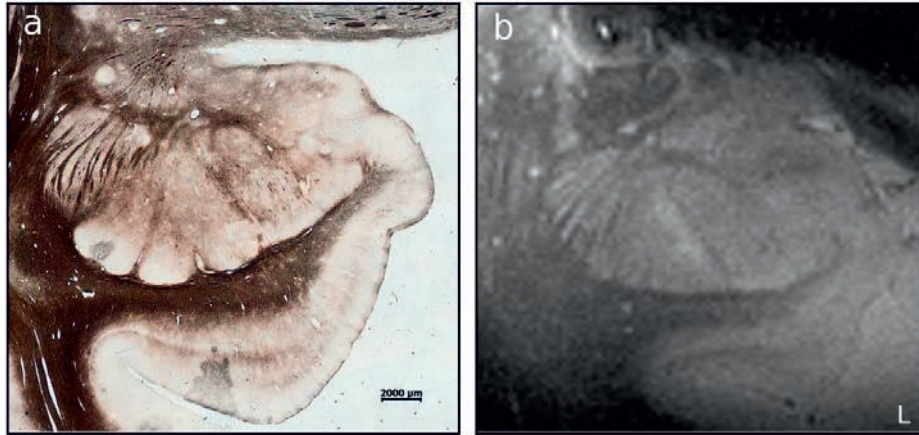
Figure 2.5. Single human brain postmortem data focused at the left temporal lobe. Coronal section. (a) Myelin stained section of the amygdala revealing few myelin features. (b) TSE image acquired on the same postmortem brain and approximated slice (Hennig, et al., 1986). We made use of a 24-channel Nova coil (Nova Medical Inc, Wilmington MA, USA) with a (0.3 mm)³ isotropic resolution (TR/TE: 11890/30 ms, 20 averages courtesy of Robert Trampel). The MR scan shows similar attributes as the histological image does.

The excellent SNR at 7 T allows for high resolution imaging. This can significantly improve non-invasive _in vivo_ human research (Li, et al., 2006; Pruessner, et al., 2000; Thomas, et al., 2008). Additional clinical applications might benefit regarding the localization of tumours, stroke, dementia and other neurological disorders (Cho, et al., 2008; Kang, et al., 2009; Mainero, et al., 2009; Zivadinov, Stosic, Cox, Ramasamy, & Dwyer, 2008).

2. 5. RF coils

Another central factor for the quality and the SNR of MR data are the RF coils used for applying the RF pulses collecting the MR signal. In our studies, two different RF coils were employed: an 8-channel phased-array coil (RAPID Biomedical, Rimpar, Germany) and a 24-channel phased-array coil (Nova Medical Inc, Wilmington MA, USA).

Within multiple reasons, principally, the coils and the number of channels influence the image quality; these are relevant for artifact minimization and SNR improvement.

2. 6. Functional magnetic resonance imaging (fMRI)

Functional MRI (fMRI) was independently developed in the early 1990's by two different research groups (Belliveau, et al., 1991; Ogawa, Lee, Kay, & Tank, 1990; Turner, Le Bihan, Moonen, Despres, & Frank, 1991). It enables non-invasive study of brain activity during task performance. The approach is based on BOLD (Blood Oxygenation Level Dependent) effect which indirectly tracks neural activity through local changes in blood flow, blood volume, and oxygen consumption, all of which affect oxygen concentration in the capillaries, venules, and arterioles.

Oxygen in blood is coupled to hemoglobin molecules (Hb), and therefore the ratio of oxyhemoglobin (HbO_2 with oxygen bound to it) and deoxyhemoglobin (Hb without oxygen) changes with the oxygen concentration in the blood. As oxyhemoglobin has different magnetic properties than deoxyhemoglobin, neural activity leads to local changes in the magnetic field. HbO_2 causes the hemoglobin to become diamagnetic, whereas hemoglobin without oxygen becomes paramagnetic.

T2* signal, as mentioned before, is depending on local field inhomogeneities and not just spin-spin interactions. The relative decrease in the concentration of Hb, can be detected by MRI as a rise in the T2* weighted signal. As a result, the T_2* relaxation time, and therefore the MR signal, changes within the activated brain area. Until today, the BOLD effect has been employed in a wealth of studies to localize functional changes in specific brain areas (Cannestra, et al., 2001; Fried, 2000; Kwong, et al., 1992; Latchaw, Ugurbil, & Hu, 1995; Maeder, et al., 2001; Mazziotta, 1994; Sharot, et al., 2007) .

Chapter 3

Diffusion tensor imaging (DTI) principles

3.1. DTI principles

DTI is a relatively new MR imaging technique, which aims to reveal the underlying anatomical connectivity in the human brain. DTI uses diffusion-weighted imaging (DWI), which is a measure of water mobility in different directions (Brownian motion). This motion is affected by the properties of the medium in which it occurs (Einstein, 1926; Le Bihan, et al., 1986; Turner, et al., 1990).

Diffusion-weighting is achieved by applying a pair of gradients with a time interval ($\varDelta$) in between. During the application of these gradients, the spins of the water molecules will be dephased by the first gradient and then rephased by the second gradient. Only the spins that have moved some distance during the time $\varDelta$ will not rephase completely resulting in a reduced signal. Diffusion-weighted imaging is thus sensitive to motional process, such as flow or water molecule diffusion.

A standard diffusion sequence used is spin echo echo planar imaging (*SE-EPI*) (Mansfield, 1977; Stehling, Turner, & Mansfield, 1991; Tanner & Stejskal, 1968) (Fig.3.1). EPI is a fast magnetic resonance imaging technique that records an entire image in a TR period. Standard sequences acquire one k-space line in one TR, EPI acquires all lines of k-space in a single TR. This sequence is commonly used for fMRI and DW imaging.

Spin Echo – Echo Planar Imaging
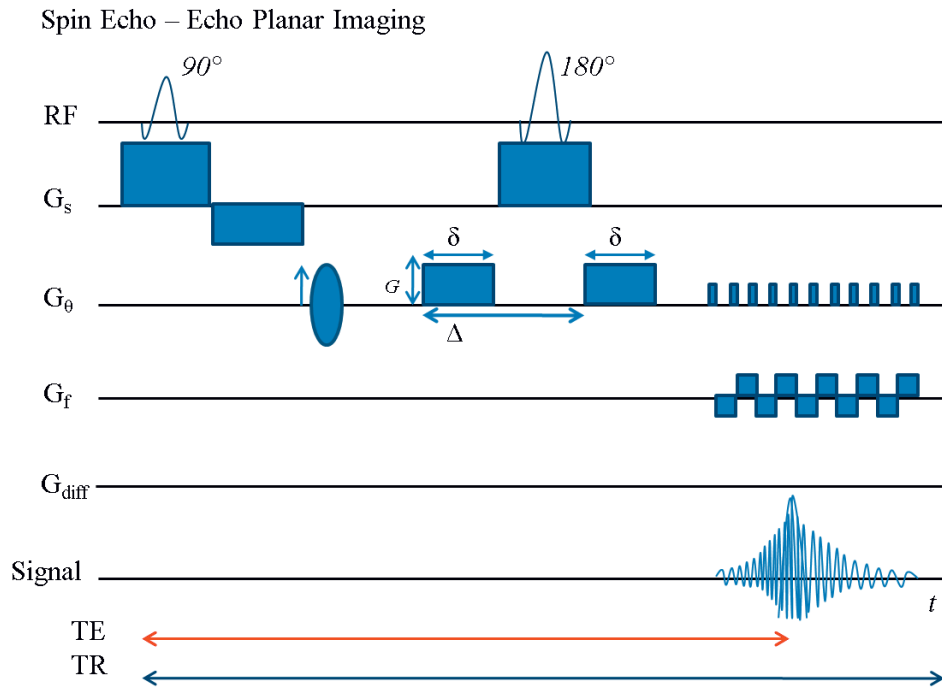
Figure 3.1. Schematic of a typical for Spin Echo - Echo Planar Imaging (SE-EPI).) including diffusion sensitizing gradients (slice direction).

The diffusion signal loss due to the application of gradients follows the Equation 3.1:

$$S/S_0 = e^{-\gamma^2 G^2 \delta^2 (\Delta^2 - \delta/3)\mathbf{D}} = e^{-b\mathbf{D}} \tag{3.1}$$

Where S_0 is the signal intensity without and S the signal with diffusion-weighting gradients applied. The gyromagnetic ratio is indicated by γ. The strength (G) and length (δ) of the diffusion gradients as well as the time between them (Δ) are summarized in the b-value b. This Equation indicates that the higher the diffusion constant D the larger the signal loss [3]. The calculated D can consequently be mapped onto an image as the spatially apparent diffusion constant (ADC) of the tissue acquired (Fig. 3.3).

The diffusion-weighting is oriented along the direction of the diffusion-sensitizing gradients. When water motion is hindered by structures in the tissue, like nerve fibres, it results in a smaller diffusion

coefficient. Any restriction will decrease the diffusion coefficient and will, hence, result in a higher signal in the diffusion-weighted image. In the case of nerve fibres, the diffusion of the molecules is less restricted parallel to the fibres. This phenomena is called diffusion anisotropy (Fig. 3.2). The lowest hindrance to water molecules provides the maximum apparent diffusion coefficient (ADC). This is reflected in the self diffusion coefficient of pure water ($\sim 2 \times 10^{-9}$ mm²/s at an average temperature of 25°C) which is, obviously, isotropic.
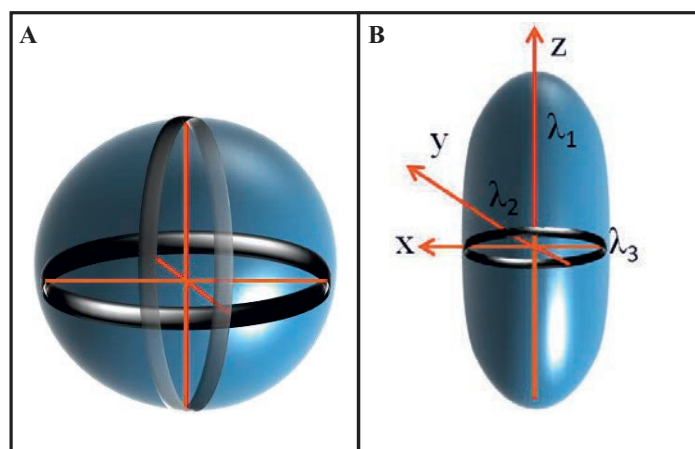

Figure 3.2. Schematic illustration of diffusion isotropy and anisotropy in the brain. When the environment is isotropic (a) water diffuses equivalently in all directions. (b) When water molecules are surrounded by restrictions, e.g., brain fibres (Fig. 3.4), they follow a principal diffusion direction. The diffusion constants (**x**, **y** and **z**) characterize the diameter of the sphere and the eigenvalues describe the length of the tensor $\lambda_1, \lambda_2, \lambda_3$. The ellipsoid computed from an anisotropic environment represents brain fibre pathways.

Using the gradients in different directions and assuming an oblique anisotropic angle provided by the surrounding media, at least six directions are needed to calculate a diffusion tensor (**D**). By adding the three orthogonal ADC maps ($\mathbf{D}_{xx} + \mathbf{D}_{yy} + \mathbf{D}_{zz}$), the diffusion tensor can be computed. This tensor, a 3 x 3 vector matrix, leads to diffusion-tensor imaging (DTI) (P. J. Basser, 1993; P.J. Basser, Mattiello, & LeBihan, 1994).

$$\mathbf{D} = \begin{bmatrix} Dxx & Dxy & Dxz \\ Dyx & Dyy & Dyz \\ Dzx & Dzy & Dzz \end{bmatrix} \tag{3.2}$$

This matrix can be normalized with three eigenvectors and three eigenvalues. The diffusion constants (Dx, Dy and Dz) characterize the diameter of the ellipsoid. The three principal axes of the diffusion tensor are termed eigenvectors. The eigenvalues describe the length of the tensor: with λ_1 being the longest, medium λ_2 and shortest λ_3 (Fig. 3.2, Eq. 3.2, Fig. 3.1). The largest eigenvector, called the "primary eigenvector", and its associated eigenvalue λ_1 indicate the direction and magnitude of the greatest diffusion. In an anisotropic environment where the water molecules are restricted by the surrounding tissue, the reconstruction of the tensor corresponds well with the fibre orientation and can be visualized as an ellipsoid (Fig. 3.3).

One commonly used parameter in DTI is the fractional anisotropy (*FA*). FA maps give information about the degree of anisotropy in different regions of interest (Fig. 3.3, Eq. 3.3).

$$\text{FA} = \frac{\sqrt{(\lambda_1 - \lambda_2)^2 + (\lambda_2 - \lambda_3)^2 + (\lambda_3 - \lambda_1)^2}}{\sqrt{2}\sqrt{\lambda_1^2 + \lambda_2^2 + \lambda_3^2}} \tag{3.3}$$

The FA values are between 0 (isotropic diffusion) and 1 (hypothetical infinite cylinder). Causes of anisotropy are not completely understood in the human brain but are found to have a close relation with the fibre orientation in white matter (P. J. Basser & Pierpaoli, 1996).
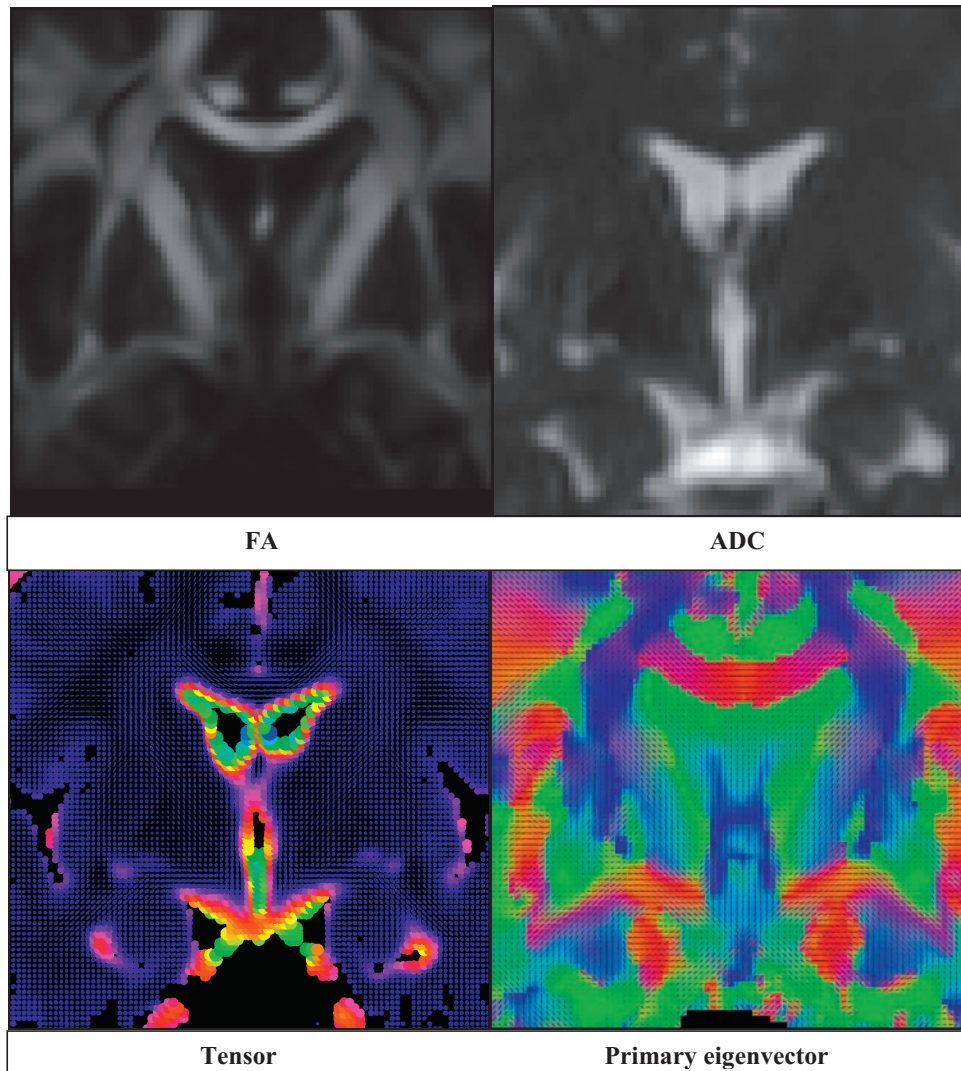
Figure 3.3. Diffusion data. The fractional anisotropy (FA) reflects degree of anisotropy with brighter contrast. The apparent diffusion coefficient (ADC) represents the degree of diffusivity. In the tensor map, each voxel is characterized with an ellipsoid. The primary eigenvector represents the average of all orientations found within one voxel. This last map is colour-coded where green labels an anterior-posterior direction; red medio-lateral ad blue indicates a dorso-ventral direction.

3.2. Diffusion on brain tissue

DTI was introduced to clinical neuroradiology during the early 1990s. It has been decisive for the characterization of neurodegenerative diseases, stroke and surgical planning (P. J. Basser & Pierpaoli, 1998; Chabriat, et al., 1999; Holodny, Schwartz, Ollenschleger, Liu, & Schulder, 2001; Le Bihan, et al., 2001; Mori & Zhang, 2006; Nakata, et al., 2009).

Diffusion magnetic resonance is the only non-invasive technique tool to obtain information about the neural architecture of the human brain white matter *in vivo* (Basser et al., 2000; Mori et al., 1999). A neuron or a series of neurons interconnect a number of areas in the brain. The axons of these neurons are myelinated. DTI allows for the reconstruction of the lattice that restricts the motion of water molecules ─ the myelinated fibres. The primary eigenvector represents the averaged diffusion orientations found within one voxel thus represents the averaged orientation of the fibre bundles (Fig. 3.4) (Wakana et al., 2004). On the basis of myelinated axons, DTI (tractography) has extensively focused on the white matter of the brain which exhibits high anisotropy.
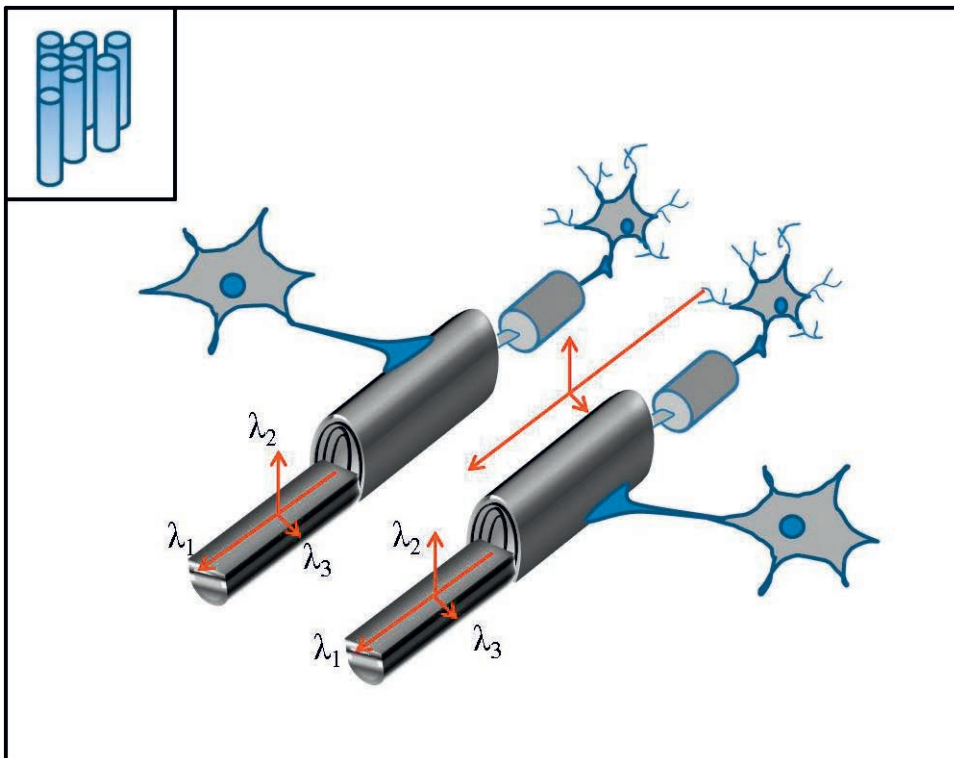
Figure 3.4. Brain natural barriers. Cell membranes, myelin sheaths, white matter fibre tracts, and protein molecules are natural barriers which restrict water molecules movement. This diffusion restriction is reconstructed on DTI as a tensor or fibre track.

Data obtained from DTI experiments can be analyzed in different ways. The visualization of an entire white matter tract in 3D can be computed by connecting individual λ_1 in each voxel. This is called fibre tracking or tractography (Anwander, Tittgemeyer, von Cramon, Friederici, & Knosche, 2007; Behrens, et al., 2003; Koch, Norris, & Hund-Georgiadis, 2002; Mori, Crain, Chacko, & Van Zijl, 1999). Tractography commonly uses two families of fibre tracking algorithms: deterministic and probabilistic methods. A deterministic algorithm computes tracts between a number of pre-defined areas while a probabilistic algorithm reconstructs the tracts arising from a specific seed point given, projecting to the rest of the brain. This latter one incorporates uncertainty but reliability due to the absence of pre-defined areas to be connected with (Fig. 3.5).
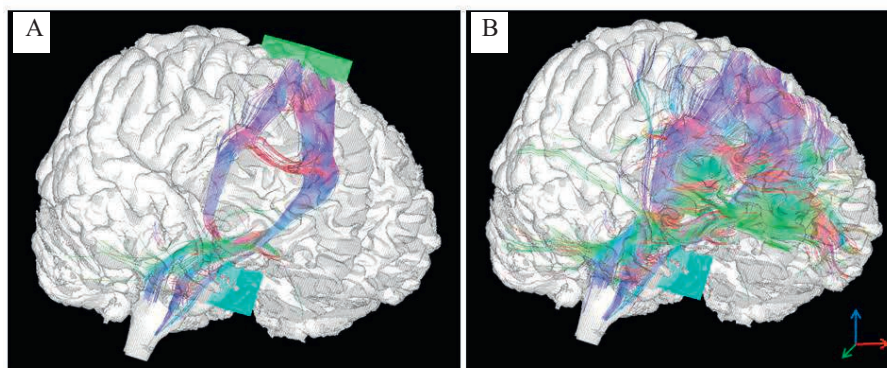

Figure 3.5. (a) A deterministic algorithm computes tracts between a number of pre-defined areas while (b) a probabilistic algorithm reconstructs the tracts arising from a specific seed point given, projecting to the rest of the brain.

Since myelin constitutes a major component on anisotropy, DTI has been mainly used on white matter brain areas. However, several studies have also successfully performed DTI experiments in grey matter (Behrens et al., 2003; DaSilva et al., 2003; Thornton et al., 1997; Tomassini et al., 2007; Wiegell et al., 2003). Myelin, however, is not the only determinant of diffusion anisotropy (Beaulieu, 2002). Given that the presented study is mainly focused on a grey matter area - the amygdala, it is

important to bear in mind that additional components of brain tissue can hinder the water molecules diffusion.

It is likely that several factors contribute to constrain diffusion. There are axons in grey matter that are myelinated, albeit to a lesser extent. In this regard, a specific organization of fibre bundles running parallel with more or less myelin might hinder extra-axonal diffusion from becoming compartmentalization (Le Bihan, et al., 2001). Similarly, dendrite density might contribute to the diffusion anisotropy in both white and grey matter (Jespersen, Kroenke, Østergaard, Ackerman, & Yablonskiy, 2007). In principle, any cell presence with long cylindrical shape and high impermeability, density and orientational distribution contributes to anisotropy of the brain (Beaulieu, 2002; Perge, Koch, Miller, Sterling, & Balasubramanian, 2009). Experiments on non-myelinated garfish have presented significant anisotropy in trigeminal, optical and olfactory nerves equivalent to that in humans despite the absence of myelination (Beaulieu & Allen, 1994a). Other experiments have focused on developmental or fetal brain (Gupta, Hasan, et al., 2005; Huang, et al., 2006; Jakovcevski, Filipovic, Mo, Rakic, & Zecevic, 2009). Any semi-impermeable cell would thus be enough to hinder water molecules from moving freely and contribute to a reduce the ADC (Fig. 3.6).
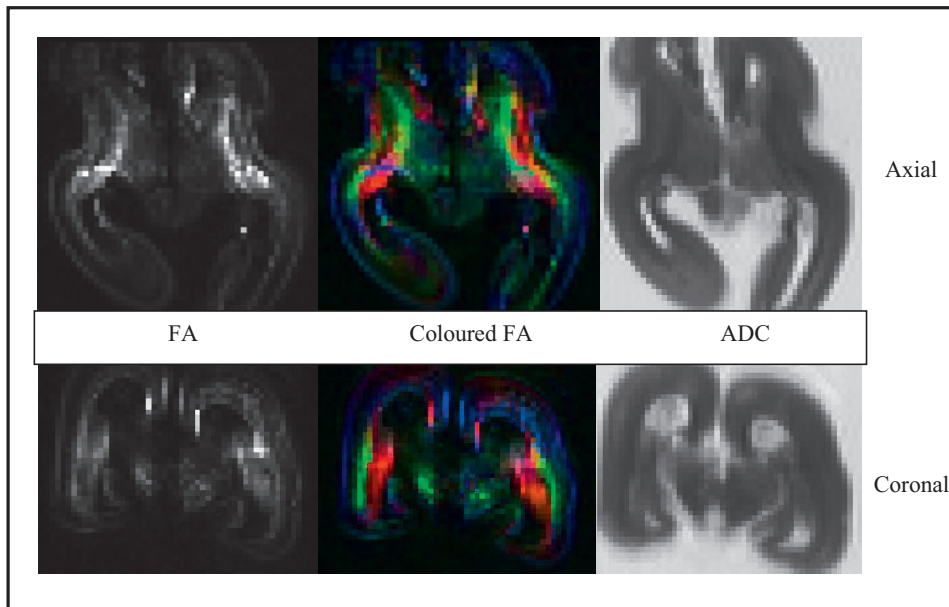
Figure 3.6. DTI at 7 T of fetal cadaver brain (29 weeks old). Upper row, mid-brain axial sections, lower row, mid-brain coronal sections. SE-EPI (TR/TE = 3000/69 ms, (0.9 mm) ³, 7 averages). Anisotropy differentiates clear cortical layers within the fetal brain.

Another candidate for causing anisotropic diffusion are glial cells. These cells, are very similar to neuron cells. First, astrocytes' mesh, can be elongated becoming comparable to neuronal networks. Unfortunately, astrocytes contain an increased number of water channels (aquaporin-4) which leads to its permeability. Another glial cell component is the oligodendrocyte. During the neuronal development, one type of oligocendrocyte constitutes the precursor of what will eventually become a neuron (Baumann & Pham-Dinh, 2001; Beaulieu, 2002; Gupta, Rao, et al., 2005; Jakovcevski, et al., 2009; Perge, et al., 2009; Rio-Hortega, 1928). Hence, this element has been recently used to explain the anisotropy found on fetal brain and non-myelinated animal brains (Avram, Guidon, & Song, 2010; Huang, 2010). These relatively recent interpretations, have opened challenging perspectives understanding adult brain anisotropy in areas such grey matter, as well as the diffusion imaging technique itself.

Chapter 4

Polarized Light Imaging (PLI)

Polarized Light Imaging (PLI) is a method currently used as a validation technique for DTI. PLI applied to brain sections of about 100 μm thickness allows the imaging of the fibre orientation at a resolution useful for cytoarchitectonic analysis.

Polarized light imaging is an ancient optical technique based on the propagation of light in anisotropic matter (Bennett, 1950; Oster, 1956; Shurcliff & Ballard, 1964) and for over a hundred years, this technique has also been applied to the myelin sheaths in the brain. The myelin sheaths have a property which is called birefringence (Klebs, 1865; Schnabel, 1966). Birefringence materials have a different refractive index (RI) (Eq. 4.1) for light of different polarization. This property makes polarized light split up into 2 light wave components which then propagate at different velocities through the substance. These two rays have orthogonal polarizations and for oblique entrance angles different directions in the material.

$$\Delta_n = n_e - n_o \tag{4.1}$$

In brain tissue, as with DTI anisotropy, birefringence is generally closely related to the orientation of myelinated nerve fibres. This can be reflected when the greatest RI runs parallel to the fibre and it produces a positive birefringence visualized as brighter.

4.1 PLI and brain tissue

In histological sections of the human brain, series of polarized light images can be used to achieve quantitative estimates of the angles of inclination (z-direction) and orientation (in xy-plane) of nervous fibres (Wolman, 1970, 1975). Since the apparent principal component related to birefringence is myelin, research has focused on brain white matter. Hence, the technique of using polarized light images has been successfully applied in structural brain classification and 3D tissue

reconstruction (H. Axer, Axer, Krings, & Keyserlingk, 2001; H. Axer, Berks, & Keyserlingk, 2000; H. Axer & Keyserlingk, 2000; H. Axer, et al., 2002; H. Axer, Lippitz, & von Keyserlingk, 1999; M. Axer, et al., 2008; Larsen, Griffin, Grassel, Witte, & Axer, 2007).

Fibre imaging using PLI requires certain specificities regarding brain tissue preparation. The specimen is first fixed in a 4% formalin solution which will not affect tissue birefringence features. This type of issue can easily occur with the use of inappropriate fixing methods such as applying paraffin. Next, the specimen is embedded in polyethylene glycol (PEG) under a scenario of temperature and time control (Romeis, 1989). After embedding, the specimen is sliced at 100 µm thickness using a cryostat microtome (CM3050 S, Leica Microsystems, Bensheim, Germany) and mounted serially on glass slides. Each series consists of one slice prepared for PLI analysis and one stained section for further investigation. The stains employed are: Cresyl violet acetat (Nissl stain) which mainly dyes cell bodies (perikarya) while myelin loses colour, and a Luxol fast blue stain which colours myelin blue (see Chapter 6).

Tissue birefringence can also be intensified with the use of metal staining and/or by employing thicker slices.

4.2 Polarized light equipment

PLI equipment consists of an specific number of light filters strategically positioned. Three plates (or filters), the polarizer, the analyzer and the quarter wave plate, are necessary for a complete visualization of all azimuths. The myelin content in the specimen is capable to split the polarized light in two components. A rotational plate will capture all athimuth present in the brain slice running parallel to the myelin sheath (see Chapter 6 for more information).
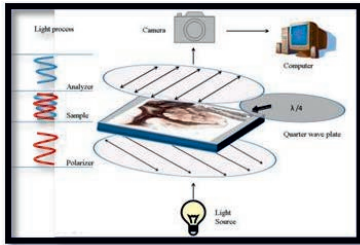
Chapter 6, Fig. 6.2

The intensity images of every possible combination of the polarizer, analyzer and the quarter wave plate are captured by a camera connected to a computer and interpreted using software written in Matlab (MathWorks Inc., Natick, MA, USA) the determined angles are then colour-coded for visualization purposes.

4.3 PLI on grey matter

Despite DTI has been successfully applied to grey matter areas such as the amygdala or the thalamus (Anwander, et al., 2007; Behrens, et al., 2003; Draganski, et al., 2008), diffusion values as the FA (see Chapter 3) still extensively used as anisotropy precursors and fibre indicators. Considering previous DTI findings obtained in the amygdala region (Solano-Castiella, et al., 2010), a logical next step, moves towards the histological study of anisotropy within this grey matter area.

Over the last 10 years, the increasing interest in grey matter has revealed several factors (e.g., crossing fibres, semi-impermeable cells) which have lent knowledge to the imaging techniques of brain water diffusion and aroused curiosity as far as myelin and fibre development are concerned (Andrews, Osborne, & Does, 2006; Mädler, Drabycz, Kolind, Whittall, & MacKay, 2008; Prayer, et al., 2001). This research will investigate the anisotropic effects of polarized light within the amygdala area.

II

Materials and Methods

Chapter 5

Experiment 1

Diffusion tensor imaging segments the human amygdala *in vivo*

The amygdala plays a substantial role in emotion, learning, and memory. It would be highly advantageous to understand more precisely its internal structure and connectivity, for individual human subjects *in vivo*. Earlier cytoarchitectural research in post-mortem human and animal brains has revealed multiple subdivisions and connectivity patterns, probably related to different functions. With standard magnetic resonance imaging (MRI) techniques, however, the amygdala appears as an undifferentiated area of grey matter. Using high quality diffusion tensor imaging (DTI) at 3 Tesla, we show diffusion anisotropy in this grey matter area. Such data allowed us to subdivide the amygdala for the first time *in vivo*. In 15 living subjects, we applied a spectral clustering algorithm to the principal diffusion direction in each amygdala voxel and found a consistent subdivision of the amygdala into a medial and a lateral region. The topography of these regions is in good agreement with the fibre architecture visible in myelin-stained sections through the amygdala of a human post-mortem brain. From these *in vivo* results we derived a probabilistic map of amygdalar fibre orientations. This segmentation technique has important implications for functional studies in the processing of emotions, cognitive function, and psychiatric disorders and in studying morphometry and volumetry of amygdala subdivisions.

5.1 MRI data Acquisition

We used data from 15 healthy subjects (7 females and 8 males between the ages of 22-35 years) selected at random from the large in-house MRI database of the Max Planck Institute for Human Cognitive and Brain Sciences. Subjects underwent a diffusion-weighted MRI (Turner et al. 1991) and T1-weighted structural scan using a whole-body 3 Tesla Trio scanner (Siemens, Erlangen, Germany) equipped with an 8-channel phased-array coil (Siemens, Erlangen). Written informed consent was obtained from all participants in accordance with ethical approval from the University of Leipzig.

The T1-weighted structural scans were used for skull-stripping, and the brain images were then co-registered into Talairach space (Talairach and Tournoux 1988). Diffusion-weighted images (DWI) were acquired with a twice-refocused spin-echo echo-planar imaging sequence (TE = 100 ms, TR = 12 s, 128 x 128 image matrix, FOV = 220 x 220 mm²) providing 60 diffusion-encoding gradient directions with a b-value of 1000 s/mm² (Reese et al. 2003; Weiskopf et al. 2007). Seven images without any diffusion weighting (b-value = 0) were obtained at the beginning of the scanning sequence and again after each block of 10 diffusion-weighted images as an anatomical reference for offline motion correction. The interleaved measurement of 72 axial slices with 1.7 mm thickness (no gap) covered the entire brain. Each DWI scan took 13 minutes. Random noise in the data was reduced by averaging 3 acquisitions, resulting in a total acquisition time of 42 minutes. Cardiac gating was not utilized, in order to limit the acquisition time. Additionally, fat saturation was employed, together with 6/8 partial Fourier imaging, Hanning window filtering, and iPAT = 2.

The 21 images without diffusion weighting distributed over the whole scan time were used to estimate motion correction parameters using rigid-body transformations (Jenkinson et al. 2002), implemented in FSL (FMRIB Software Library, University of Oxford, 2006, http://www.fmrib.ox.ac.uk/fsl). Motion correction for the 180 diffusion-weighted images was combined with a global registration to the T1 anatomy computed with the same method. The gradient direction for each volume was corrected using the rotation parameters. The registered images were interpolated to the new reference frame with an isotropic voxel resolution of 1 mm and the three corresponding acquisitions and gradient directions were averaged. A diffusion tensor and the fractional anisotropy (FA) were computed from the DWI data of each voxel.

5.2 Amygdala Segmentation

Automatic segmentation tools, while under active development in several laboratories, are still not fully reliable. Several boundaries of the amygdala complex are subtly defined in MR images. We decided to use a more robust manual delineation of the amygdala (Horinek et al. 2007) to exclude extraneous tissue, as far as possible (see Chapter 1). Individual masks were created for each brain, guided by the 2 mm thick anatomical sections of human cadaver brains shown in the Duvernoy (1999) atlas. The resulting masks were conservatively small.

5.3 Amygdala Parcellation

All 15 anatomical and DWI data sets were subsequently nonlinearly aligned (Thirion 1998) with a single subject template brain, based on the FA contrast of all images, so that the amygdala regions were located approximately at the same position in all transformed data sets. The masks were transformed likewise. We then computed an intersection across all masks so that the resulting single mask was common to all data sets.

For each voxel, a diffusion tensor was fitted to the spatially normalized DWI data. The preferential fibre direction in each voxel is characterized by the principal eigenvector of the diffusion tensor. The angular direction of the diffusion tensors can be conveniently visualized using an RGB colour coding, so that a specific colour represents a particular fibre orientation (Douek et al. 1991).

In order to group voxels with comparable tissue orientation within the mask of the amygdala, the similarities between two voxels were computed as the cosine of the angle between the principal diffusion directions. For each hemisphere in each of the 15 data sets, we obtained a similarity matrix in which entries s_{ij} represented the similarity of orientations in voxels i and j. The second and third eigenvector of the diffusion tensor were not used due to the higher noise level in these components related to the low anisotropy in the amygdala which is below 0.2 (Fig. 5.1).
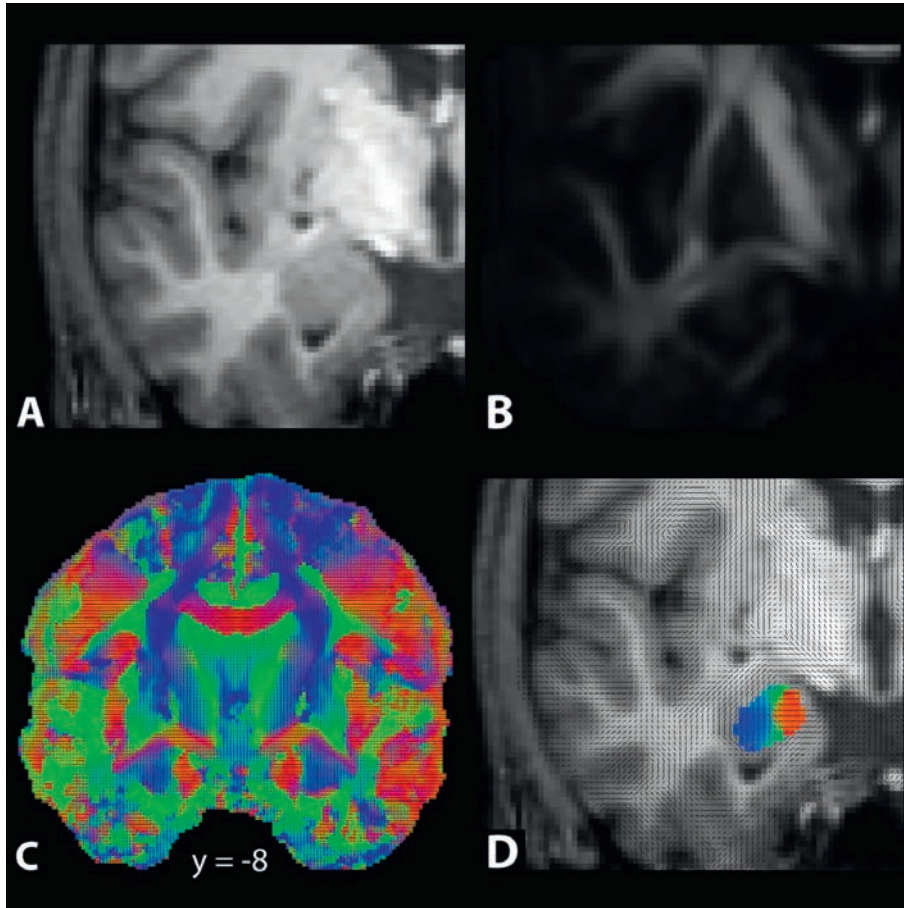
Figure 5.1. Diffusion data. Coronal MR sections of a single human subject. (a, b, d) Enlarged view of the left temporal lobe. (a) T1-weighted structural image. (b) Fractional anisotropy (FA) map derived from the diffusion-weighted data. (c) Diffusion orientation map from the group mean DTI data. Red colour corresponds to medio-lateral direction, green to anterior-posterior, and blue to dorso-ventral orientation. (d) Averaged orientation map superimposed on the anatomy of a single subject (amygdala is colour-coded). In C and D the data reveal 3 compact groups of differently oriented voxels not identifiable in panel A and B. Coordinates are in Talairach space.

5.4 Spectral Clustering

We averaged the similarity matrices across all subjects and applied spectral clustering to it (Ng et al. 2002). In order to avoid an arbitrary choice of the number of clusters, we used cross-validations to

determine the number of clusters which yielded optimal consistency across subjects and hence the optimal number of clusters. Specifically, we employed a leave-one-out method where each subject's data is left out from the averaging. For each subject, we checked the consistency between the clustering results of the single subject and the average across the remaining subjects. We used Cramer's V for this purpose (Cramer, 1946). This tool is a widely used measure of nominal association based on chi-square which tests variables relationship. Then is normalized for table size (Cramer, 1946). This procedure provides an index of the strength of association between the results found. In this particular case, it evaluates the association of the resulting clusters across subjects. Cramer's V gives values within the range [0,1]. Values above 0.5 would indicate good consistency with a value of 1 indicating a perfect match. The inter-subject consistency check, was performed for $k =3, 4, 5$ clusters. The results are listed in Table 5.1. The most consistent result was found for $k= 2$ in both hemispheres.

	$k= 2$	$k= 3$	$k= 4$	$k= 5$
Left hemisphere	0.72 ± 0.026	0.58 ± 0.019	0.49 ± 0.012	0.47 ± 0.009
Right hemisphere	0.73 ± 0.034	0.57 ± 0.008	0.52 ± 0.011	0.50 ± 0.011

Table 5.1. Inter-subject consistency for different numbers of clusters using Cramer's V. The numbers shown are averages across subjects with standard errors.

In order to further check whether a clear separation between at least two clusters exists, we applied spectral re-ordering to the averaged similarity matrix. This ordering is obtained via the so-called Fiedler vector which corresponds to the second smallest eigenvector of the graph Laplacian (Higham et al. 2007). When the groups of similar vectors show a clear separation within each other, indicates a reliable possible clustering of the data.

In order to study the inter-subject variability, the spectral clustering was applied separately to all subjects. The non-normalized DTI data of the individual amygdala segmentation was separated into two clusters for each hemisphere. The individual results were transformed to the template brain. By voxel-wise counting the number of times each subregion was found, a probability map of the clustering result was created.

5.5 Myeloarchitectonic comparison

In order to understand the effect of myelinated tissue within the amygdala on the DTI images, we included in this study histological data from one human cadaver brain. The post-mortem period before staining was less than one month. The specimen was preserved in formalin. Blocks containing the amygdala were sliced with a thickness of 30 μm , and its in-plane resolution is only 2 μm, while the MR image resolution is $(1.7 \text{ mm})^3$ (cf. box in Fig. 10.1.1). The sections were stained for myelin using the Gallyas (1979) technique. This approach is highly specific for myelin and can visualize thin fibres.

Chapter 6

Experiment 2

Polarized light imaging (PLI) of the human amygdala

The intricate neuronal network within the extended amygdala supports a diversity of human emotions. Diffusion tensor imaging (DTI) has showed anisotropic grouping within the human amygdala based on the orientation of the main eigenvector for each voxel (see Chapter 5). This can be achieved because this grey matter area has a non-zero fractional anisotropy in DTI. Polarized light imaging (PLI) is a basic technique which also measures brain tissue anisotropy. This technique has been also used for structural brain classification (Axer et al., 2002; Axer et al., 2008). The following study compares PLI data obtained for 100 μm thick slices through the amygdala of human cadaver brain with our previously acquired *in vivo* DTI data.

6.1 Tissue preparation

A human cadaver brain donated to our laboratory was fixed in 4% formalin, and a coronal slab containing the amygdala was dissected. Because paraffin embedding destroys the tissue's birefringence, the specimen was embedded in 10% gelatine/polyethylene glycol (PEG). Once the block was hardened by applying low temperatures (a traditional fridge), a 10% saccharose solution was applied for cryoprotection. This last procedure was repeated 24 hours later but this time increasing the concentration of saccharose to 25%.

The slab was serially sectioned into 100 μm thick coronal slices using a cryostat microtome (CM3050 S, Leica Microsystems, Bensheim, Germany). The sectioning table was tilted 3° at a temperature of 17°C for an optimal slicing. The sections were finally coverslipped with aquatex on a glass slide. The sections needed about 4 weeks to dehydrate.

In addition to the sections already prepared for PLI purposes, each slice was also accompanied by a stained section interleaved. As already mentioned in Chapter 4, the stains used were Luxol fast blue and Cresyl violet acetat (Nissl staining). The combination of these particular stains on one section

permits the visualization of both myelin and cell bodies which could either belong to neurons but also to glial cells. As a result, this additional technique assists the microscopical imaging of the specific organized compounds that can be found in the specimen (Fig.6.1).
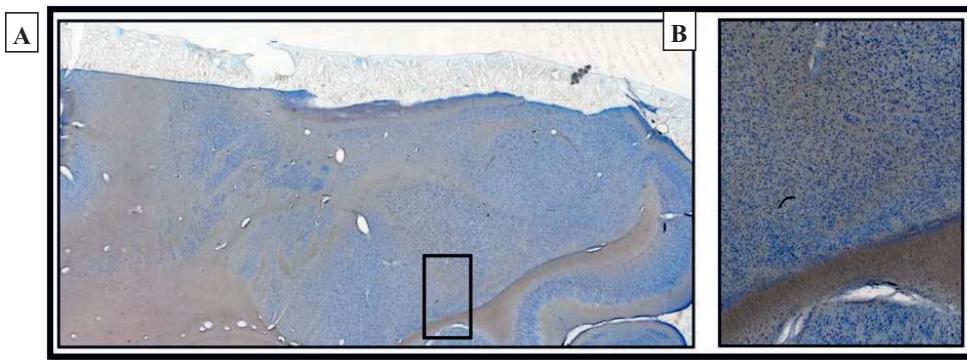

Figure 6.1. Tissue stain used for microspic inspection. Cresyl violet acetat (Nissl stain) which mainly dyes cell bodies (perikarya) while myelin loses colour, and a Luxol fast blue stain which will colour the myelin. (a) Coronal section of the left amygdala. The box represents the enlarged region shown in (b).

6.2 Polarized light imaging equipment

PLI equipment uses three separate filters (Fig. 6.2). First, light is plane polarized by the polarizer filter before arriving at the specimen. The optically polarized light then passes through a sample of tissue and into a second polarizer (analyzer), which polarizes light in a perpendicular plane relative to the first polarizer. The anisotropic, organized components of the tissue split the polarized beam into two light wave components with orthogonal polarizations and different directions, depending on the relative orientations of the tissue optical axis, the direction of the incident light, and the incident plane of polarization. The second filter is the analyzer, with a plane of polarization independent from that of the polarizer. This second filter can be rotated through azimuthal angles between 0-80° in steps of 10°. Thus, the orientation of the fibres influences the transmission of plane-polarized light at different azimuths, so that a fraction of light can pass through a second filter – the analyzer – and be imaged. The series of polarization images under rotation of the filter combination can be used to quantitatively calculate the inclination angle of fibres in the depth of the section. Finally, a third filter

– the quarter wave plate – can selectively be introduced into the light beam and is used to unambiguously estimate the direction angle of fibres in the plane of a section (0-60° in steps of 20°), enabling the complete characterization of the polarization characteristics of the emerging light and, in particular, estimation of the direction of the optic axis of the tissue. Using Matlab software (MathWorks Inc., Natick, MA, USA), the different intensities are interpreted as specific angles of orientation of the tissue optic axis, colour-coded for visualization purposes.
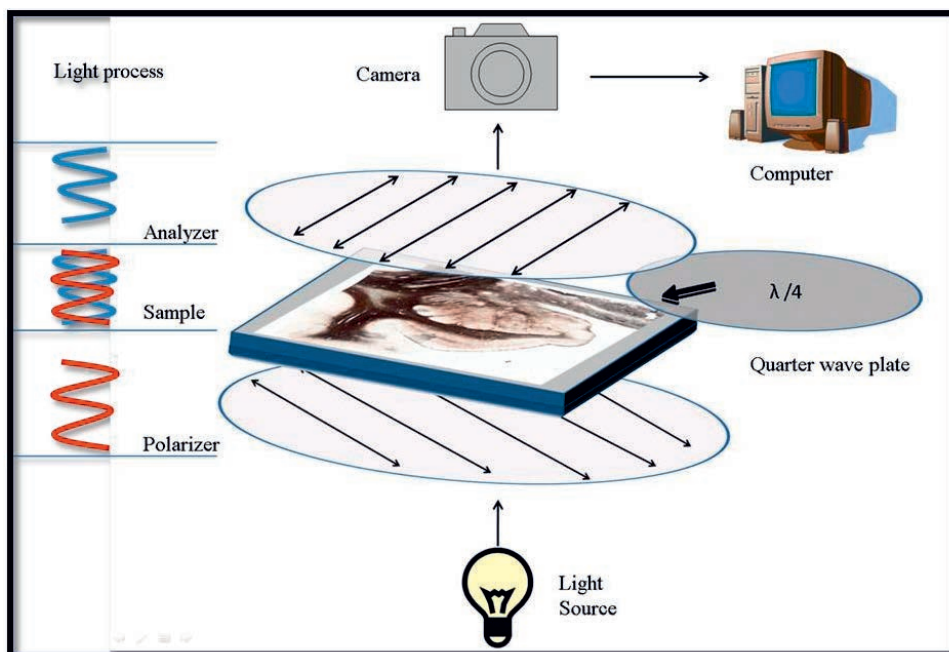
Figure 6.2. Polarized light equipment. The figure represents the different filters used for the optimal imaging of all azimuths.

Chapter 7

Experiment 3

Diffusion tensor imaging (DTI) with a non-myelinated fetal brain using ultra-high field strength (7 Tesla)

Diffusion tensor imaging technique is capable to distinguish groups within the grey matter amygdala region (see chepter 3). The FA values, in this regard, are often misunderstood as fibre integrity and myelin reduction indicators. A deeper look at water molecule motion in non myelinated brains might provide new keys to brain development knowledge but also to diffusion imaging techniques. In the 1930s, research made initial observations on the patterns of infant myelination (Brody, Kinney, Kloman, & Gilles, 1987; Langworthy, 1933). However, these studies were limited by poorly quantitative methods. Today's technology enables the characterization of developmental processes in the brain. The comprehension of inherent myelin and glial variation leads to an understanding of adult brain degeneration. Since the initial process of myelination occurs near the second trimester of fetal development, any imaging technique applied before or during this period becomes an interesting information source for histological data.

7.1 MRI data Acquisition

Fourteen postmortem fetal brains of gestational age of between 15 and 30 weeks, were donated to our institute for medical research. Brains were investigated by means of diffusion-weighted MRI (Turner et al. 1991) and T1-weighted structural scanning on a 7 Tesla Magnetom MRI system (Siemens, Erlangen, Germany) equipped with a 24 channel phased-array coil (Nova Medical Inc, Wilmington MA, USA). The study was in accordance with ethical approval from the University of Leipzig.

Diffusion-weighted images (DWI) were acquired with a Spin-echo echo-planar imaging sequence (SE-EPI) (TE = 72 ms, TR = 10 s) providing 67 diffusion-encoding gradient directions with a b-value of 1000 s/mm² (Reese et al. 2003; Weiskopf et al. 2007). The isotropic voxel resolution was (1

mm)³. Depending on the fetus gestational week (gw) the brain size varied and consequently so did the number of axial slices (from 20 to 45 slices) required to cover the entire brain. Total acquisition time was approximately 4 hours, resulting from a scan with 20 averages. A 5/8 partial Fourier imaging together with a parallel generalized autocalibrating partially parallel acquisition (GRAPPA, reduction factor = 4) was employed. A diffusion tensor and the fractional anisotropy (FA) were computed from the DWI data of each voxel.

For a more comprehensive analysis, 2 brains with different gestational development (16 gw, 19 gw) were scanned with slightly different parameters. Isotropic voxel resolution was reduced to (0.9 mm)³ (TE = 69-71 ms, TR = 3-4 s). Two different number of diffusion encoding directions were applied for replicability check: DTI (SE-EPI), with 256 diffusion-encoding gradient directions and DTI, with 201 encoding directions. The measurement of approximately 40 axial slices of 0.9 mm thickness (no gap) covered the entire brain. In addition to these diffusion modes, this study added a magnetization transfer preparation pulse (MTC) to the diffusion scan, according to some recently found changes on the diffusion-weighted when MTC was applied (Gupta, Rao, et al., 2005; Ronen, Moeller, Ugurbil, & Kim, 2006). Based on the literature, the MT technique, uses and off-resonance pulse to selectively excite water molecules and saturate macromolecules. The application of MT-DTI becomes then sensitive to the tissue selection due to the non-aqueus tissue components and the diffusion of water associated with macromolecules (Baumann & Pham-Dinh, 2001; Mulkern, Vajapeyam, Haker, & Maier, 2005; Ronen, et al., 2006).

Chapter 8

Experiment 4

Parcellation of human amygdala *in vivo* using ultra-high field MRI

Histological studies show that human amygdala is subdivided into nuclei with specific connections to other brain areas. One such study has been recently used as the basis of a probabilistic amygdala map, to enable *in vivo* identification of specifically located functions within the amygdala and connections to it (Solano-Castiella, et al., 2010). However, structural MRI scans of the human amygdala at field strengths ($\leq$ 3 T), show a region of generally featureless grey matter. The use of different MRI tissue contrast mechanisms at high field strengths has yet been little explored. The involvement of the amygdala in cognition, emotion and action, which may underlie several psychiatric disorders, points to a need for discrimination of these nuclei in living human brains. The goal of this study is the *in vivo* anatomical segmentation of the amygdala. The higher sensitivity available at 7 T, in combination with the information from different MRI contrasts, together with the powerful technique of spectral clustering, may allow the discrimination of amygdaloid subregions.

8.1 Data acquisition

Ten healthy volunteers (five male and five female) underwent MRI scanning. One subject was excluded due to poor image quality. All subjects were healthy, with ages between 21-29 years (mean age 25.2). None of the subjects had a history of neurological or psychiatric conditions. Written informed consent was obtained from all participants in accordance with ethics requirements from the University Hospital of Leipzig.

Subjects were scanned using a 7 Tesla Magnetom MRI system (Siemens, Erlangen, Germany) equipped with an 8-channel head-array RF coil (RAPID Biomedical, Rimpar, Germany). A whole brain data set was first acquired using a magnetization prepared rapid gradient echo (MP-RAGE) sequence, resulting in T1 contrast which allowed precise anatomical localization of the region of interest (TR=3000 ms, TE=2.95 ms, TI=1100 ms, voxel size: $(1.2 \text{ mm})^3$, flip angle=6°, iPAT=2). Additionally, 30 coronal slices (FOV 230x230 mm², matrix 192x192, thickness 1.2 mm, no gap) were acquired using a fully flow compensated spoiled gradient echo (GRE) resulting in T2* contrast

(TR=2000 ms, TE=20.2 ms, flip angle=70°) and a turbo spin echo (TSE) sequence resulting in T2 contrast (TR=9130 ms, TE=22 ms, flip angle=60°).

To determine replicability of the results, all acquisitions were repeated within session, and subjects were re-scanned one week later. Total acquisition time was 40 minutes for each session.

A final additional acquisition was performed for consistency check. A 24-channel phased array coil (Nova Medical Inc, Wilmington MA, USA) with an improved SNR was employed on five individuals from the same data set. The protocol used, followed the same sequence parameters previously described including a repetition within one session.

8.2 Definition of the region of interest (ROI)

Given the high degree of inter-subject variability, to define subcomponents of the amygdala properly requires an accurate delineation of the complete amygdala for every data set. However, the vagueness of the amygdala's boundaries with neighbouring brain areas hinders the work of automatic segmentation tools (e.g. Freesurfer). An amygdala mask was therefore manually created for each subject (Horínek, Varjassyová, & Hort, 2007; Morey, et al., 2009). Boundaries were defined based on the structural identification of anatomical features observed in human cadaver brains (Duvernoy, 1999). The use of known landmarks ensures the exclusion of extraneous tissue which would contaminate the results. In the coronal orientation, the limits from rostral to caudal were defined by the gyrus ambiens, lateral ventricle, entorhinal area, semilunar gyrus, anterior perforated substance and hippocampal formation. The sagittal boundaries were defined, from lateral to medial, by the peduncle of the lentiform nucleus, hippocampus, anterior commissure, temporal gyrus and optic tract. Lastly, boundaries in axial sections from ventral to dorsal were given by the edges of the hippocampus, parahippocampal gyrus, piriform lobe, entorhinal area, gyrus ambiens, temporal horn of lateral ventricle and semilunar gyrus (Fig. 8.1). Additionally, the comparison with an automatic segmentation tool (Freesurfer) shows the necessity of manual segmentation.
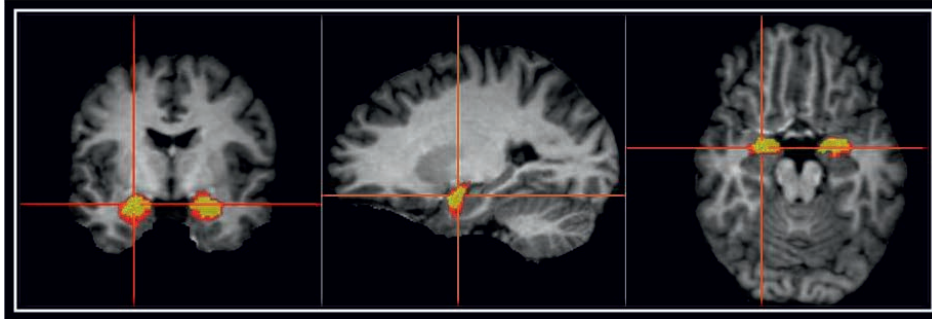
Figure 8.1. Manual segmentation of the amygdala. The segmentation provided by Freesurfer automatic tools is labelled on red and the manual segmentation is coloured on yellow. Freesurfer's automatic segmentation covers extraneous tissue.

8.3 Clustering methods

The data used for clustering were obtained using two types of MRI acquisition, TSE and GRE, each performed twice in two sessions a week apart. All images for each subject were linearly co-registered to the GRE image. In total, 8 data sets acquired with the 8-channel rapid coil (two repetitions on two weeks) were co-registered and 4 in case for the 24-channel coil (two repetitions on one session). Correlations of the intensities of voxels within the amygdala between acquisitions were computed.

The use of different contrasts provides additional information regarding amygdalar tissue properties. False colour images were computed in order to study the contribution of each particular contrast to a final combined image. For this reason, all three contrasts were initially included (T1, T2 and T2*) to study the principal contributions to the image (see Chapter 10, Fig. 10.4.1). After selecting the contrasts which had a high weighting to the image (GRE, TSE), a similarity matrix s was computed for each hemisphere in all data sets in which the components s_{ij} represented the similarity of vectors in voxels i and j. These vectors were defined in terms of image intensity and a normalized spectral clustering algorithm (Ng, Jordan, & Weiss, 2002) based on multivariate feature vectors (GRE, TSE) was then applied to the similarity matrices. This procedure was employed on the average data from all subjects but also, separately for each subject's data and for each hemisphere to allow the study of inter-subject variability.

To check for consistency of the resultant clusters, cross-validation techniques were employed. This reduces the possibilities of a randomized choice of the number of clusters found. In this case, a test-re-test correlation method was applied to the individual clustering results. Measurements were correlated within acquisition and between both sessions. Additionally, Cramer's V was used to assess the consistency of clustering. This tool is a widely used measure of nominal association based on chi-square which tests variables relationship. Then is normalized for table size (Cramer, 1946). This procedure provides an index of the strength of association between the results found. In this particular case, it evaluates the association of the resulting clusters from two acquisitions on one session and also across weeks. Cramer's V gives values within the range [0,1]. Values above 0.5 would indicate good consistency with a value of 1 indicating a perfect match. The consistency check for each subject's clusters k, was performed for $k =3, 4, 5$ clusters.

8.4 Inter-subject registration and averaging

In order to assess the stability of the results, images of the five subjects, scanned with the two different coils, were linearly co-registered to the image data from a single subject. Registration, averaging, and the consecutive clustering, were computed in two different ways: First, co-registration, clustering and create a probabilistic map from the resulting clusters and, secondly co-registration, averaging and clustering. Thereby, the study tests the variability and consistency of the clusters found across subjects.

First, every single subject data was linearly co-registered to the first GRE acquisition taken and individual masks were created. Next, an spectral clustering was applied to the similarity matrix containing both sequences. By counting the times a voxel appeared across subjects, a probabilistic map was created (see Chapter 10, Fig. 10.4.5). Secondly, all subject's sequences were linearly co-registered to an individual data set. A single mask adapted for all subjects was used. The co-registered TSE and GRE images from every subject were averaged separately and an spectral clustering was applied (see Chapter 10, Fig. 10.4.4). This process was applied to the data acquired with the two different coils.

Chapter 9
Experiment 5

fMRI of the human amygdala using ultra-high field MRI. Parcellation of emotional human non-linguistic sounds

In the course of this thesis, several *in vivo* probabilistic maps of the amygdala are presented. In order to optimally use these maps on a single fMRI study, the stimuli used aimed to arouse different parts of the amygdala. Although the literature relating the amygdala to emotions with negative valence is vast, a large number of studies have also linked this structure with a variety of positive emotions. Despite the complicated location of the amygdala and the standard voxel resolution commonly used, the literature has postulated a general indication of where positive and negative emotions occur within the amygdala *in vivo*. However, the precise location of each of these emotions within this structure has rarely been described. After a careful study of the experimental design and hardware improvement, together with the higher resolution acquired at 7 T, this experiments aims to locate different emotions with the assistance of the probabilistic maps generated on this thesis.

Stimuli selection

As previously mentioned, extensive literature has shown the role of the amygdaloid complex as a key component in the processing of different emotional states (J. LeDoux, 2003; J.E. LeDoux, 2000; Morris, Scott, & Dolan, 1999; Murray, Izquierdo, & Malkova, 2009; Robinson, 1963; K. Sander, Brechmann, & Scheich, 2003; Vollm, et al., 2006). Darwin (1872) postulated that emotional expression is related to natural selection in both humans and animals. The negative emotional dimension appears to have an instinctive, rapid reaction. Fear, for instance, induces an automatic animal-like response in the amygdala, with the consequent behavioural response (Mineka & Ohman, 2002; E. A. Phelps & LeDoux, 2005). An acute positive emotional state, however, seems to not evoke amygdaloid responses of the same dimension (Meyer, Baumann, Wildgruber, & Alter, 2007). Many studies have revealed strong amygdaloid implication in empathy, social awareness, reward and emotional face recognition (Anderson & Phelps, 2000; Breiter & Rosen, 1999; Fecteau, Belin, Joanette, & Armony, 2007; Martel, Nishi, & Shumyatsky, 2008; Olsson, Nearing, & Phelps, 2007; E. A. Phelps, 2006; D. Sander, et al., 2005; Simon, Craig, Miltner, & Rainville, 2006; Vollm, et al.,

2006; Vuilleumier, 2009; Williams, 2008). Considering this functional mixture, the approach decided upon was the use of non-verbal auditory human emotional stimuli. Non-verbal human sounds may elicit the personal and social involvement of a subject, thereby increasing the likelihood of a strong response to positive and negative emotional stimuli.

This study aimed to accurately localize different emotions within the amygdala *in vivo*. The combination of stimuli, field strength and data analysis result in a novel study. In order to facilitate the data interpretation, this project aimed to remain as simple as possible. In principle, the categories decided upon were based on Ekman's six basic emotions: Happiness, Sadness, Surprise, Anger, Fear and Disgust (Paul Ekman, 1992). However, this categorization consists of two positive and four negative valence emotions. In order to avoid an overall negative influence, just four stimuli types (two positive and two negative) were chosen. These were: happiness, surprise, sadness and disgust. Some studies have reported the amygdala to be reactive to both laughter and crying (Fecteau, et al., 2007; Klinge, Roder, & Buchel, 2010; K. Sander, et al., 2003; K. Sander & Scheich, 2005; Wild, Rodden, Grodd, & Ruch, 2003). The location of a crying sound in the amygdala is more lateral in both hemispheres, while laughter shows a trend towards centromedial areas of the right amygdala (Ball, et al., 2007; Fecteau, et al., 2007; K. Sander, et al., 2003). In addition, disgust was chosen due to the strong link between the amygdala and the olfactory system (Zald, Lee, Fluegel, & Pardo, 1998).

Design of fMRI condition

Detecting amygdala response to certain emotional sounds has been reported to pose a number of difficulties. In particular, how natural an emotion sounds and its intensity seems to be relevant. Some participants also demonstrate a gender preference when perceiving the emotion as contagious or real. The length of blocks has been reported to be crucial in the appreciation of amygdaloid activation. This could be due to the participation of the subject in the emotional context presented (Fecteau, et al., 2007; Meyer, et al., 2007; D. Sander, Grafman, & Zalla, 2003; K. Sander, et al., 2003).

Sounds were recorded from professional actors of both genders resulting in a total of 300 sounds. Fourteen volunteers were then asked to identify each sound and rate its naturalness and intensity.

Considering the highly rated the sounds on both conditions and the correct identification of these ones, we accumulated an amount of 30 sounds/condition (15 female and 15 male). These sounds from all conditions had an average rate above 66 % for intensity and 59 % for naturalness. The highest rated stimuli were selected for inclusion in the study.

Stimuli length and presentation blocks were adapted from the literature (Meyer, et al., 2007; K. Sander, et al., 2003). To avoid gender bias, both male and female emotional vocalizations were presented to the subjects. Commercial Presentation software (Neurobehavioral Systems, Inc.) was used to randomize the blocks and stimuli within the blocks. Since subjects' personal involvement in each emotional condition may assist in the intensification of the stimuli, participants were asked to actively evoke personal emotional situations related to the acoustic stimuli.

Each subject was presented 30-second-long conditions. Each of the four emotions was presented for male and female voices, and the condition of silence was also considered. Male and female blocks were separated. Stimuli of 3 s duration were presented in 30 s blocks to allow for the subject to respond. All conditions were repeated at least six times for each subject.

Data acquisition

Eleven healthy volunteers, with no known history of any neurological or pathological condition, were scanned using a 7 Tesla Magnetom MRI system (Siemens, Erlangen, Germany) equipped with a 24-channel phased array coil (Nova Medical Inc, Wilmington MA, USA). Written informed consent was obtained from all participants in accordance with ethics requirements from the University Hospital of Leipzig.

A whole brain data set was first acquired using a magnetization prepared rapid gradient echo (MP2-RAGE) sequence, resulting in a T1 contrast which allowed precise anatomical localization of the region of interest. The images obtained were used to place fMRI acquisition volume exactly on the amydala bilaterally. The resolution for this sequence was $(0.7 \text{ mm})^3$ isotropic (TR/TE= 4000/2.4 ms). This sequence allows the reduction of B1 inhomogeneities characteristic of higher field strengths

(Marques, et al., 2010; Van de Moortele, et al., 2005). In particular, images with two different inversion times are acquired and next divided, resulting in a flat image.

For functional imaging, an interleaved silent steady state (ISSS) sequence was used (Schwarzbauer, Davis, Rodd, & Johnsrude, 2006). In order to maintain subjects' comfort levels and ensure active participation, the acquisition was divided into 6 or 8 different runs of 4 and half minutes each. A protocol used, followed a standard GE-EPI (TR/TE = 2500 ms / 25 ms) (*see Chapter 2*). A partial Fourier transform of 6/8 was used with GRAPPA acceleration factor of 3. Forty-six coronal slices covered the amygdala region. The total scan time was about 45 min. The particular feature of this sequence is the interleaved silence periods (no gradient noise) together with the acquisition blocks. This way, the participant can listen to long blocks and experience clear acoustic timings. Despite the benefits of the ISSS sequence, an improved auditory system was also used for clear audition (http://www.sens.com). The system consists of specially designed non-magnetic earphones which are correctly shielded. This intensifies the audio and reduces the outside noise. Sander et al. (2003) have reported that low-noise fMRI is beneficial for obtaining the amygdala response. The conditions used consisted of the four emotional non-linguistic human acoustic stimuli described previously. The blocks used had a length of 30 s in which 20 s was used to collect 8 volume acquisitions and the remaining 10 s for clear stimulus presentation. Stimuli were also presented during the data acquisition period with the noise from EPI acquisition. The blocks used had a length of 30 s in which 20 s corresponds to 8 acquisitions and the remaining 10 s to 4 silent blocks. After acquisition, the silent volumes were excluded from the data, resulting in 432 real volumes/subject for the whole acquisition (Fig. 9.1).
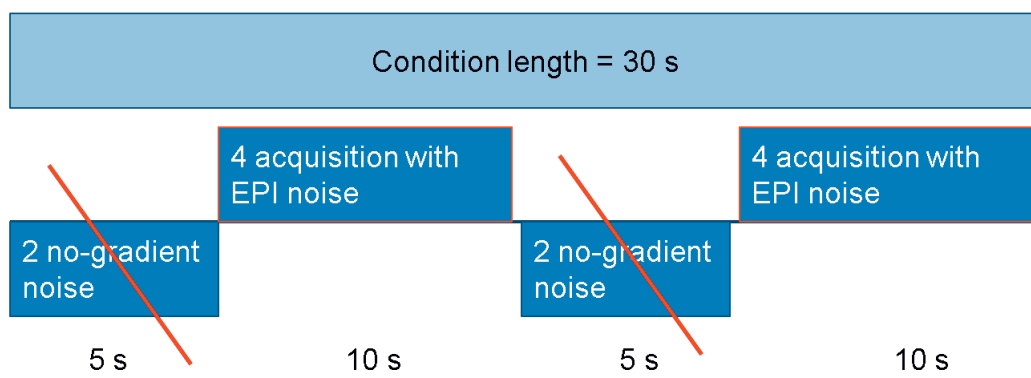
Figure 9.1. Representation of a condition block during ISSS image acquisition. In total, the block has 8 real volumes.

After scanning, participants were asked questions about their personal involvement in the emotions heard and the experiences evoked. They were also asked to rate the naturalness, intensity and contagiousness of the stimuli on a scale from 0-10, with 10 being a perfect emotional weight in a particular category.

Statistical analysis

Data analysis was performed in several steps. First, the silent periods were excluded and the different runs were concatenated in time using the fsl-merge tool from FSL software (Smith, et al., 2004; Woolrich, et al., 2009). The combined data was motion-corrected and the correction parameters were applied to the model. BOLD responses from each participant for the four categories were modelled using a general linear model (GLM) and a finite-impulse-response (FIR) basis function using feat – FSL software (Worsley, 2001). A spatial smoothing of 3 mm and highpass temporal filtering were applied. The *t*-statistics (transformed to *Z*-statistics) were threshold using clusters determined by $Z > 2.3$ and a cluster significance threshold of $p < 0.05$ (corrected for multiple comparisons). Statistical comparisons involved contrasts between different experimental conditions. This resulted in: laughter vs. crying, laughter vs. disgust, crying vs. surprise, crying vs. laughter, disgust vs. surprise, disgust vs. laughter, surprise vs. disgust, surprise vs. crying, laughter vs. surprise, and crying vs. disgust.

Finally, since data was individually checked, centroids from each subject responses to a particular condition were manually plotted to provide an overview of emotions distribution across the amygdala. Next, both probabilistic maps achieved in this thesis were 3D rendered using FSL (Smith, et al., 2004; Woolrich, et al., 2009). Each emotional category across all data sets was also 3D rendered in order to to systematically classify the position of the response associated with each amygdala probabilistic maps.

Data registration

Because of the high SNR at 7 T, the functional images therefore show great detail regarding activation specificity. The positions of small but significant responses are sensitive to spatial displacement when the data is smoothed or co-registered to a standard space. Since the aim of this

experiment is to precisely localize different emotions within the amygdala, care was taken to avoid any possible corruption of the data.

Initially, each subject's functional data was linearly registered to the individual MP2-RAGE (anatomical image) using statistical parametric mapping 8 software (SPM) (http://www.fil.ion.ucl.ac.uk/spm). Next, the *in vivo* probabilistic maps obtained from high field structural imaging and DTI were linearly co-registered to the individual brains using flirt – FSL software (Jenkinson, Bannister, Brady, & Smith, 2002). Both anatomical brains used to superimposed the maps were registered to the individual brains using an affine model with 12 degrees of freedom, correlation ratio as cost function and a tri-linear interpolation or to the nearest neighbour. Next, the transform matrices were applied to the probabilistic maps.

III

Results

Chapter 10

Experiment 1

Diffusion tensor imaging segments the human amygdala *in vivo*

10.1.1 Results

Diffusion anisotropy in a grey matter region

Figure 5.1 shows examples of the general appearance of the amygdala in MR images. Neither the T1-weighted image (A) nor the FA map (B) show definable internal structure, consistent with the relatively low myelin content of this area. However, when images were colour-coded for the main diffusion direction in each voxel, a high degree of organization into compact subregions was revealed (C, D). Groups of amygdalar voxels show characteristically different orientations of the diffusion tensors with relatively sharp boundaries (see Chapter 5, Fig. 5.1). The red colour component corresponds to medio-lateral orientation, green labels anterior-posterior, and blue a dorso-ventral dominance.
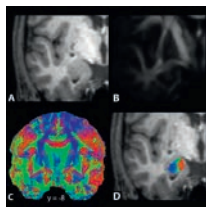
 (Chapter 5, Fig 5.1)

Myelin stained sections of the amygdala revealed relatively few fibre bundles, visible as darker features, within the regions generally accepted as the amygdaloid nuclei. However, at the boundaries (septa) of the nuclei a higher fibre concentration can sometimes be seen. The fibre directions within these septa vary across the amygdala, in accordance with the DTI data. Medially, a band of fibres extends in a roughly lateral-to-medial direction, separating the medial amygdaloid nuclei from the others. This is consistent with the more medial of the two DTI clusters found. More laterally, a nearly vertical band of fibres extends through the amygdala from its dorsal surface to the ventral

temporal lobe white matter, separating the lateral nuclei from the others, and possibly accounting for the dorso-ventral orientation found by DTI here (Fig. 10.1.1).
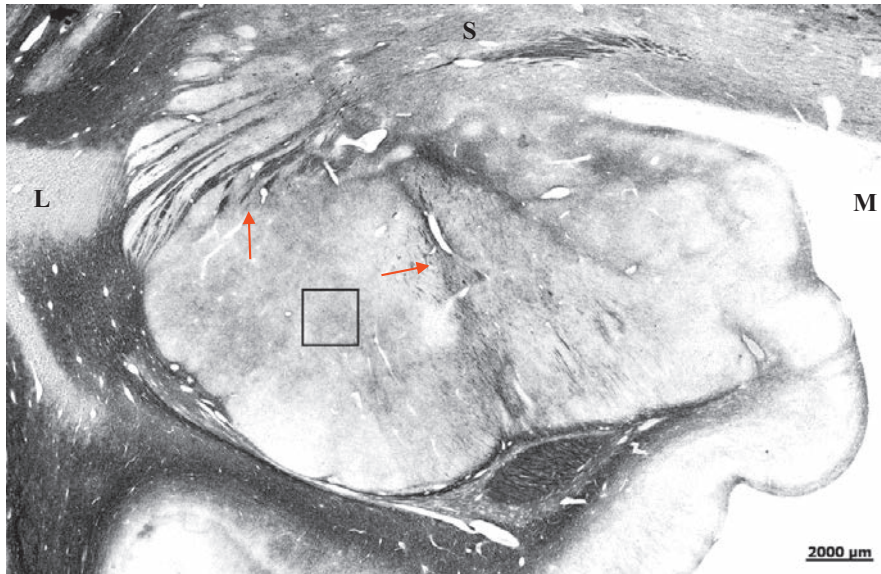
Figure 10.1.1. Myelin-stained coronal section (30 µm thick) of a human post-mortem brain. The medial, lateral and superior areas are indicated in the picture. This figure shows relatively low myelin content in the amygdaloid complex, with markedly higher fibre density at some boundaries (septa) between the nuclei. The fibre orientations shown in this section may underlie some features of the DTI data set (see arrows). In order to indicate the effect of partial voluming, the box represents the size (1.7 mm) of the MRI voxel.

Clusters found

The mean similarity matrix uses the orientation of the principal eigenvector for every voxel averaged across all 15 data sets after normalization. Using Fiedler vector analysis, this matrix is re-ordered by minimizing the angular differences between adjacent feature vectors. This formalism can provide information regarding the number of clusters that gives maximum reliability. Figure 10.1.2 reflects this re-ordering. Note that at least two clearly defined regions are visible along the diagonal of the re-ordered matrix. These areas represent a large number of voxels characterized by similar orientations.

A third cluster may possibly reside between the two major compartments but is not clearly distinguishable.

In the search for robust clusters, the spectral clustering was carefully tested. The most coherent and reproducible clustering result for both hemispheres was achieved by a subdivision into two groups of voxels. The left and the right amygdalae were subdivided into compact lateral and medial regions as revealed in Figure 10.1.3. The number of clusters was determined by the values of Cramer's V. For two clusters V had an average value of 0.73 ± 0.03, whereas for 3 clusters V was decreased to 0.58 ± 0.01. The inter-subject variability is included in this analysis.
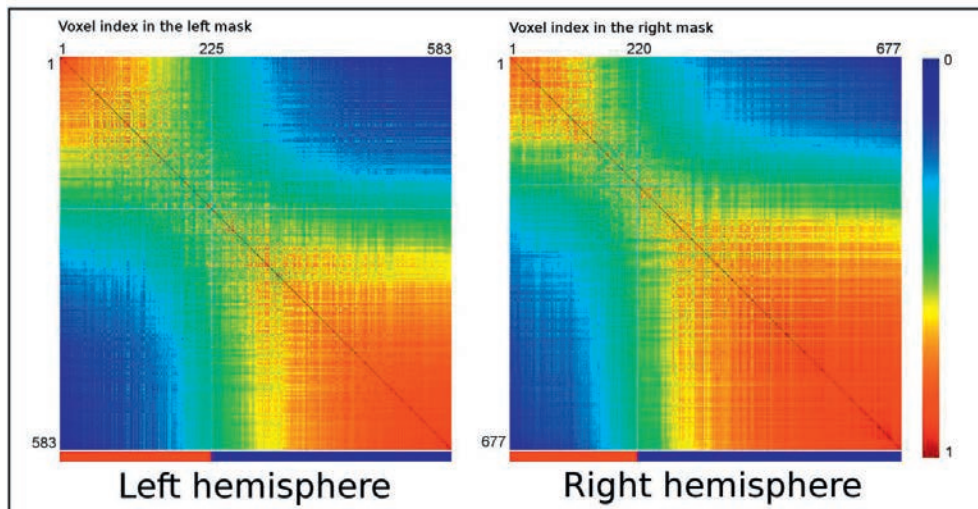
Figure 10.1.2. Averaged similarity matrix for diffusion orientation for each hemisphere. The matrix represents the similarity between all pairs of voxels within the amygdala (Left = 583 voxels, Right = 677 voxels). Each voxel is characterized with a main orientation. Spectral re-ordering minimizes the angular distances between feature vectors, providing regions categorized by a particular direction. A perfect orientation match is one. Parallel orientations are labelled in red while orthogonal directions are blue following the displayed colour map. Projection of the resulting matrices onto the images of each hemisphere reveals two main compact regions (top-left, bottom-right), although the matrices do not in themselves provide this spatial information. The resulting clusters are indicated by the coloured bar below the reordered matrices. The number of voxels corresponding to the smaller clusters are shown for each hemisphere (Left = 225, Right = 220). An additional transition area is present between the main compartments which suggest the possible existence of a third smaller group (cf. green region Chap.5 Fig. 5.1 d).
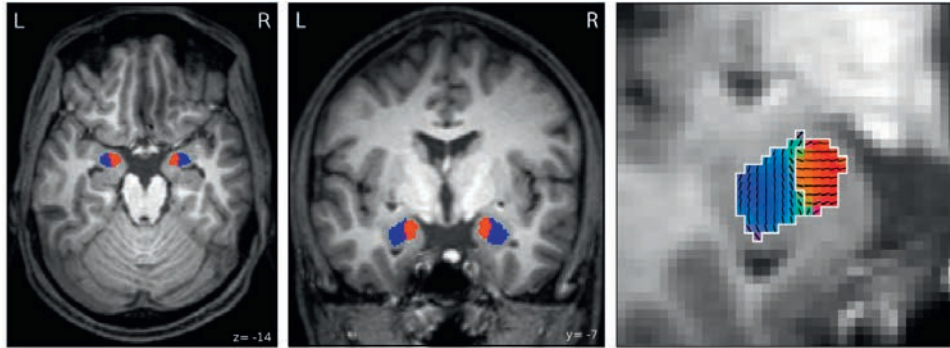
Figure 10.1.3. Result of spectral clustering using the averaged similarity matrix. The two main areas are superimposed on a single subject's T1-weighted image (left and middle). The amygdala segments are colour-coded. The medial region is labelled in red and the lateral region in blue. The right panel shows the enlarged left temporal lobe. The averaged diffusion directions are indicated by short lines and superimposed on the amygdala. The colour also represents the diffusion orientation. The white lines correspond to the boundaries computed by the clustering algorithm.

Probabilistic map of the amygdala based on directions of maximum diffusion

From the parcellation results of the individual subjects a probabilistic map was determined characterizing inter-subject variability. It was created by clustering the individual DTI data, followed by spatial normalization and averaging across subjects. The map is in good agreement with the clustering of the averaged DTI data (Fig. 10.1.4). We also computed the distribution of the centroids of each cluster across subjects. These centroids revealed a similarity of localization of the clusters (Fig. 10.1.5). In all subjects, the FA values found in the amygdala were much lower than in the white matter. The mean FA values and standard deviation for the lateral subdivision were 0.128 ± 0.024 and for the medial region 0.116 ± 0.024, with no remarkable differences between both hemispheres.
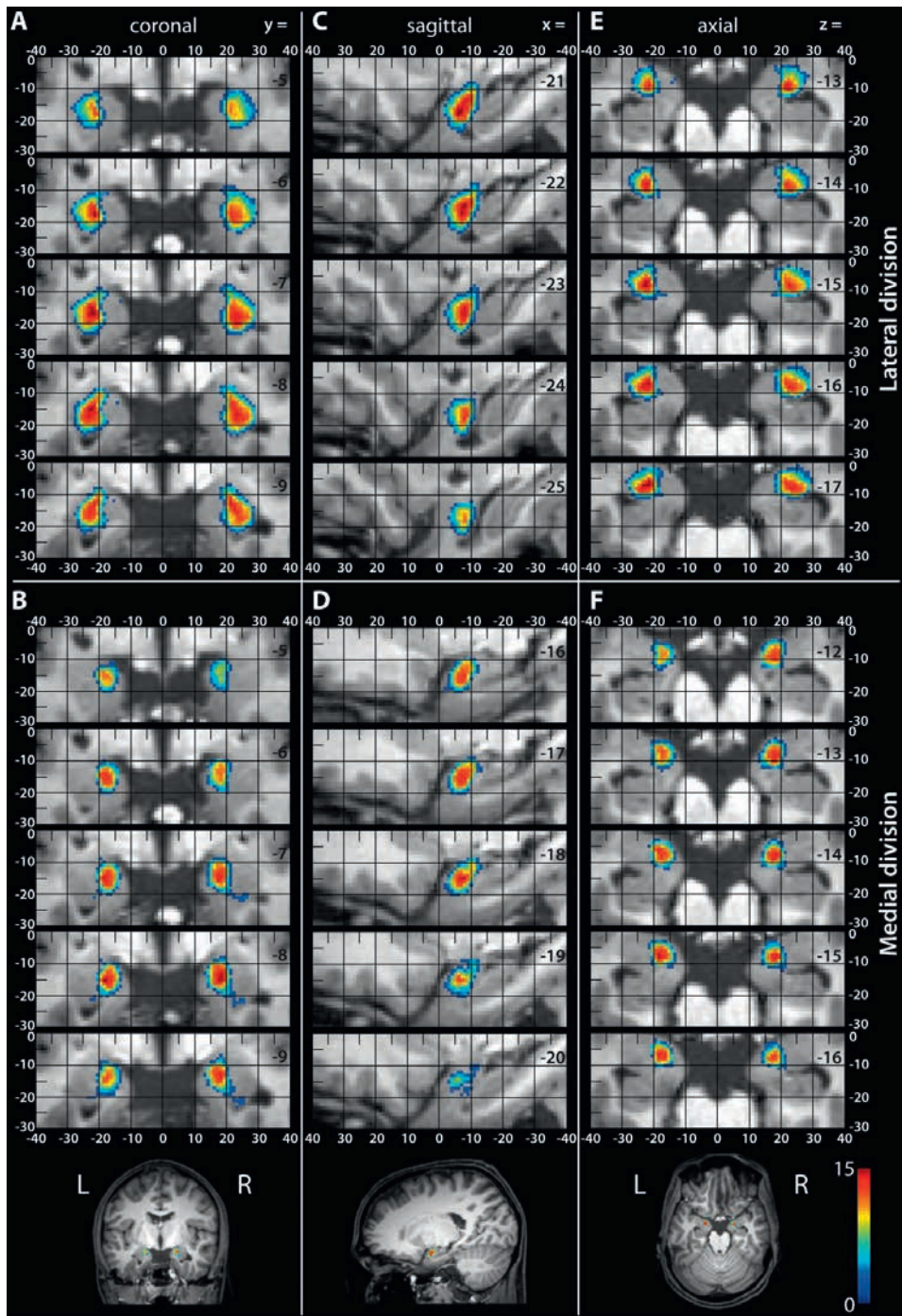
Figure 10.1.4. Probabilistic maps of amygdala data. The two amygdaloid subregions derived from individually clustered DTI maps (15 subjects) are superimposed on the structural T1 image of one subject. Left column, coronal sections; middle column, sagittal sections of the left amygdala; right column, axial sections. Maps of the lateral (a, c, e) and medial (b, d, f) cluster across several sections. Coordinates are in Talairach space. The overlap of the regions from all subjects is colour-coded using the indicated colour map with a minimum overlap of two subjects. An overlap of all 15 subjects is labelled in red. A volumetric reading (grid system) assist to a better localization.
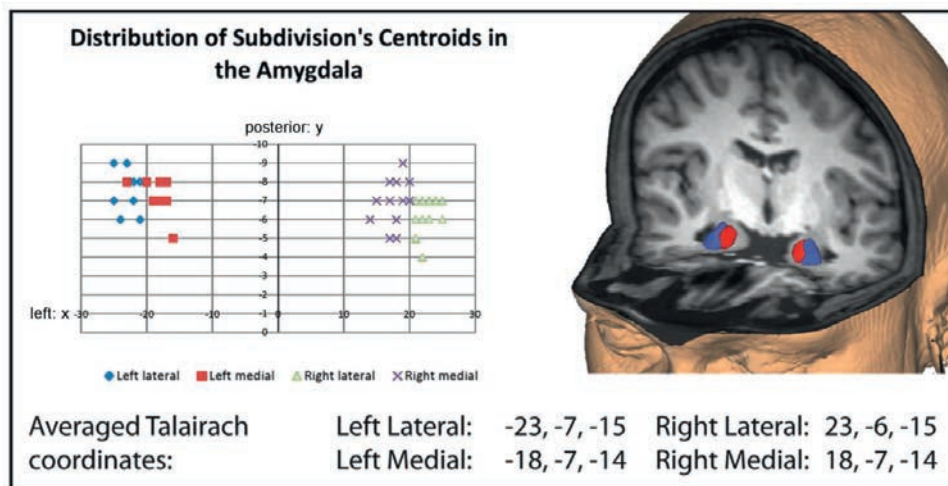
Figure 10.1.5. Centroid distribution. (Left) Location of the computed centroids of each subject's subregions. Left and right side of the chart indicate cerebral hemispheres. Vertical axis corresponds to the posterio-anterior axis. Coordinates are averaged and given in Talairach space. (Right) 3-D reconstruction of the probabilistic amygdaloid subregions superimposed on a single subject's T1-weighted image.

10.1.2 Discussion

This non-invasive method for subdividing the amygdala may allow structure and function to be directly correlated within the same living human subjects (cf. Johansen-Berg et al. 2005).

It is instructive to compare these maps with careful microscopic examination of sections through the amygdala of a human cadaver brain (Fig. 10.1.1). The bundles of myelinated fibres are not resolved in the lower resolution MR images, and a significant partial voluming effect is apparent. These bundles may contribute to the main orientations found using DTI. The spatial resolution of the DTI data does not allow discrimination of finer scale structures in the amygdala, but apparently it can distinguish the lateral group of nuclei from the medial nuclear complex.

The precise relationship of the clusters we have found with the known amygdaloid nuclei remains, however, a topic for further investigation. The main orientations appear to correspond to amygdalar connectivity pathways documented in animal brains. On the Figure 5.1 from Chapter 5 and the Figure 10.1.3 on this chapter, show the blue component labelling the dorso-ventral orientation. Experimental findings describe a well established connection between the lateral amygdala and somatosensory cortical areas (Shi and Cassell 1998; Pikkarainen and Pitkänen 2001; Grossman et al. 2008). The latero-medial direction is labelled in red. Tract tracing studies have reported that the medial part of the amygdala plays an essential role in intra-amygdaloid connections, as well as forming the main output source of the amygdaloid complex (Jolkkonen and Pitkänen 1998; Cassell et al. 1999; Fudge and Tucker 2009). The green-coded group of voxels has a generally anterior-posterior orientation. This region is relatively compact. Fiedler graph analysis reveals a transition area, which could perhaps also be considered as a subpart (de Olmos 2004). However, due to the inter-subject size variability and the lower coherence values given by Cramer's V, we are reluctant to include this as a separate subregion, and it will be the object of future investigation.

Fibrearchitectonic preparations (de Olmos 2004) reveal that the lateral and basolateral nuclei are characterized by numerous small fibre bundles running diagonally in a dorsolateral-to-ventromedial direction – a potential microanatomical substrate for the blue cluster found in the DTI data. In the medial nuclear complex (medial, anterior cortical, and ventral cortical nuclei) fibres have a tendency to run in a transverse direction – a possible correlate for the red cluster. The intermediate group of nuclei (central and basomedial nuclei) could be the microstructural substrate of the green cluster.

The probabilistic atlas provided by cytoarchitectonic studies has been increasingly used as a guide for *in vivo* studies of areas within the amygdala. Indeed, this methodology constitutes the first

classification tool for a better understanding of the amygdala. However, the resolution used at MR standard field strength ($\leq$ 3 Tesla) is generally no better than 3 mm isotropic for functional studies, and 1 mm isotropic for structural images. Given the fine detail of the amygdala just discussed, significant partial-volume effects are likely to appear from these cytoarchitectonic maps. This *in vivo* segmentation of the amygdala based on DTI data suffers less from interpolation. Thus, the study presented may assist identification of the amygdaloid subregions for MR images at standard field strength.

A general question arising from the study presented is how does diffusion anisotropy arises in a grey matter structure like the amygdala?. The diffusion coefficient of water in grey matter is about 2.5 times smaller than in pure water at body temperature, because tissue water diffusion is hindered by cell membranes, intracellular organelles, cytoskeletal structures, and the extracellular glycocalyx (Le Bihan et al. 1995; Le Bihan and Basser 1995). A non-isotropic arrangement consequently leads to anisotropic diffusion. Hence, myelin contributes to diffusion anisotropy, but it is not essential. For instance, diffusion anisotropy has been observed in non myelinated olfactory nerves (Beaulieu and Allen 1994a; Beaulieu and Allen 1994b). Thalamic fractional anisotropy (FA) values are approximately 0.3. Other factors clearly play a role, such as water restriction in the interstitial space between fibres (perpendicular to the axon), cell shape distributions, membrane permeability, and fibre organization (Hille 1971; Vasilescu et al. 1978; Szafer et al. 1995; Andrews et al. 2006). Furthermore, diffusion anisotropy has been shown in unmyelinated neonatal brain tissue (Wimberger et al. 1995).

The data presented here constitute the first MRI evidence for identification of internal structure within the amygdala *in vivo*, robustly partitioning this brain region. In this region there is not only tissue anisotropy, but also a characteristic orientation pattern. Use of this parcellation could form the basis of functional studies of amygdalar-directed structural networks *in vivo*. This methodology also opens a new way to study morphometry and volumetry of amygdala subdivisions in large groups of living human subjects.

Experiment 2

Polarized light imaging (PLI) of the human amygdala

10.2.1 Results

PLI is a DTI validation technique frequently applied to white matter tissue. This is due to the birefringent properties that myelinated fibres entail. However, for poorly myelinated grey matter tissue like the human amygdala, the simple finding of birefringent properties represented a noticeable result.

The PLI filters are carefully prepared for white matter requiring a particular adaptation regarding light post-processing for the grey matter tissue. After contrast enhancement and the consecutive informatics transformation into colour-coded azimuths, PLI confirmed the presence of anisotropy in the grey matter area of the amygdala. Furthermore, this optical technique showed directional groups in the 100 μm thick coronal sections comparable to a certain degree to those found with DTI at an isotropic resolution of (1.72 mm)³. Figure 10.2.1 illustrates a lateral to medial direction within the amygdala similar to the centro-medial cluster found with DTI (Fig. 10.2.1 b, lower right panel). These directions, as in DTI, are colour-coded where green indicates and anterior-posterior direction, dorso-ventral is labelled in blue and red shows the medio-lateral course.

Fiber inclination map (Z)

Fiber direction map (XY)
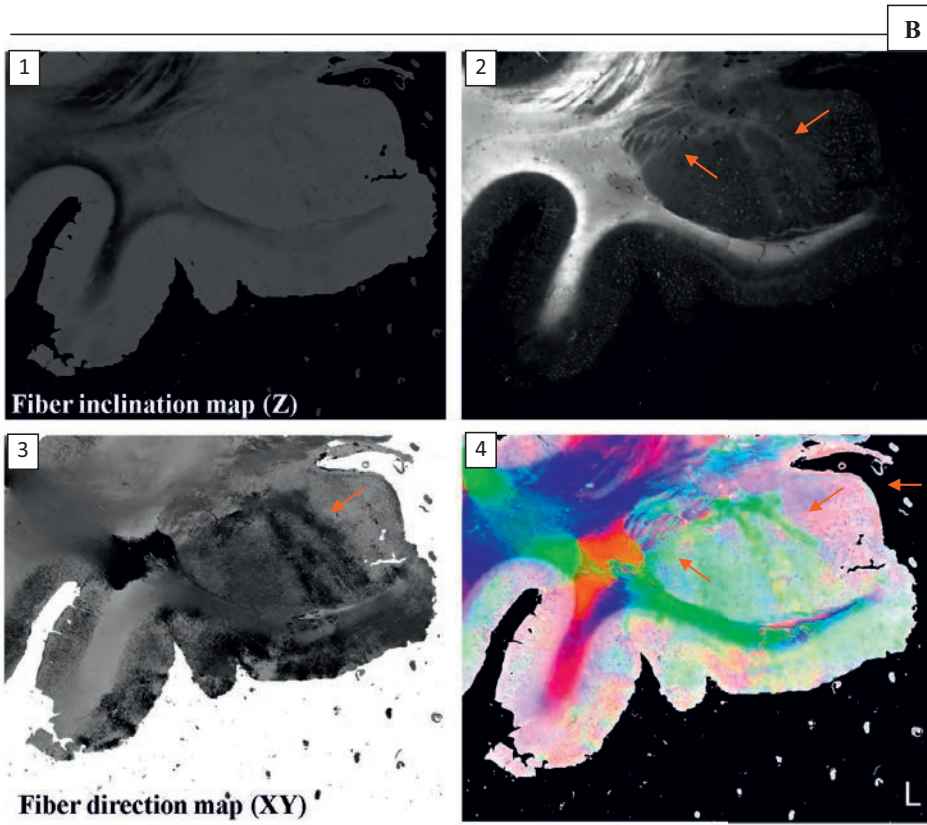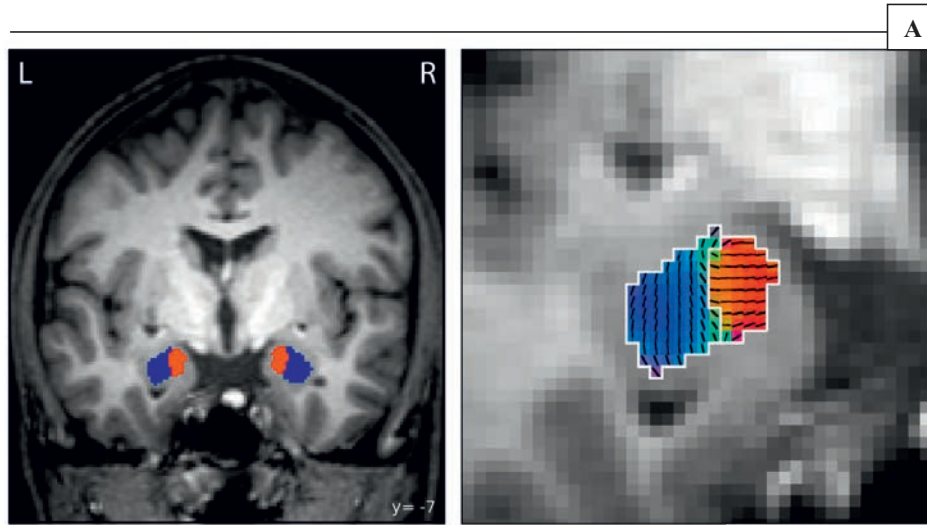
Figure 10.2.1. Polarized light imaging (PLI) confirms *in vivo* diffusion data (DTI). (a) Averaged *in vivo* diffusion data of 15 subjects, voxel resolution of (1.72 mm)³. Coronal sections. On the top left figure, the clusters found within the amygdala using DTI are illustrated. On the right side, the mask from both clusters to the main eigenvector raw data of 15 subjects' left amygdala is superimposed. (b) PLI of the left hemisphere, 100 µm slice thickness. Coronal section. (b.1) Fibre inclination map (z), (b.2) Maximum intensity map, (b.3) Fibre direction map (xy) (quarter wave plate), (b.4) Coloured fibre orientation map. The arrows indicate apparent myelinated fibres which suggest similar orientation and localization to those found in DTI.

10.2.2 Discussion

White matter has always been considered to be the suitable target tissue for both DTI and PLI techniques. In the presented thesis it could be shown, that a careful analysis of amygdaloid data acquired with both techniques reveals anisotropic features in this grey matter area. However, one has to mention that the PLI optical analysis is not sensitive to crossing fibres, Therefore, the application of techniques which are able to recognize crossing fibres could even improve the results of this study.

A simplistic macroevaluation of the amygdala through PLI, could also rely upon the possibility of an absence or a reduced amount of crossing fibres. This idea would stress the importance of components within the amygdaloid tissue, additional to the myelin, which would be capable to provide birefringence. Following this path, in order to check for any particular cell organization, the Nissl sections of the amygdala were also studied. A first closer inspection at these stained sections, have not revealed a particular preferred orientation of the cell bodies dyed (see Chapter 6, Fig. 6.1 b). However, the results obtained with PLI suggest that the amygdaloid tissue has certain features capable to bend polarized light.
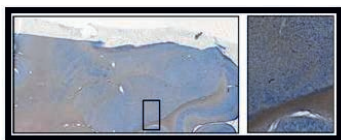
(Chapter 6, Fig. 6.1 b)

Additional, specific staining methods might be utilized for the investigation of the amygdala. For instance, RIP staining dyes particularly mature glial components components which could identify their influence on the obtained anisotropy (Friedman, Hockfield, Black, Woodruff, & Waxman, 1989).

Finally, since PLI, as an optical technique, has much higher spatial resolution than DTI, it may offer a means to validate claims based on MRI data regarding structural anisotropy within grey matter, as well as providing much richer information for white matter axonal orientation. However, this technique can only be applied *ex vivo*.

Experiment 3

Diffusion tensor imaging (DTI) with a non-myelinated fetal brain using ultra-high field strength (7 Tesla)

10.3.1 Results

In order to further investigate the diffusion properties of a poorly myelinated structure like the amygdala, this study applied DTI to the extreme case of non-myelinated fetal brain. When 7 Tesla diffusion-weighted MRI was applied, the DTI images showed clear anisotropy revealing marked cortical layers. These layers could already be depicted in an early gestational stage (15 gestational weeks (gw)) (Fig 10.3.1). Moreover, tractography enabled the reconstruction of apparent fibres at all different developmental stages (Fig 10.3.1).

Given the low FA values that this developing brain and the amygdaloid tissue present, both experiments revealed tissue differentiation based on its diffusion properties. This fact reinforces the argument that FA does not necessary indicate fibre integrity. Organized water diffusion can occur with a lack of myelin and the resulting low FA values (Fig. 10.3.1).
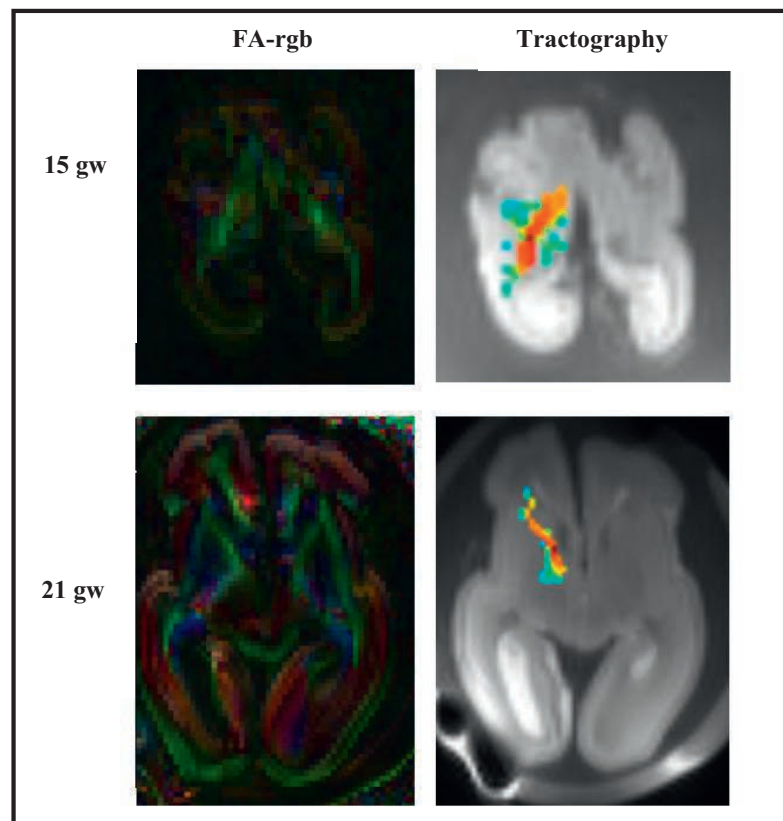
Figure 10.3.1. Fetal brain data at 15 gw and 21 gw. Axial orientation. (Left column) FA-rgb. FA is colour-coded, indicating the diffusion directions. The red component corresponds to medio-lateral orientation, green indicates anterior-posterior, and blue a dorso-ventral dominance. Both brains present differentiated cortical layers. The FA values within the region of interest for the 15 gw brain are 1.91 e^{-01}, and 2.30 e^{-01} for the 21 gw fetal brain. (Right column) Tractography.

In order to investigate the diffusion properties of this non-myelinated tissue, the following research applied a supplementary technique, magnetization transfer (MT). As already mentioned in Chapter 7, the MT preparation pulse makes DTI sensitive to free water diffusing in the vicinity of non-aqueous components. Since the amygdala has a reduced amount of myelin, other possible components could contribute to DTI hindering the movement of the water molecules. When MT-DTI is utilized in the developing brains, a general change in the diffusion (FA values) was shown.

These results confirm recent literature applying MT-DTI in other specimens (Avram, et al., 2010; Gupta, Rao, et al., 2005; Ronen, et al., 2006) as well as the presence of additional components acting as diffusion barriers within this tissue. Furthermore, when MT-DTI and only DTI are repeated in the same session, similar FA changes can be found (Table 10.3.1).

Anatomical Coordinates x, y, z	1st MT-DTI	2nd MT-DTI	1st DTI	2nd DTI
72,65,18	5.04e-02	4.34 e-02	3.93 e-02	2.81 e-02
87,93,21	8.09 e-02	7.25 e-02	6-47 e-02	6.51 e-02
73,88,29	1.85 e-01	2.99 e-01	2.43 e-01	2.66 e-01

Table 10.3.1. Three randomly selected locations on a fetal brain of 16 gw. Differences in the FA values were found in these three locations. MT-DTI was repeated in the same session as well as DTI. The use of MT-DTI in contrast to DTI reveals differences in the FA values.

10.3.2 Discussion

During the course of this thesis, the reduced amount of myelin within the amygdala complex has been constantly referred to the reduced amount of myelin within the amygdala complex. The complementary study of non-myelinated fetus brain allows a test of the usefulness of DTI in adult amygdala, where it appears to show robust. The results obtained in this experiment indicate that organized water diffusion can occur with a lack of myelin and the resulting low FA values as occurs with the amygdaloid tissue (Fig. 10.3.1). Myelination is typically associated with anisotropic diffusion in the brain, although the work published by Beaulieu et al. in (1994b) showed that this is not always required. This suggests the presence of additional components (besides myelin) that can behave as myelinated barriers for the water molecules.

Recalling some fetal literature, radial glial cells represent a key component for the development of the fetal brain (Noctor, Flint, Weissman, Dammerman, & Kriegstein, 2001) and could therefore become one of reasons explaining the anisotropy found in the developing brain. In addition, olygodendrocytes precursors (non proliferative) appear around the ninth gestation week in the ganglionic eminence spreading to the cortex in the next weeks. The DTI data of the 16-week-old shows anisotropy around this particular area which expands to the cortex perceptible in Figure 10.3.2. Late oligodendrocyte precursors appear around 15 weeks of gestation. Olygodentrocyte maturation appears with the expression of myelin basic protein (MBP+) when the first myelin sheaths are shown. This has been shown in an 18-gestation-week fetus in the thalamic region and three weeks later in the internal capsule (Filipovic, Jakovcevski, & Zecevic, 2003; Huang, et al., 2009; Huang, et al., 2006; Jakovcevski, et al., 2009; Jakovcevski, Mo, & Zecevic, 2007; Jakovcevski & Zecevic, 2005).
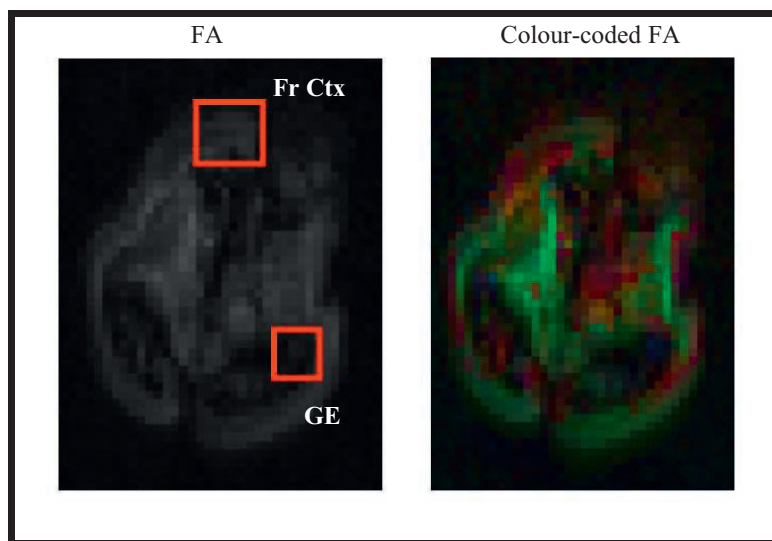
Figure 10.3.2. Diffusion data from fetal brain at 16 gestational weeks' development. The ganglionic eminence (GE) and the frontal cortex (Fr Ctx) are indicated with the box. Left image shows a non-zero fractional anisotropy (FA) where GE has an FA of 1.23 e^{-01} and Fr Ctx 1.60 e^{-01}. The figure on the right is the colour-coded FA showing clear organized orientations.

Hence, the fetal brain tissue contains a high number of radial glial cells (which can later become astrocytes) and oligodendrocytes precursors. These last, are later expressed on a myelin basic protein (MBP+). Therefore, an interesting result was obtained from the application of MT-DTI to non-myelinated brains. Although this technique still not-fully understood, the application of the MT preparation pulse revealed a considerable change in FA values. This confirms not only the large presence of glial components, but also its influence in DTI when there is an absence of myelin (Fig. 10.3.1 and Fig. 10.3.2). Indeed, the clear distinction of cortical layers has been recently attributed to the large presence of these glia cells (Huang, 2010).

These results seen in the context of the adult human amygdala raise questions about the existence of elements in the amygdala in addition to myelin (e.g. glia cells). This hypothesis could shed light on the robust anisotropy found within the amygdala when DTI was applied (see Chapter 10, Experiment 1). As a consequence, future research is encouraged to further investigate the presence of specific components within the amygdala tissue. One possible *in vivo* experiment would be the application of MT-DTI or, as it has recently been called, myelin water-weighted diffusion tensor imaging (MWW) (Avram, et al., 2010).

Experiment 4

Parcellation of human amygdala *in vivo* using ultra-high field MRI

10.4.1 Results

Contrast contribution to the clustering

Figure 10.4.1 shows a false-colour image based on the image intensities of all voxels within the amygdala. The weight of each sequence is represented by a different colour, where red corresponds to TSE data, green shows GRE data, and blue indicates the MP-RAGE data. This figure reveals a clear distribution of image intensities within amygdaloid tissue. The higher CNR found at 7 T allowed easier analysis of image intensity variation. Combining the image intensity maps given by each sequence, produced coherent subdivisions. While the clusters thus formed are not compact, they are reproducible across weeks. Two contrasts were finally chosen for clustering purposes based on the main weight shown: The TSE, or T2 MRI contrast, and the GRE, or T2* contrast.
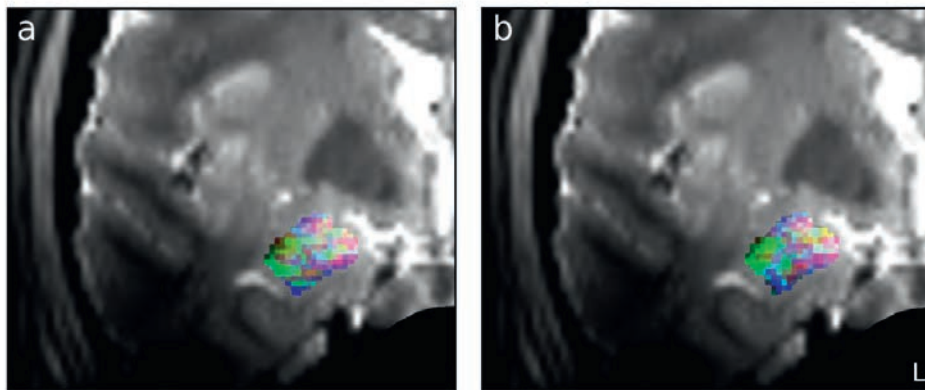
Figure 10.4.1. False colour images of the amygdala superimposed on a TSE image of one subject coronal section. Images are zoomed at the left temporal lobe. (a-b) Two different acquisitions on single session. The false colour image represents the weight of the contribution of the data from each sequence to the resultant contrast. TSE was assigned to the red colour channel, GRE to the green, and MP-RAGE was labelled in blue. Figures show tissue heterogeneity within the amygdala. The features variability similar in both images yields consistency between measurements.

Cross-validation techniques

The high correlation of image intensities (> 70%) across sequence repetitions and across different RF coils indicates a consistent distribution of intensity values in the amygdala area.

The data acquired with the Rapid coil was analyzed for ten different subjects and two different weeks. When Cramer's V was computed across repetitions and sessions, good consistency was found when three clusters were specified: ($k = 3$, V = 0.65).

In order to assess replicability of the results, the data scanned with the two different coils was compared. This likewise confirmed that specification of $k = 3$ gave the highest consistency. When Cramer's V was computed, the 8-channel Rapid coil for three specified clusters $k = 3$ gave V = 0.65 for the left hemisphere and V = 0.65 for the right hemisphere. When all subjects were registered to one individual's data acquired with the 24-channel Nova coil, V 0.66 ($k = 3$), for the left hemisphere, and V = 0.53 for the right hemisphere was obtained. Clustering the averaged data resulted in V = 0.57 ($k = 3$) for both, right and left hemisphere.

Because histological data reveals much more than three nuclei within the amygdala, a range of k values was explored for each subject. However, Cramer's V showed no further increase for k greater than 5, a result typical for automatic clustering tools which are applied in small areas.

.

Figure 10.4.2 further supports the initial clustering results. One subject's clusters are superimposed on the structural data. This image shows a T2-weighted coronal section of the left temporal lobe. As an illustration of the coherence of the given divisions, a scatter diagram shows the grouping of feature vectors using spectral clustering. The distribution of all voxels forming the amygdala is characterized by a particular intersection in a 2D scatter diagram. This consists of two contrasts

(TSE, GRE) and the image intensity given by these two sequences on a particular voxel. The resultant outcome consists of a logical grouping of the vectors into three different areas.

The cluster number most commonly found is consistent with the main grouping of amygdalar nuclei found in histological studies, although the cluster boundaries are not in full agreement. In regard to the spatial distribution of putative nuclei within the amygdala, all ten subjects revealed clear similarities (Fig 10.4.3). However, the positions of the boundaries found and the size of each subfield does not precisely agree closely with the histological data.
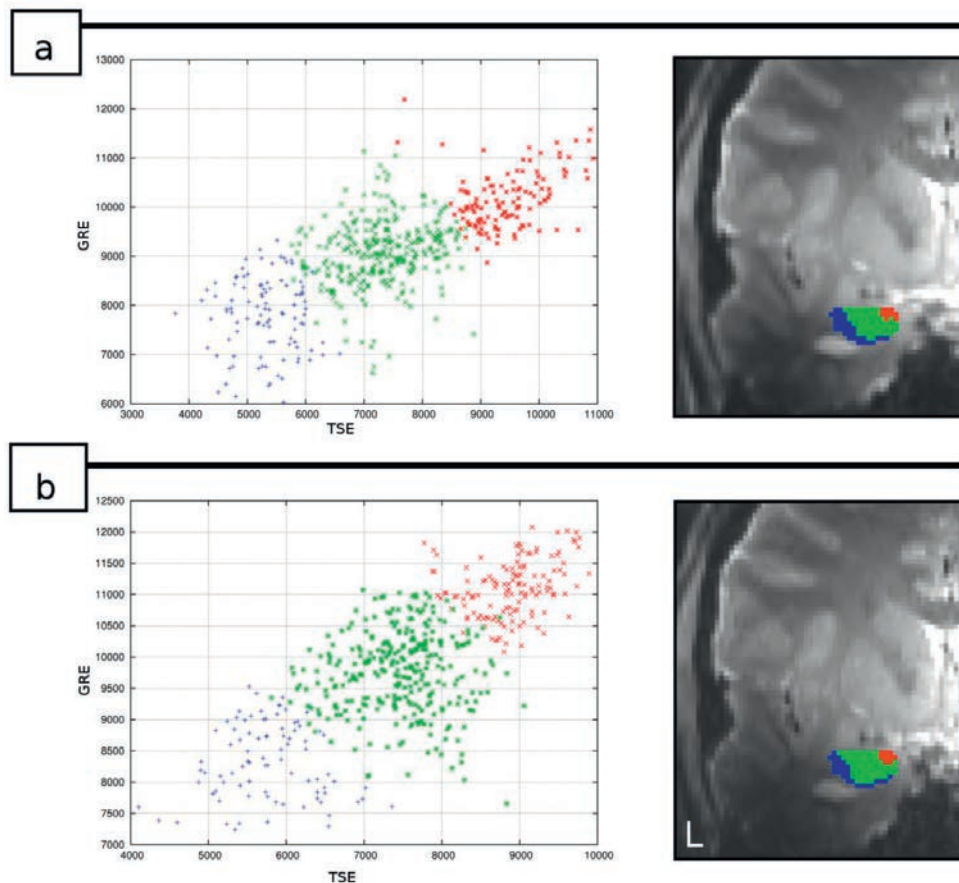
Figure 10.4.2. Amygdala spectral clustering based on two contrast's grey values (TSE, GRE). Coronal sections of an individual data set. (a-b) The left side of the figure presents a 2D scatter

diagram. This represents all voxels comprised in the amygdala in relation with all contrast's grey values scale and the spectral clustering applied. Clusters found are shown on the right side. The colours in this figure just differentiate the clusters found. The groups shown are based on both sequences. (a) Constitutes the clustering results from the first week acquisition. (b) Illustrates the second week clustering results from the same subject. Resultant clusters have correspondence across weeks.
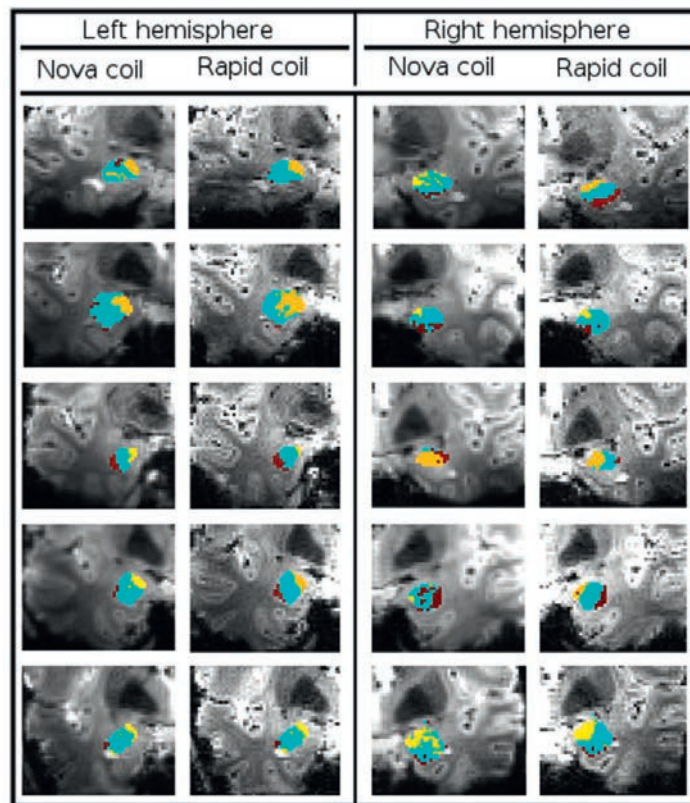
Figure 10.4.3. Inter-subject variability. Left and right hemisphere, coronal sections shown at the position giving maximal lateral extent of the amygdala. 24-channel coil and 8-channel coil. Arbitrary colour scale. Most of the subjects present a similar parcellation, although variability across subjects and coils.Inter-subject variability on the first week.

After averaging the data acquired with two different coils, the spatial distribution of the putative nuclei was consistent with previous results shown. This similarities, were found despite coil-specific

differences or inter-subject variability. One of the resulting segments coloured in blue, is located at the lateral and superficial regions of the amygdala. The axial sections reveal this nucleus to be situated towards the rostral sections of this structure. A second centro-medial cluster is labelled in red. Finally, a third cluster can be distinguished in green. This last segment, is located at the posterior-ventral regions of the amygdala. (Fig. 10.4.4). Finally, counting the times a particular voxel appeared across subjects, a probabilistic map was generated (Fig. 10.4.5).
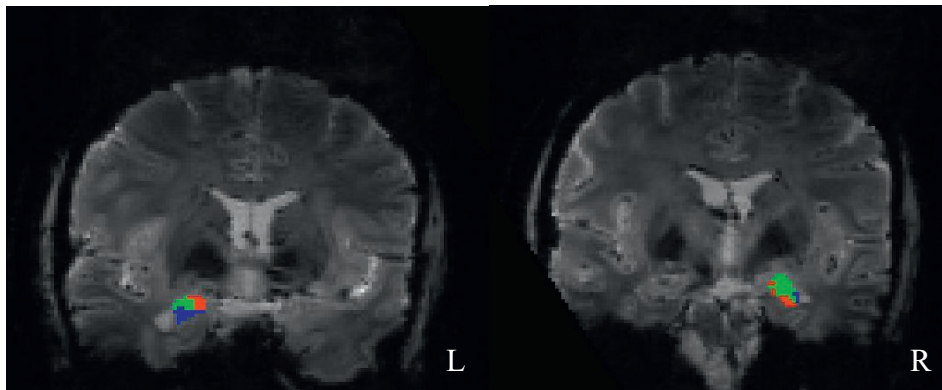
Figure 10.4.4. Spectral clustering of the averaged data. The data has been acquired with the 24-ch Nova coil. Both right and left hemispheres' clusters, have been acquired after averaging all subjects data. The resulting segments confirm the individual results (Fig. 10.4.3). The three nuclei found reveal spatial consistency across coils and subjects.
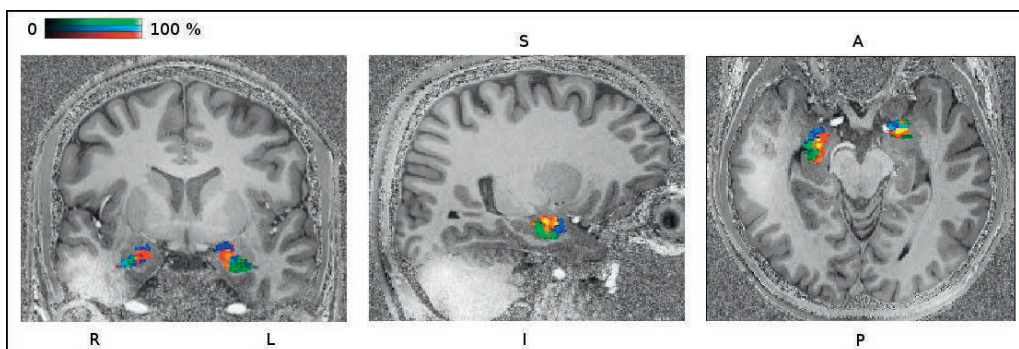
Figure 10.4.5. Probabilistic map. The data has been acquired with the 24-ch Nova coil. The probabilistic map from all subjects has been superimposed to a coronal (first image left), sagittal (middle) and axial (first image right) sections. Counting the times a particular voxel appeared across

subjects, a probabilistic map was generated. Three different clusters are shown here. Labelled in blue, a lateral-superficial region located towards the rostral sections of the amygdala (see axial section). A centro-medial cluster is coloured in red. Finally, an posterior-ventral group is labelled in green.

10.4.2 Discussion

Several studies have investigated the anatomical complexity of the amygdala. However, this studies have mainly focus on histological procedures. At standard MR field strength (≤ 3 T), MRI shows few internal details and it is unlikely that similar results could be obtained. Since the amygdala is not entirely devoid of myelin, we could show that MRI reveals features, given a high enough field strength and spatial resolution. The increased CNR available at 7 T has allowed this study to distinguish subfields which can be analyzed by the appropriate clustering methods.

In order to give adequate SNR, the relatively coarse resolution of $(1.2 \text{ mm})^3$ isotropic was employed for the data analyzed here. The present study initially used a $(0.6 \text{ mm})^3$ isotropic resolution, but due to inadequate SNR the clusters found showed poor consistency. Further work is needed to optimize voxel size in relation to RF coil sensitivity. After employing a 24-channel RF coil with equal resolution, this research assumes that the higher SNR provided by this coil predicts more reliable clusters than the 8-channel coil. Furthermore, the 8-channel coil, in particular, suffers from B1 inhomogneities. Thus, the slight differences in the subregions found when using the 24-channel coil are likely due to the better performance of this coil.

Histological studies of postmortem brain converge to a consensus number of three main clusters of nuclei, consistent with our findings (Amunts, et al., 2005; de Olmos, 2004). Our techniques identified three set of robustly distinguishable areas in the living human brain based on structural images. Finding three areas consistent across subjects and with the use of both coils provides additional support to our findings. A consistent relationship between the three sets of subregions can probably be established, perhaps using a series of cadaver brains which underwent high resolution

MRI scans and subsequent histological analysis. This study could also be applied to similar complex brain regions for instance regions as the nucleus accumbens, caudate nucleus or the substantia nigra.

While the presented results are promising, certain limitations should also be mentioned. Spectral clustering has been a reliable tool for cluster exploration. The amygdala is well known to have multiple subregions besides the three main ones. Even when higher field strenghts allow higher resolution, partial volume effect may cause small clusters to be missed. Furthermore, reproducibility is decreased when the number of clusters sought is too high.

Furthermore, the use of 7 Tesla MRI entails some limitations which need to be mentioned. The amygdala is located adjacent to the sinus sphenoidalis. Here, GRE images can show signal dropouts and distortions caused by susceptibility artifacts. On the other hand, TSE images can suffer from intensity and contrast non-uniformities due to significant variations of the RF field (Van de Moortele, et al., 2005). Combining both sequences may reduce these artifactual effects.

Since the relative position of the subject varies across sessions, B0 inhomogeneities may change. Regarding B1 inhomogeneities, the use of different coils does not lead to consistent image intensity differences. The use of two different coils reflects the variable SNR and artifacts characteristics of each. Increasing the number of channels leads to an increase of SNR. Additionally, the 24-channel coil suffers less from B1 inhomogeneities compared to the 8-channel coil. By applying both coils repeatedly, this study tested the stability of the results acquired. The good agreement of the clusters obtained supports our findings. In addition, spectral clustering uses a matrix formed from image intensities produced by both sequences. In consequence, the resulting clusters may be common to both contrasts. Where this is the case, the high correlation of image intensity will ensure robustness against the type of artifact described above.

Experiment 5

fMRI of the human amygdala using ultra-high field MRI. Parcellation of emotional human non-linguistic sounds

10.5.1 Behavioural results

When asked which stimuli were more contagious or real, seven out of eleven participants showed a preference for the stimuli performed by the opposite sex. Volunteers were asked to rate stimuli from 0 to 10, with 10 being a perfect emotional weight in a particular category. Ratings of naturalness, contagiousness and intensity of each category had an average of 6.8 ± 1.7 for the laughters, 6.09 ± 1.8 for crying, 5.45 ± 2.11 for surprise and 6.7 ± 1.5 for the emotional sound of disgust. The ratings for all categories combined yielded an average of 6.2 ± 0.2, which is consistent with the *a priori* ratings obtained from 14 volunteers when selecting these stimuli. All participants reported feeling comfortable with the length of the study.

10.5.2 Neuroimaging results

To the best of our knowledge, this experiment is the first to show a precise anatomical assignment of four different auditory non-human emotional vocal sounds (positive and negative) within different parts of the amygdala.

Functional responses revealed involvement of several brain regions while processing emotional human vocalizations. Specific parts of thalamic nuclei were active in several conditions. The fornix was particularly sensitive to sadness. Among the structures which respond to all emotional conditions we found the insula, the putamen, the superior temporal gyrus, the cingulate and central gyri, auditory cortex, globus pallidus and caudate nucleus. Also, the hippocampus showed strong activity with negative emotional conditions (disgust and sadness). Figure 10.5.1 shows these activations with a given threshold of $z>2.7$ and $p<0.05$ corrected for multiple comparisons. Although we found multiple reactions from different parts of the brain, this study mainly focuses on the reactivity of the amygdala to these stimuli and its anatomical specificity.

Previous studies have shown the lateral regions of the amygdala to be more reactive to negative emotional valence. Also, a trend for lateralization stronger in right than in left centromedial amygdala has been shown to be elicited by positive valence emotions (Ball, et al., 2009; Ball, et al., 2007; Fecteau, et al., 2007).

The current experiment has confirmed these standard localizations known from the literature (Fig. 10.5.1). However, our study also provides additional category-dependent locations using a threshold of $z>2.7$ and $p<0.05$ (corrected). The comparisons of emotional contrasts were not exclusive (e.g. crying vs. laughter + surprise + disgust) but inclusive (e.g. crying vs. laugh, crying vs. surprise and crying vs. disgust). This analysis allows one to see the overlap between categories, possible incongruities and common pathways for all positive (laughter and surprise) and all negative (crying and disgust) emotional valances.

Hence, when crying was compared to laughter, surprise, and disgust, bilateral activations were found in the lateral regions of the amygdala. An apparently lateralized active group in the right superficial amygdala was also revealed. Contrasting laughter with other conditions (laughter vs. cry, laughter vs. disgust and laughter vs. surprise) showed bilateral centromedial responses and an additional possible location in the right lateral area. A contrast of disgust (disgust vs. surprise, disgust vs. laughter) was mainly shown in the superficial medial regions of both amygdalae. Finally, a comparison of surprise with other categories (surprise vs. disgust and surprise vs. crying) mainly appeared in the left superficial medial amygdala areas. Some individual results can be seen in Figure 10.5.1. In a zoomed coronal picture of the amygdala region, the figure reveals several small category-dependent activations distributed in different parts of the right amygdala. In this particular case, it is possible to visualize activations related to crying (coloured in blue), laughter (in red), surprise (in magenta) and disgust (labelled in green). To visualize the centroids of all emotional activations, see Figure 10.5.2.
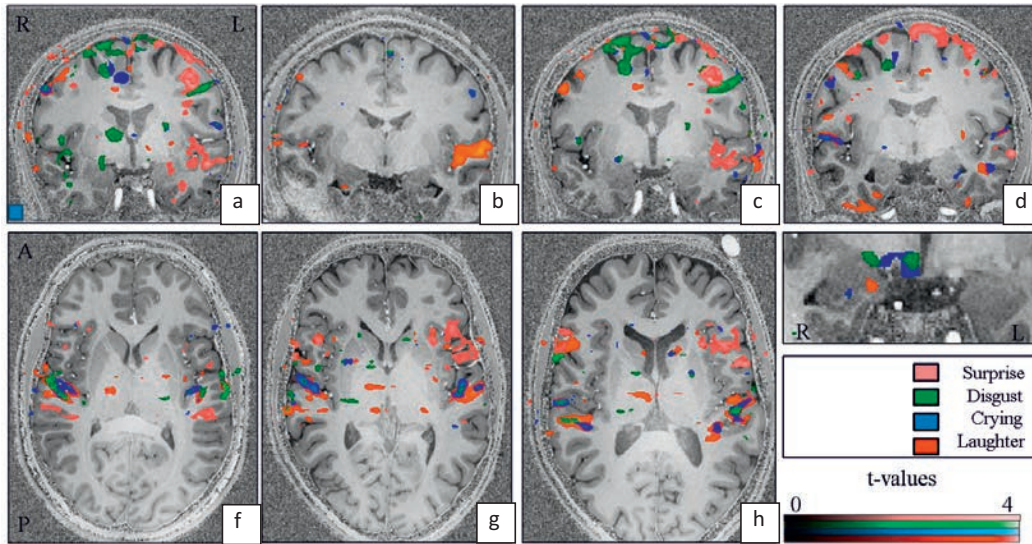
Figure 10.5.1. Functional responses to emotional human vocalisations across the brain and within the amygdala. Single subject's results. Top row, coronal sections. Bottom row, axial sections. First figure right, bottom row, zoomed picture of a coronal section showing the amygdala region. Emotional categories are colour-coded. Surprise (surprise vs. disgust and surprise vs. crying) is labelled in magenta, disgust (disgust vs. surprise, disgust vs. laughter) in green, crying (crying vs. laughter, crying vs. surprise and crying vs. disgust) in blue and laughter (laughter vs. crying, laughter vs. disgust and laughter vs. surprise) in red. Although the insula and superior temporal gyrus (STG) were reactive to all emotional conditions, Figure (a) shows an insular response to surprise and the STG active with disgust. Different parts of the thalamus responded to laughter and disgust and the fornix reacted to crying. The central and cingulate gyrus are active with all conditions. Most importantly, right superior region of the amygdala shows a response to disgust together with the globus pallidus internal segment. The left lateral superficial region of the amygdala presents a reaction to surprise. In (b), the superior temporal gyrus as well as the right basolateral amygdala respond to laughter. Figure (c) adds right superior amygdala activation elicited by crying and disgust. Figure (d) shows a STG bilateral response to crying and laughter and a left lateral amygdala reaction to crying. The axial figures (f, g, h) show a reaction to all emotions from the auditory cortex, putamen, caudate nucleus, thalamus and globus pallidus. Finally, the zoomed coronal figure of the amygdala region (first Figure right, bottom raw), reveals specific areas reacting to different emotions in the right amygdala: the medial part is active with laughter, the bottom lateral and the superior

region (together with the globus pallidus internal segment) reacts to crying and nearby, a small cluster reactive to disgust can be seen.

Since a group data analysis was avoided in order to protect the spatial distribution of small activations, individually following the spatial location of activations within the amygdalae, centroids of all subjects' responses to all categories (laughter, crying, surprise and disgust) were manually plotted on a 2D figure (Fig. 10.5.2). This allows to have an overview of the activations (category-dependent) across subjects. The centroids shown in Figure 10.5.2 show a bilaterally coherent grouping in different parts of the amygdala. As already mentioned above, the crying condition is bilaterally distributed towards the lateral regions and suggests and additional location in the superior areas of the right hemisphere. The laughing condition is grouped in different amygdala areas. Confirming previous results, there are several centroids perceived on the medial right area of the amygdala but also on the right lateral side of this structure and the left superficial region (Ball, et al., 2007; Fecteau, et al., 2007; K. Sander, et al., 2003). Interestingly, disgust and surprise were also consistently concentrated towards the superficial medial areas. Since the surprise category is not only compared to laughter but also to disgust, as well as laughter being compared not only to surprise but to crying and disgust, the left superior amygdala exposes an overlap between both positive conditions.
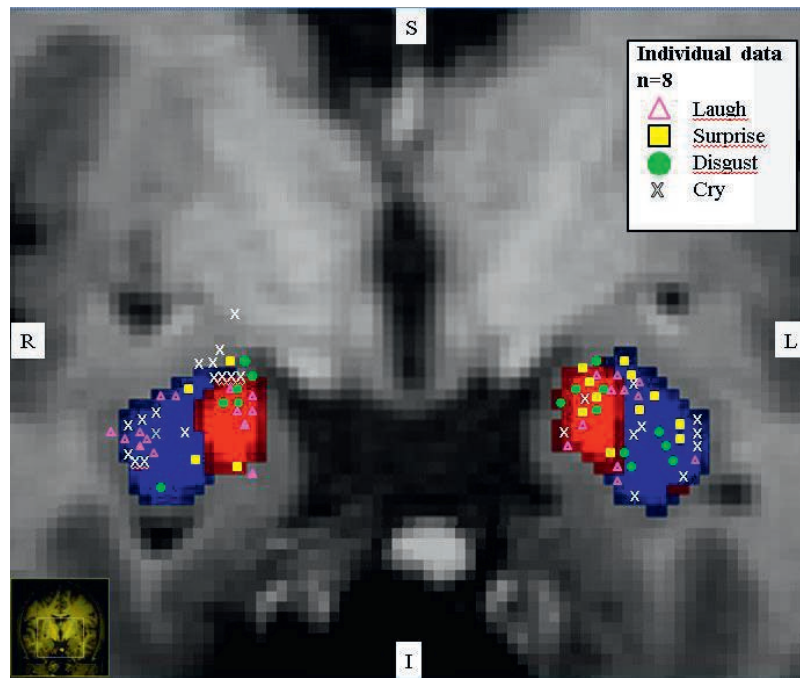
Figure 10.5.2. Centroid distribution of the functional data. Coronal section. The centre of the activations to the emotional categories across subjects reveal a coherent grouping in different parts of the amygdala. Laughter is labelled with magenta triangles, the white crosses represent the crying condition, surprise is labelled with yellow squares and the disgust is labelled with green circles.

In vivo probabilistic maps and emotion localization

Functional responses to different emotional categories could be located after registering DTI and structurally derived probabilistic maps to the individual data set. Figure 10.5.3 shows individual results for these maps and their relation to the different emotions.

The DTI probabilistic maps have two different segments, one medial and one lateral (see Chapter 10, Experiment 1). The structural maps have a certain agreement with the medial-superficial cluster and the lateral division, with an additional third segment located towards the anterior-lateral sections of the amygdala. This third cluster naturally rearranges the other two, contributing to the difference between both modalities (see Chapter 10, Experiment 4). For this reason, a certain agreement exists

with similar clusters but there are some differences in particular cases. This difference has the added benefit of providing an additional assessment to localize the emotional categories not easily discernable in the DTI maps. For instance, Figure 10.5.3 shows this cluster to be a better fit to individual functional responses to disgust and laugh.
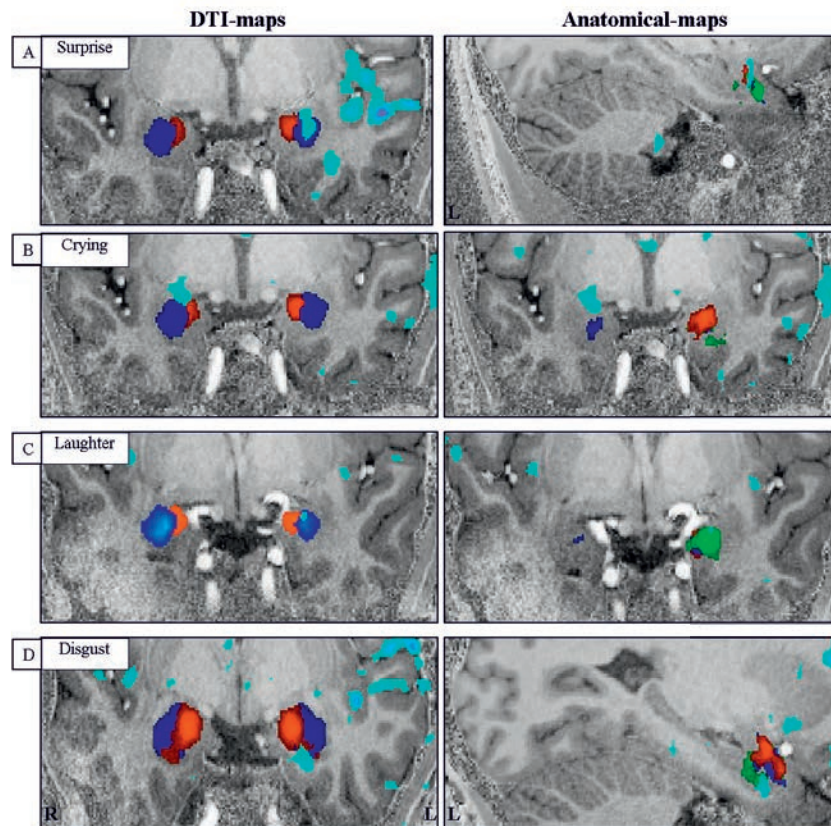
Figure 10.5.3. Probabilistic maps registered to the individual brains. Right column, structurally derived maps. Left column, DTI-derived maps. Coronal sections and sagittal (a right, d right). Individual results. Within the maps, medial clusters are labelled in red, lateral in blue and the third cluster from structural data is coloured green. In light blue, (a) surprise condition, (b) crying condition, (c) laughing condition and (d) disgust condition. In some cases, the functional responses match a cluster given by both maps (see also Fig. 10.5.5 and Fig. 10.5.6). (c,d) The anatomical

cluster labeled in green suggests a better fit to laughter and disgust. For the original probabilistic maps see Fig. 10.1.4 and Fig. 10.4.5.

Next, both probabilistic maps from different modalities were 3D rendered. Following all subjects' functional activation patterns, a 3D rendering of all functional responses (laughing, surprise, crying, disgust independently) was manually created. The threshold used to visualize these functional patterns was $z>2.7$ and $p<0.05$ (corrected). This enables the systematic classification of emotional distribution within the amygdala. Fig. 10.5.4, presents both probabilistic maps achieved registered to MNI space for a direct comparison.

First, the DTI clusters presented in Figure 10.5.5 (medial labelled in red and lateral in blue), reveals a correlation of the functional categories with the probabilistic maps (threshold 70 %). As previously seen, the laughter condition (coloured in red) shows a clear bilateral activation in the medial segments and an additional activation in the right lateral group. 3D blue activation that represents the crying condition is mainly located in the lateral maps together with a small group towards the medial superficial region of the right amygdala, which corresponds to the medial segment. However, surprise (labelled in yellow) and disgust (coloured in green) do not show an entirely clear location within these segments. The surprise condition reveals a trend towards the lateral segment while disgust is located towards the medial cluster.

Next, the anatomical probabilistic maps were also 3D rendered (70 % threshold). The beneficial distribution of the anatomically derived segments assisted with the better identification of some emotional conditions. While laughter and crying remained constant with the DTI probabilistic maps (superficial segment and lateral segment, respectively), surprise (labelled in yellow) fitted better to the centromedial segment (labelled in yellow). Furthermore, activation related to disgust, which was not easy to visualize in the DTI maps, is now presented in a clear bilateral location in the superficial anatomical-derived maps and a left laterally positioned group (Fig. 10.5.6).
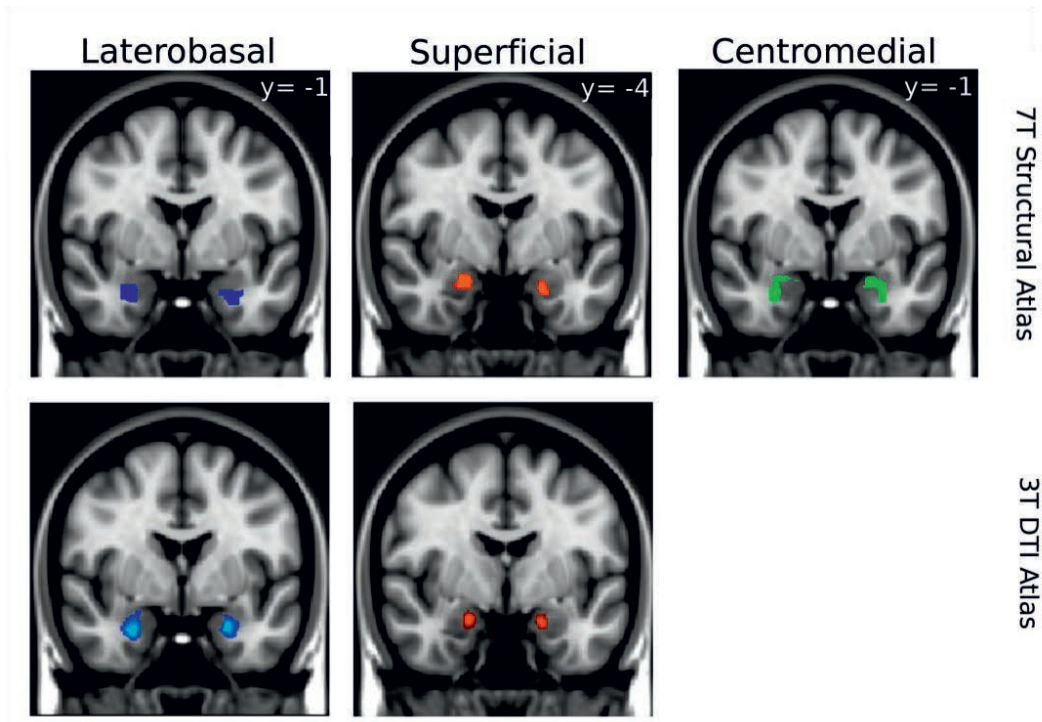
Figure 10.5.4. Probabilistic parcellations of the amygdala. First row, in vivo 7 Tesla structurally derived maps. Bottom row, in vivo 3 Tesla DTI derived maps. All probabilistic maps are in MNI space. The laterobasal and superficial nuclei of both probabilistic maps show similar spatial locations.
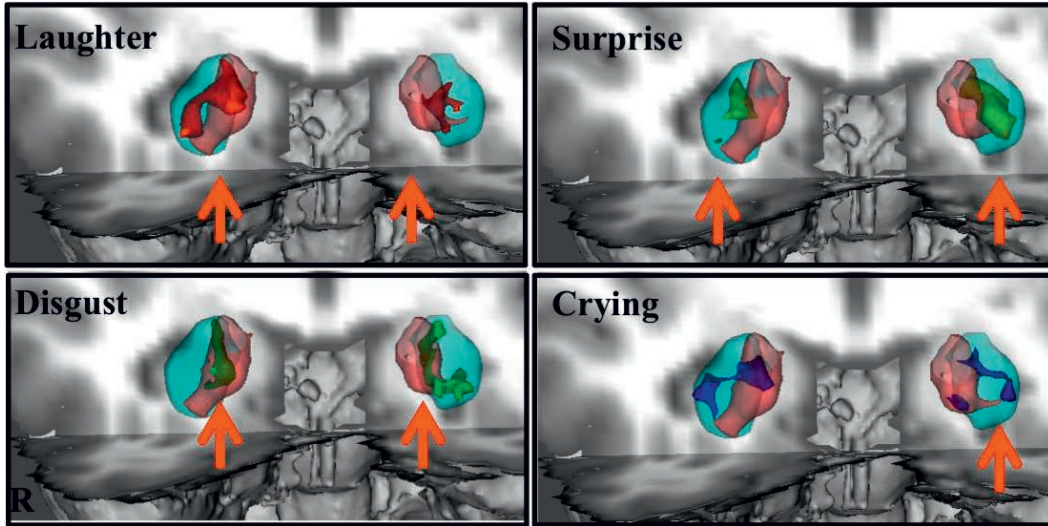
Figure 10.5.5. 3D rendering of the DTI-derived probabilistic maps. Coronal sections. The medial cluster is labelled in red and the lateral cluster is coloured in blue. Laughing condition is labelled in red, surprise in yellow, disgust in green and crying in blue,. The functional activity related to different emotions is shown in these maps for a direct correlation between function and its anatomical substrate. For original DTI-derived clusters see Fig. 10.1.4. or Fig. 10.5.4.
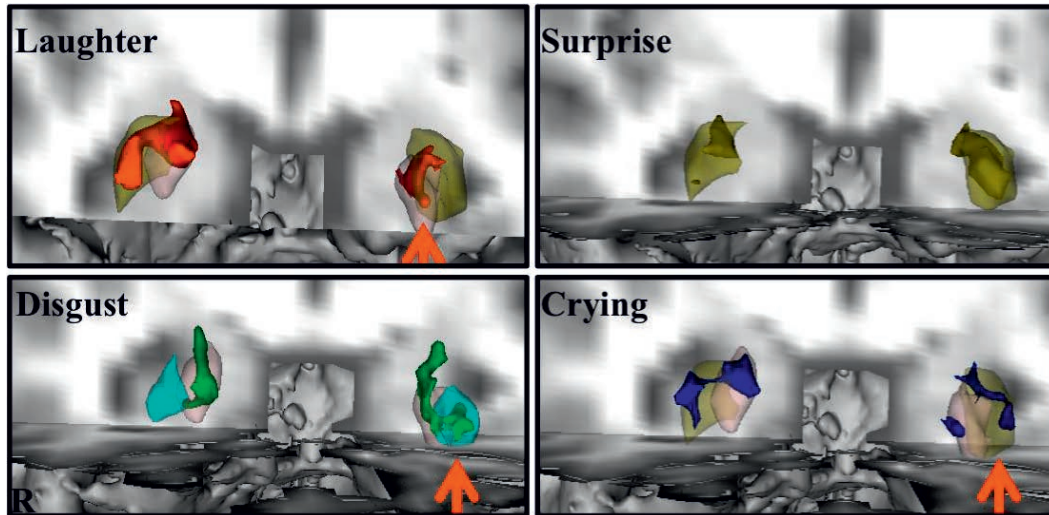
Figure 10.5.6. 3D rendering of the structurally derived probabilistic maps. Coronal sections. The lateral cluster is labelled in blue, the superficial segment in red and the centromedial division is coloured in yellow. Laughing condition is labelled in red, surprise in yellow, disgust in green and crying in blue. Top row, the distribution of the clusters assists the functional distinction in the left hemisphere for the laughing condition and bilaterally for the surprise category. Bottom row, the disgust condition shows a clear bilateral localization towards the most medial segment (or superficial subdivision). Also, the left hemisphere shows a certain tendency towards the most lateral segment. For the crying category both centromedial and superficial segments cluster bilaterally the functional activity. For original structural-derived clusters see Fig.10.4.5. or Fig. 10.5.4.

.

Due to the way the fMRI data was analysed (e.g. crying vs. laughter, crying vs. surprise and crying vs. disgust), an overlap between emotions could be detected. This enabled the study of common regions for positive (happiness and surprise) and negative emotions (sadness and disgust). Interestingly, both the positive valence stimuli (surprise and happiness) had overlapping clusters bilaterally at the centromedial segment of the structural probabilistic maps. Furthermore, the cluster revealing a negative emotional valence (sadness and disgust common pathway) could be identified in the most medial segment (or superficial) of the structural probabilistic maps. These positive and negative pathways represent an interesting finding due to the unexpected clusters to which they are related (Fig. 10.5.7).
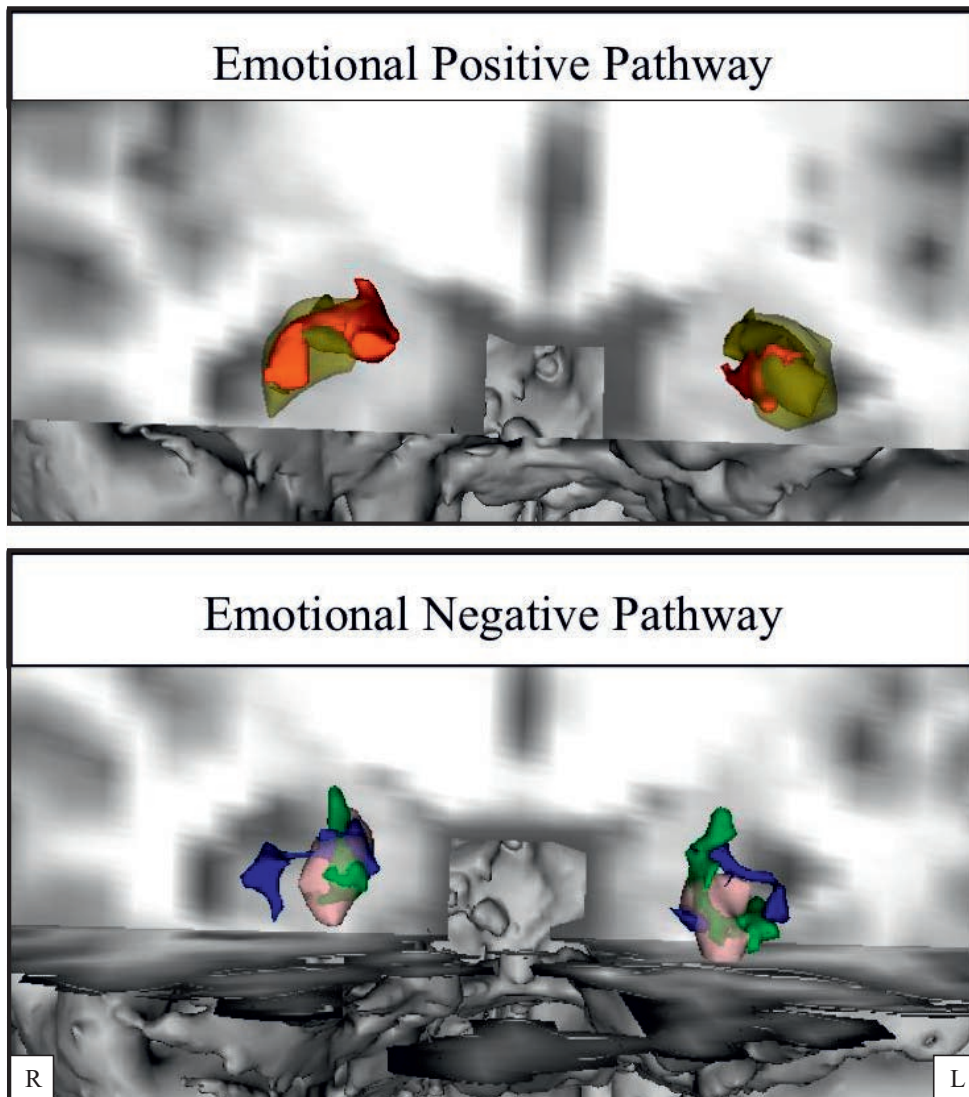
Figure 10.5.7. Common areas for positive and negative emotions. Coronal sections. Top row, positive valence pathway. The laughter condition is labelled in red and the surprise category in yellow. The centromedial segment of the structural-derived probabilistic map (yellow cluster) suggests a common location of the positive emotions. Bottom row, negative valence pathway. The crying condition is labelled in blue, and the disgust category in green. The superficial segment from

the anatomical-derived map (red cluster) clusters around the common region of these two negative emotions.

10.5.3 Discussion

The aim of the present study was to assess anatomical specificity of different types of emotions within the amygdala. The findings of the experiment conducted indicate different regions of the amygdala are directly related to auditory positive and negative emotional vocal sounds. Additionally, the probabilistic maps achieved in the current thesis assigned high anatomical specificity to different conditions.

In order to visualize a general tendency of where some emotional responses occur, the DTI maps provided a useful overview to this question. When one category was not clearly identified with these maps, the structural maps assisted in confirming the anatomical substrate underlying a particular emotional category.

Furthermore, the common pathways of all positive as well as all negative emotions were also assigned a particular cluster given. Surprisingly, the common pathways between the laughing and surprise conditions had a better fit in the most lateral segment (centromedial subdivision) provided by the structurally derived maps and the common regions for crying and disgust were better clustered at the most medial segments (superficial subdivision) of the amygdala. These novel results do not entirely follow the general common standards of the location of positive and negative valence emotions. We think this could be due to the use of higher resolution and the experimental design. However, this study present preliminary results which need further investigation.

Anatomical specificity is crucial for the successful functional imaging of the amygdala. Although the interpolation of post-mortem-based probabilistic maps has successfully assisted in the functional location within the amygdala, some limits have been shown due to vague borders with neighbouring

regions (Ball, et al., 2009). The actual *in vivo* probabilistic maps created here are most likely to be a useful tool to assist in this issue.

Future work will consider the application of a small volume correction, which could increase the significance of the activations found, perhaps revealing their better identification. Additionally, masking out the individual amygdala could assist in the co-registration across subjects, conserving the spatial localization of the small activations found. Further analysis of the data, such as the study of the time series, may provide useful information regarding emotion-related reaction times of the amydala.

In summary, one of the key components that this experiment enhances is the successful integration of some of the *in vivo* methods used in the course of this thesis, together with the probabilistic maps also achieved *in vivo*. To our knowledge, this is the first time that the aim of this study relating functional emotional diversity to its anatomical substrate within the amygdala *in vivo* has been successfully achieved.

IV

Final Conclusions

Final conclusions

The optimum approach leading towards a deep understanding of the limbic system and, consequently, the emotional system, is based on the *in vivo* segmentation and parcellation of their components. This may finally lead to an accurate functional correlation with the specific anatomical substrate. Therefore, the goal of the experiments conducted in the present thesis has been to explore the amygdala complex and its components through different MR perspectives *in vivo*.

Despite certain challenges due to the properties of the amygdaloid tissue and the intrinsic MR limits, the parcellation of the human amygdala was successfully achieved *in vivo* for the first time. Subsequent *ex vivo* studies confirmed these findings.

It is important to stress that the widely used mask that was acquired in cytoarchitectonic studies, represents a big step forward in nuclei localization within the amygdala. However, it is equally important to consider the limitations of this approach. Additionally, a perfect correlation between function and structure is only possible if both are determined in the same subject *in vivo*.

A first main result of the thesis was that techniques which have found their most popular applications in white matter brain regions have provided striking results in the human amygdala. Firstly, diffusion tensor imaging has not only shown prominent anisotropy in this grey matter area but also these diffusion groups were robustly clustered in amygdala subregions. The probabilistic maps resulting from this data constitute a step towards the *in vivo* study of the subregions of the amygdala, and its specific tissue characteristics.

Secondly, in cadaver brain samples, polarized light imaging confirmed the presence of anisotropy in the grey area of the amygdala, and showed directional groups comparable to those found with DTI *in vivo*. This optical technique then constitutes a good validation of MR diffusion results, even for grey matter.

The complementary microscopical investigation of the amygdaloid cell bodies, unfortunately, did not show any particular pattern related to the DTI or PLI data. However, staining glial cells via RIP staining could be a solution to this problem.

Employing dedicated techniques, a fourth experiment was performed to determine whether DTI contrast is possible in a structure with little to no myelin. The use of MT-DTI at the non-myelinated fetal brain and the consequent diffusion changes confirms the presence of a large amount of glial cells in fetal tissue. The literature has also confirmed these findings *ex vivo*. These glial components could be one of the reasons by which we find water diffusion restrictions in the amygdala grey matter.

Besides DTI, a second MRI approach was used to further improve the *in vivo* parcellation of the human amygdala. Aware of the difficulties in imaging the amygdala using MRI, a dedicated experimental setup was employed. Firstly, it was shown that the higher signal and contrast at higher magnetic field strengths, such as 7 Tesla, resulted in visible internal structures within the amygdala, whereas, at 3 T field strength, this structure is merely seen as an undifferentiated area. Next, the combination of different MR contrasts and the latest resources available in image analysis led to a robust clustering of the amygdala. Although the relatively coarse resolution of $(1.2 \text{ mm})^3$ was used because of the improved robustness of the analysis technique, the future goal should be a decrease in voxel size. Then, the full potential of 7 Tesla imaging could be tapped and the parcellation could presumably be improved.

A comparison between the clusters found in the amygdala using DTI and structural high field MRI showed similarities but also differences. This is not surprising because both parcellation approaches are based upon two separate information sources - connectivity (diffusion weighted MRI) and anatomical differences in general (structural MRI).

A sixth and final experiment was conducted as an fMRI study. This last experiment incorporated the main general hypothesis as well as the different approaches shown in the course of this thesis. Using both positive and negative human emotions as stimuli, the probabilistic maps achieved with different MR techniques, the latest improvements in audio hardware, ultra-high field MRI and high resolution, this study was able to accurately localize specific human emotions within the amygdala, and present some preliminary results employing our probabilistic maps.

To our knowledge, this is the first study to identify robust amygdaloid components *in vivo,* providing deeper insight into the amygdaloid tissue itself. The direct correlation between function and its anatomical substrate obtained here opens new perspectives for the understanding of the amygdala and, consequently, of human emotions.

References

Alheid, G.F., de Olmos, J.S., & Beltramino, C.A. (1995). Amygdala and extended amygdala. In G. Paxinos (Ed.), *The Rat Nervous System* (2nd ed., pp. 495-578). San Diego: Academic Press,.

Amaral, D., & Price, J. (1984). Amygdalo-cortical projections in the monkey (Macaca fascicularis). *J Comp Neurol, 230*(4), 465-496.

Amaral, D., Price, J., Pitkänen, A., & Carmichael, S. (1992). Anatomical organization of the primate amygdaloid complex. In J.P. Aggelton (Ed.), *The Amygdala: Neurobiological Aspects of Emotion, Memory and Mental Dysfunction.* (pp. 1-66). New York: Wiley.

Amunts, K., Kedo, O., Kindler, M., Pieperhoff, P., Mohlberg, H., Shah, N. J., et al. (2005). Cytoarchitectonic mapping of the human amygdala, hippocampal region and entorhinal cortex: intersubject variability and probability maps. *Anat Embryol (Berl), 210*(5-6), 343-352.

Anderson, A. K., & Phelps, E. A. (2000). Expression without recognition: contributions of the human amygdala to emotional communication. *Psychol Sci, 11*(2), 106-111.

Andrews, T.J., Osborne, M.T., & Does, M.D. (2006). Diffusion of myelin water. *Magn Reson Med, 56*(2), 381-385.

Anwander, A., Tittgemeyer, M., von Cramon, D.Y., Friederici, A.D., & Knosche, T.R. (2007). Connectivity-based parcellation of Broca's area. *Cereb Cortex, 17*(4), 816-825.

Avram, A. V., Guidon, A., & Song, A. W. (2010). Myelin water weighted diffusion tensor imaging. *Neuroimage, 53*(1), 132-138.

Axer, H., Axer, M., Krings, T., & Keyserlingk, D. G. (2001). Quantitative estimation of 3-D fiber course in gross histological sections of the human brain using polarized light. *J Neurosci Methods, 105*(2), 121-131.

Axer, H., Berks, G., & Keyserlingk, D. G. (2000). Visualization of nerve fiber orientation in gross histological sections of the human brain. *Microsc Res Tech, 51*(5), 481-492.

Axer, H., & Keyserlingk, D. G. (2000). Mapping of fiber orientation in human internal capsule by means of polarized light and confocal scanning laser microscopy. *J Neurosci Methods, 94*(2), 165-175.

Axer, H., Leunert, M., Murkoster, M., Grassel, D., Larsen, L., Griffin, L. D., et al. (2002). A 3D fiber model of the human brainstem. *Comput Med Imaging Graph, 26*(6), 439-444.

Axer, H., Lippitz, B. E., & von Keyserlingk, D. G. (1999). Morphological asymmetry in anterior limb of human internal capsule revealed by confocal laser and polarized light microscopy. *Psychiatry Res, 91*(3), 141-154.

Axer, M., Dammers, J., Gräzel, D., Amunts, K., Pietrzyk, U., & Zilles, K. (2008). Nerve fiber mapping in histological sections of the human brain by means of polarized light. . In Australia. 14th Annual meeting on Human Brain Mapping in Melbourne (Ed.), *Neuroimage* (Vol. 41).

Aylward, E. H., Minshew, N. J., Goldstein, G., Honeycutt, N. A., Augustine, A. M., Yates, K. O., et al. (1999). MRI volumes of amygdala and hippocampus in non-mentally retarded autistic adolescents and adults. *Neurology, 53*(9), 2145-2150.

Ball, T., Derix, J., Wentlandt, J., Wieckhorst, B., Speck, O., Schulze-Bonhage, A., et al. (2009). Anatomical specificity of functional amygdala imaging of responses to stimuli with positive and negative emotional valence. *J Neurosci Methods, 180*(1), 57-70.

Ball, T., Rahm, B., Eickhoff, S. B., Schulze-Bonhage, A., Speck, O., & Mutschler, I. (2007). Response properties of human amygdala subregions: evidence based on functional MRI combined with probabilistic anatomical maps. *PLoS One, 2*(3), e307.

Basser, P. J. (1993). Cable equation for a myelinated axon derived from its microstructure. *Med Biol Eng Comput, 31 Suppl*, S87-92.

Basser, P. J., & Pierpaoli, C. (1996). Microstructural and physiological features of tissues elucidated by quantitative-diffusion-tensor MRI. *J Magn Reson B, 111*(3), 209-219.

Basser, P. J., & Pierpaoli, C. (1998). A simplified method to measure the diffusion tensor from seven MR images. *Magn Reson Med, 39*(6), 928-934.

Basser, P.J., Mattiello, J., & LeBihan, D. (1994). Estimation of the effective self-diffusion tensor from the NMR spin echo. *J Magn Reson B, 103*(3), 247-254.

Baumann, N., & Pham-Dinh, D. (2001). Biology of oligodendrocyte and myelin in the mammalian central nervous system. *Physiol Rev, 81*(2), 871-927.

Beaulieu, C. (2002). The basis of anisotropic water diffusion in the nervous system - a technical review. *NMR Biomed, 15*(7-8), 435-455.

Beaulieu, C., & Allen, P.S. (1994a). Determinants of anisotropic water diffusion in nerves. *Magn Reson Med, 31*(4), 394-400.

Beaulieu, C., & Allen, P.S. (1994b). Water diffusion in the giant axon of the squid: implications for diffusion-weighted MRI of the nervous system. *Magn Reson Med, 32*(5), 579-583.

Behrens, T. E. , Johansen-Berg, H., Woolrich, M. W., Smith, S. M., Wheeler-Kingshott, C. A. , Boulby, P. A., et al. (2003). Non-invasive mapping of connections between human thalamus and cortex using diffusion imaging. *Nat Neurosci, 6*(7), 750-757.

Belliveau, J.W., Kennedy, D.N. Jr., McKinstry, R.C., Buchbinder, B.R., Weisskoff, R.M., Cohen, M.S., et al. (1991). Functional mapping of the human visual cortex by magnetic resonance imaging. *Science, 254*(5032), 716-719.

Bennett, H.S. (1950). The microscopical investigation of biological materials with polarized light. In R. McClung-Jones (Ed.), *McClung's Handbook of Microscopical Techniques for Workers in Animal and Plant Tissues* (3 ed., pp. 591-677). New York: Hafner.

Bernard, J. F., Peschanski, M., & Besson, J. M. (1989). A possible spino (trigemino)-ponto-amygdaloid pathway for pain. *Neurosci Lett, 100*(1-3), 83-88.

Bizzi, A., Righini, A., Turner, R., Le Bihan, D., Bockhorst, K.H. , & Alger, J.R. (1996). Imaging focal reperfusion injury following global ischemia with diffusion-weighted magnetic resonance imaging and 1H-magnetic resonance spectroscopy. *Magn Reson Imaging, 14*(6), 581-592.

Blood, A. J., & Zatorre, R. J. (2001). Intensely pleasurable responses to music correlate with activity in brain regions implicated in reward and emotion. *Proc Natl Acad Sci U S A, 98*(20), 11818-11823.

Boccardi, M., Pennanen, C., Laakso, M. P., Testa, C., Geroldi, C., Soininen, H., et al. (2002). Amygdaloid atrophy in frontotemporal dementia and Alzheimer's disease. *Neurosci Lett, 335*(2), 139-143.

Bordi, F., & LeDoux, J. E. (1994). Response properties of single units in areas of rat auditory thalamus that project to the amygdala. II. Cells receiving convergent auditory and somatosensory inputs and cells antidromically activated by amygdala stimulation. *Exp Brain Res, 98*(2), 275-286.

Breiter, H. C., & Rosen, B. R. (1999). Functional magnetic resonance imaging of brain reward circuitry in the human. *Ann N Y Acad Sci, 877*, 523-547.

Brockhaus, H. (1938). Zur normalen und pathologischen Anatomie des Mandelkerngebietes. *J Psychol Neurol, 49*, 1-136.

Brody, B. A., Kinney, H. C., Kloman, A. S., & Gilles, F. H. (1987). Sequence of central nervous system myelination in human infancy. I. An autopsy study of myelination. *J Neuropathol Exp Neurol, 46*(3), 283-301.

Burdach, KF. (1826). *Vom Baue und Leben des Gehirns*: Dyk.

Burnett, A. C., Reutens, D. C., & Wood, A. G. (2010). Social cognition in Turner's Syndrome. *J Clin Neurosci, 17*(3), 283-286.

Butler, T., Pan, H., Tuescher, O., Engelien, A., Goldstein, M., Epstein, J., et al. (2007). Human fear-related motor neurocircuitry. *Neuroscience, 150*(1), 1-7.

Campeau, S., & Davis, M. (1995). Involvement of subcortical and cortical afferents to the lateral nucleus of the amygdala in fear conditioning measured with fear-potentiated startle in rats trained concurrently with auditory and visual conditioned stimuli. *J Neurosci, 15*(3 Pt 2), 2312-2327.

Cannestra, A. F., Pouratian, N., Bookheimer, S. Y., Martin, N. A., Beckerand, D. P., & Toga, A. W. (2001). Temporal spatial differences observed by functional MRI and human intraoperative optical imaging. *Cereb Cortex, 11*(8), 773-782.

Carr, H. Y., & Purcell, E. M. (1954). Effects of Diffusion on Free Precession in Nuclear Magnetic Resonance Experiments. *Physical Review, 94*(3), 630.

Chabriat, H., Pappata, S., Poupon, C., Clark, C. A., Vahedi, K., Poupon, F., et al. (1999). Clinical severity in CADASIL related to ultrastructural damage in white matter: in vivo study with diffusion tensor MRI. *Stroke, 30*(12), 2637-2643.

Cho, Z. H., Kang, C. K., Han, J. Y., Kim, S. H., Park, C. A., Kim, K. N., et al. (2008). Functional MR angiography with 7.0 T Is direct observation of arterial response during neural activity possible? *Neuroimage, 42*(1), 70-75.

Clugnet, M. C., & LeDoux, J. E. (1990). Synaptic plasticity in fear conditioning circuits: induction of LTP in the lateral nucleus of the amygdala by stimulation of the medial geniculate body. *J Neurosci, 10*(8), 2818-2824.

Collins, C.M., & Smith, M.B. (2001). Signal-to-Noise Ratio and Absorbed Power as Functions of Main Magnetic Field Strength and Definition of "90°" RF Pulse for the Head in the Birdcage Coil. *Magn. Reson. Med., 45*, 684-691.

Cramer, H. . (1946). *Mathematical Methods of Statistics*. Princeton, NJ.: Princeton University Press.

Dammers, J., Axer, M., Grassel, D., Palm, C., Zilles, K., Amunts, K., et al. (2010). Signal enhancement in polarized light imaging by means of independent component analysis. *Neuroimage, 49*(2), 1241-1248.

Darwin, C. (1872). *The Expression of the Emotions in Man and Animals*. Chicago: Univ. of Chicago Press.

de Olmos, J.S. (2004). The Amygdala. In G. Paxinos & J.K. Mai (Eds.), *The Human Nervous System* (2 ed., pp. 739-868). San Diego: Elsevier Academic Press.

Dong, H. W., Petrovich, G. D., & Swanson, L. W. (2001). Topography of projections from amygdala to bed nuclei of the stria terminalis. *Brain Res Brain Res Rev, 38*(1-2), 192-246.

Douaud, G., Gaura, V., Ribeiro, M. J., Lethimonnier, F., Maroy, R., Verny, C., et al. (2006). Distribution of grey matter atrophy in Huntington's disease patients: a combined ROI-based and voxel-based morphometric study. *Neuroimage, 32*(4), 1562-1575.

Draganski, B. , Kherif, F., Klöppel, S., Cook, P.A., Alexander, D.C., Parker, G.J., et al. (2008). Evidence for segregated and integrative connectivity patterns in the human basal ganglia. *J Neurosci, 28*(8), 7143-7152.

Duvernoy, H. (1999). *Human Brain: Surface, Three-Dimensional Sectional Anatomy with MRI, and Blood Supply* (2 ed.). New York: Springer.

Einstein, A. (1926). *Investigations on the theory of the Brownian movement.* New York: Dover Publications, Inc.

Ekman, P. (1977). Biological and cultural contributions to body and facial movement. In j. Blacking (Ed.), *Anthropology of the Body.* (pp. 34-38). London: Academic Press.

Ekman, Paul. (1992). An argument for basic emotions. *Cognition & Emotion, 6*(3), 169-200.

Fecteau, S., Belin, P., Joanette, Y., & Armony, J. L. (2007). Amygdala responses to nonlinguistic emotional vocalizations. *Neuroimage, 36*(2), 480-487.

Fendt, M., & Fanselow, M. S. (1999). The neuroanatomical and neurochemical basis of conditioned fear. *Neurosci Biobehav Rev, 23*(5), 743-760.

Filipovic, R., Jakovcevski, I., & Zecevic, N. (2003). GRO-alpha and CXCR2 in the human fetal brain and multiple sclerosis lesions. *Dev Neurosci, 25*(2-4), 279-290.

Floresco, S. B., St Onge, J. R., Ghods-Sharifi, S., & Winstanley, C. A. (2008). Cortico-limbic-striatal circuits subserving different forms of cost-benefit decision making. *Cogn Affect Behav Neurosci, 8*(4), 375-389.

Frahm, J., Haase, A., & Matthaei, D. (1986). Rapid three-dimensional MR imaging using the FLASH technique. *J Comput Assist Tomogr, 10*(2), 363-368.

Fried, I. (2000). Functional neuroimaging in presurgical localization of essential cortical processing zones. *Adv Neurol, 83*, 297-303.

Friedman, B., Hockfield, S., Black, J. A., Woodruff, K. A., & Waxman, S. G. (1989). In situ demonstration of mature oligodendrocytes and their processes: an immunocytochemical study with a new monoclonal antibody, rip. *Glia, 2*(5), 380-390.

Gallagher, M., & Holland, P. C. (1994). The amygdala complex: multiple roles in associative learning and attention. *Proc Natl Acad Sci U S A, 91*(25), 11771-11776.

García-Martí, Gracián, Aguilar, Eduardo J., Lull, Juan J., Martí-Bonmatí, Luis, Escartí, María J., Manjón, José V., et al. (2008). Schizophrenia with auditory hallucinations: A voxel-based morphometry study. *Prog Neuropsychopharmacol Biol Psychiatry, 32*(1), 72-80.

Gaykema, R. P., Chen, C. C., & Goehler, L. E. (2007). Organization of immune-responsive medullary projections to the bed nucleus of the stria terminalis, central amygdala, and paraventricular nucleus of the hypothalamus: evidence for parallel viscerosensory pathways in the rat brain. *Brain Res, 1130*(1), 130-145.

Ghashghaei, H. T., & Barbas, H. (2002). Pathways for emotion: interactions of prefrontal and anterior temporal pathways in the amygdala of the rhesus monkey. *Neuroscience, 115*(4), 1261-1279.

Ghods-Sharifi, S., St Onge, J. R., & Floresco, S. B. (2009). Fundamental contribution by the basolateral amygdala to different forms of decision making. *J Neurosci, 29*(16), 5251-5259.

Goldman, M.R., Pohost, G.M., Ingwall, J.S., & Fossel, E.T. (1980). Nuclear magnetic resonance imaging: potential cardiac applications. *Am J Cardiol., 46*(7), 1278-1283.

Gupta, R. K., Hasan, K. M., Trivedi, R., Pradhan, M., Das, V., Parikh, N. A., et al. (2005). Diffusion tensor imaging of the developing human cerebrum. *J Neurosci Res, 81*(2), 172-178.

Gupta, R. K., Rao, A. M., Mishra, A. M., Chawla, S., Sekar, D. R., & Venkatesan, R. (2005). Diffusion-weighted EPI with magnetization transfer contrast. *Magn Reson Imaging, 23*(1), 35-39.

Hahn, E. L. (1950). Spin Echoes. *Physical Review, 80*(4), 580.

Hamann, S. (2009). The Human Amygdala and Memory. In P.J. Whalen & E. A. Phelps (Eds.), *The Human Amygdala*. New York: The Guilford Press.

Hayman, L. A., Rexer, J. L., Pavol, M. A., Strite, D., & Meyers, C. A. (1998). Klüver-Bucy syndrome after bilateral selective damage of amygdala and its cortical connections. *J Neuropsychiatry Clin Neurosci, 10*(3), 354-358.

Hennig, J., Nauerth, A., & Friedburg, H. (1986). RARE imaging: a fast imaging method for clinical MR. *Magn Reson Med, 3*(6), 823-833.

Holodny, A. I., Schwartz, T. H., Ollenschleger, M., Liu, W. C., & Schulder, M. (2001). Tumor involvement of the corticospinal tract: diffusion magnetic resonance tractography with intraoperative correlation. *J Neurosurg, 95*(6), 1082.

Horínek, Daniel, Varjassyová, Alexandra, & Hort, Jakub. (2007). Magnetic resonance analysis of amygdalar volume in Alzheimer's disease. *Curr Opin Psychiatry, 20*(3), 273-277.

Huang, H. (2010). Structure of the Fetal Brain: What We Are Learning from Diffusion Tensor Imaging. *Neuroscientist*.

Huang, H., Xue, R., Zhang, J., Ren, T., Richards, L. J., Yarowsky, P., et al. (2009). Anatomical characterization of human fetal brain development with diffusion tensor magnetic resonance imaging. *J Neurosci, 29*(13), 4263-4273.

Huang, H., Zhang, J., Wakana, S., Zhang, W., Ren, T., Richards, L. J., et al. (2006). White and gray matter development in human fetal, newborn and pediatric brains. *Neuroimage, 33*(1), 27-38.

Humphrey, T. (1968). The Development of the Human Amygdala during Early Embryonic Life. *J Comp Neurol, 132*(1), 135-165.

Jakovcevski, I., Filipovic, R., Mo, Z., Rakic, S., & Zecevic, N. (2009). Oligodendrocyte development and the onset of myelination in the human fetal brain. *Front Neuroanat, 3*, 5.

Jakovcevski, I., Mo, Z., & Zecevic, N. (2007). Down-regulation of the axonal polysialic acid-neural cell adhesion molecule expression coincides with the onset of myelination in the human fetal forebrain. *Neuroscience, 149*(2), 328-337.

Jakovcevski, I., & Zecevic, N. (2005). Olig transcription factors are expressed in oligodendrocyte and neuronal cells in human fetal CNS. *J Neurosci, 25*(44), 10064-10073.

Jenkinson, M., Bannister, P., Brady, M., & Smith, S. (2002). Improved optimization for the robust and accurate linear registration and motion correction of brain images. *Neuroimage, 17*(2), 825-841.

Jespersen, S.N., Kroenke, C.D., Østergaard, L., Ackerman, J.J., & Yablonskiy, D.A. (2007). Modeling dendrite density from magnetic resonance diffusion measurements. *Neuroimage, 34*(4), 1473-1486.

Johnston, JB. (1923). Further contributions to the study of the evolution of the forebrain. *J Comp Neurol, 35*, 337-481.

Kang, C. K., Park, C. W., Han, J. Y., Kim, S. H., Park, C. A., Kim, K. N., et al. (2009). Imaging and analysis of lenticulostriate arteries using 7.0-Tesla magnetic resonance angiography. *Magn Reson Med, 61*(1), 136-144.

Killcross, S., Robbins, T. W., & Everitt, B. J. (1997). Different types of fear-conditioned behaviour mediated by separate nuclei within amygdala. *Nature, 388*(6640), 377-380.

Klebs, E. (1865). Die Nerven der organischen Muskelfasern. *Virchows Arch., 32*(2), 168-198.

Klinge, C., Roder, B., & Buchel, C. (2010). Increased amygdala activation to emotional auditory stimuli in the blind. *Brain, 133*(Pt 6), 1729-1736.

Klüver, H., & Bucy, P. C. (1937). "Psychic blindness" and other symptoms following bilateral temporal lobectomy in rhesus monkeys. *Am J Physiol 119*, 352-353.

Koch, M. A., Norris, D. G., & Hund-Georgiadis, M. (2002). An investigation of functional and anatomical connectivity using magnetic resonance imaging. *Neuroimage, 16*(1), 241-250.

Kwong, K. K., Belliveau, J. W., Chesler, D. A., Goldberg, I. E., Weisskoff, R. M., Poncelet, B. P., et al. (1992). Dynamic magnetic resonance imaging of human brain activity during primary sensory stimulation. *Proc Natl Acad Sci U S A, 89*(12), 5675-5679.

Langworthy, O.R. (1933). Development of behavior patterns and myelinization of the nervous system in the human fetus and infant. *Contributions to embryology* (Vol. 26, pp. 1-13). Washington, DC: Carnegie Institute of Washington.

Lanteaume, Laura, Khalfa, Stéphanie, Régis, Jean, Marquis, Patrick, Chauvel, Patrick, & Bartolomei, Fabrice. (2007). Emotion induction after direct intracerebral stimulations of human amygdala. *Cereb Cortex, 17*(6), 1307-1313.

Larsen, L., Griffin, L. D., Grassel, D., Witte, O. W., & Axer, H. (2007). Polarized light imaging of white matter architecture. *Microsc Res Tech, 70*(10), 851-863.

Latchaw, R. E., Ugurbil, K., & Hu, X. (1995). Functional MR imaging of perceptual and cognitive functions. *Neuroimaging Clin N Am, 5*(2), 193-205.

Le Bihan, D., Breton, E., Lallemand, D. , Grenier, P., Cabanis, E., & Laval-Jeantet, M. (1986). MR imaging of intravoxel incoherent motions: application to diffusion and perfusion in neurologic disorders. *Radiology, 161*(2), 401-407.

Le Bihan, D., Mangin, J.F., Poupon, C., Clark, C.A., Pappata, S., Molko, N., et al. (2001). Diffusion tensor imaging: concepts and applications. *J Magn Reson Imaging., 13*(4), 534-546.

LeDoux, J. (2003). The emotional brain, fear, and the amygdala. *Cell Mol Neurobiol, 23*(4-5), 727-738.

LeDoux, J. E., Farb, C., & Ruggiero, D. A. (1990). Topographic organization of neurons in the acoustic thalamus that project to the amygdala. *J Neurosci, 10*(4), 1043-1054.

LeDoux, J.E. (2000). Emotion circuits in the brain. *Annu Rev Neurosci, 23*, 155-184.

Li, T.Q., van Gelderen, P., Merkle, H., Talagala, L., Koretsky, A.P., & Duyn, J. (2006). Extensive heterogeneity in white matter intensity in high-resolution T2*-weighted MRI of the human brain at 7.0 T. *Neuroimage, 32*(3), 1032-1040.

MacLean, P. D. (1949). Psychosomatic disease and the visceral brain; recent developments bearing on the Papez theory of emotion. *Psychosom Med, 11*(6), 338-353.

Mädler, B., Drabycz, S.A., Kolind, S.H., Whittall, K.P., & MacKay, A.L. (2008). Is diffusion anisotropy an accurate monitor of myelination? Correlation of multicomponent T2 relaxation and diffusion tensor anisotropy in human brain. *Magn Reson Imaging, 26*(7), 874-888.

Maeder, P. P., Meuli, R. A., Adriani, M., Bellmann, A., Fornari, E., Thiran, J. P., et al. (2001). Distinct pathways involved in sound recognition and localization: a human fMRI study. *Neuroimage, 14*(4), 802-816.

Mainero, C., Benner, T., Radding, A., van der Kouwe, A., Jensen, R., Rosen, B. R., et al. (2009). In vivo imaging of cortical pathology in multiple sclerosis using ultra-high field MRI. *Neurology, 73*(12), 941-948.

Mansfield, P. (1977). Multi-planar image formation using NMR spin echoes *J Phys C, 10*, L55-L58.

Marques, J. P., Kober, T., Krueger, G., van der Zwaag, W., Van de Moortele, P. F., & Gruetter, R. (2010). MP2RAGE, a self bias-field corrected sequence for improved segmentation and T1-mapping at high field. *Neuroimage, 49*(2), 1271-1281.

Martel, G., Nishi, A., & Shumyatsky, G. P. (2008). Stathmin reveals dissociable roles of the basolateral amygdala in parental and social behaviors. *Proc Natl Acad Sci U S A, 105*(38), 14620-14625.

Mazziotta, J. C. (1994). Mapping human brain activity in vivo. *West J Med, 161*(3), 273-278.

McDonald, A. J. (1987). Organization of amygdaloid projections to the mediodorsal thalamus and prefrontal cortex: a fluorescence retrograde transport study in the rat. *J Comp Neurol, 262*(1), 46-58.

McDonald, A. J. (1991). Topographical organization of amygdaloid projections to the caudatoputamen, nucleus accumbens, and related striatal-like areas of the rat brain. *Neuroscience, 44*(1), 15-33.

McDonald, A. J. (1998). Cortical pathways to the mammalian amygdala. *Prog Neurobiol, 55*(3), 257-332.

McDonald, A. J., & Jackson, T. R. (1987). Amygdaloid connections with posterior insular and temporal cortical areas in the rat. *J Comp Neurol, 262*(1), 59-77.

McDonald, A. J., & Mascagni, F. (1997). Projections of the lateral entorhinal cortex to the amygdala: a Phaseolus vulgaris leucoagglutinin study in the rat. *Neuroscience, 77*(2), 445-459.

McDonald, A.J. (1992). Cell types and intrinsic connections of the amygdala. In J.P. Aggelton (Ed.), *The amygdala: neurobiological aspects of emotion, memory, and mental dysfunction.* (pp. 67-96). New York: Wiley-Liss.

Meyer, M., Baumann, S., Wildgruber, D., & Alter, K. (2007). How the brain laughs. Comparative evidence from behavioral, electrophysiological and neuroimaging studies in human and monkey. *Behavioural Brain Research, 182*(2), 245-260.

Mineka, S., & Ohman, A. (2002). Phobias and preparedness: the selective, automatic, and encapsulated nature of fear. *Biol Psychiatry, 52*(10), 927-937.

Morey, R.A., Petty, C.M., Xu, Y., Hayes, J.P., Wagner, H.R. 2nd., Lewis, D.V., et al. (2009). A comparison of automated segmentation and manual tracing for quantifying hippocampal and amygdala volumes. *Neuroimage, 45*(3), 855-866.

Mori, S., Crain, B.J. , Chacko, V.P. , & Van Zijl, P.C.M. (1999). Three-dimensional tracking of axonal projections in the brain by magnetic resonance imaging. *Ann Neurol, 45*, 265-269.

Mori, S., & Zhang, J. (2006). Principles of diffusion tensor imaging and its applications to basic neuroscience research. *Neuron, 51*(5), 527-539.

Morris, J. S., Scott, S. K., & Dolan, R. J. (1999). Saying it with feeling: neural responses to emotional vocalizations. *Neuropsychologia, 37*(10), 1155-1163.

Mugler, J. P., 3rd, & Brookeman, J. R. (1990). Three-dimensional magnetization-prepared rapid gradient-echo imaging (3D MP RAGE). *Magn Reson Med, 15*(1), 152-157.

Mulkern, R. V., Vajapeyam, S., Haker, S. J., & Maier, S. E. (2005). Magnetization transfer studies of the fast and slow tissue water diffusion components in the human brain. *NMR Biomed, 18*(3), 186-194.

Murray, E. A., Izquierdo, A, & Malkova, L. (2009). Amygdala Function in Positive Reinforcement. In P.J. Whalen & E. A. Phelps (Eds.), *The human amygdala*. New York: The Guilford Press.

Nakashima, M., Uemura, M., Yasui, K., Ozaki, H. S., Tabata, S., & Taen, A. (2000). An anterograde and retrograde tract-tracing study on the projections from the thalamic gustatory area in the rat: distribution of neurons projecting to the insular cortex and amygdaloid complex. *Neurosci Res, 36*(4), 297-309.

Nakata, Y., Sato, N., Nemoto, K., Abe, O., Shikakura, S., Arima, K., et al. (2009). Diffusion abnormality in the posterior cingulum and hippocampal volume: correlation with disease progression in Alzheimer's disease. *Magn Reson Imaging, 27*(3), 347-354.

Ng, A.Y., Jordan, M.I., & Weiss, Y. (2002). On spectral clustering: analysis and an algorithm. *Proc. Neural Information Processing Systems (NIPS), 14*, 849-856.

Noctor, S. C., Flint, A. C., Weissman, T. A., Dammerman, R. S., & Kriegstein, A. R. (2001). Neurons derived from radial glial cells establish radial units in neocortex. *Nature, 409*(6821), 714-720.

Ogawa, S., Lee, T.M., Kay, A.R., & Tank, D.W. . (1990). Brain magnetic resonance imaging with contrast dependent on blood oxygenation. *Proc Natl Acad Sci, 87*(24), 9868-9872.

Olsson, A., Nearing, K. I., & Phelps, E. A. (2007). Learning fears by observing others: the neural systems of social fear transmission. *Soc Cogn Affect Neurosci, 2*(1), 3-11.

Oster, G. (1956). *Birefringence and dichroism. Physical Techniques in Biological Researchs*. New York: Academic Press.

Perge, J. A., Koch, K., Miller, R., Sterling, P., & Balasubramanian, V. (2009). How the optic nerve allocates space, energy capacity, and information. *J Neurosci, 29*(24), 7917-7928.

Phelps, E. A. (2004). Human emotion and memory: interactions of the amygdala and hippocampal complex. *Curr Opin Neurobiol, 14*(2), 198-202.

Phelps, E. A. (2006). Emotion and cognition: insights from studies of the human amygdala. *Annu Rev Psychol, 57*, 27-53.

Phelps, E. A., & LeDoux, J. E. (2005). Contributions of the Amygdala to Emotion Processing: From Animal Models to Human Behavior. *Neuron, 48*(2), 175-187.

Phelps, Elizabeth A., LaBar, Kevin S., & Spencer, Dennis D. (1997). Memory for Emotional Words Following Unilateral Temporal Lobectomy. *Brain and Cognition, 35*(1), 85-109.

Pitkänen, A. (2000). Connectivity of the rat amygdaloid complex. In J.P. Aggelton (Ed.), *The amygdala: A Functional Analysis* (pp. 31-115). Oxford: Oxford Univ. Press.

Pitkänen, A., & Amaral, D. G. (1994). The distribution of GABAergic cells, fibers, and terminals in the monkey amygdaloid complex: an immunohistochemical and in situ hybridization study. *J Neurosci, 14*, 2200–2224.

Pitkänen, A., Savander, V., & LeDoux, J. E. (1997). Organization of intra-amygdaloid circuitries in the rat: an emerging framework for understanding functions of the amygdala. *Trends Neurosci, 20*(11), 517-523.

Prayer, D., Barkovich, A. J., Kirschner, D. A., Prayer, L. M., Roberts, T. P., Kucharczyk, J., et al. (2001). Visualization of nonstructural changes in early white matter development on diffusion-weighted MR images: evidence supporting premyelination anisotropy. *AJNR Am J Neuroradiol, 22*(8), 1572-1576.

Price, J.L., Russchen, F.T., & Amaral, D.G. (1987). *The limbic Region II: The Amygdaloid Complex*. New York: Elsevier Science.

Pruessner, J.C., Li, L.M., Serles, W., Pruessner, M., Collins, D.L., Kabani, N., et al. (2000). Volumetry of Hippocampus and Amygdala with High-resolution MRI and Three-dimensional Analysis Software: Minimizing the Discrepancies between Laboratories. *Cereb Cortex, 10*, 433-442.

Rabinak, C. A., & Maren, S. (2008). Associative structure of fear memory after basolateral amygdala lesions in rats. *Behav Neurosci, 122*(6), 1284-1294.

Raslan, A.M., DeJesus, R., Berk, C., Zacest, A., Anderson, J.C., & Burchiel, K.J. (2009). Sensitivity of high-resolution three-dimensional magnetic resonance angiography and three-dimensional spoiled-gradient recalled imaging in the prediction of neurovascular compression in patients with hemifacial spasm. *J Neurosurg. , 111*(4), 733-736.

Rio-Hortega, P. Del. . (1928). *Tercera aportación al conocimiento morfológico e interpretación funcional de la oligodendroglía.* (Vol. 14): Mem. Real Soc. Espan. Hist. Nat. .

Robinson, E. (1963). EFFECT OF AMYGDALECTOMY ON FEAR-MOTIVATED BEHAVIOR IN RATS. *J Comp Physiol Psychol, 56*, 814-820.

Romeis, B. (1989). *Mikroskopische Technik*. München: Urban und Schwarzenberg.

Ronen, I., Moeller, S., Ugurbil, K., & Kim, D. S. (2006). Investigation of multicomponent diffusion in cat brain using a combined MTC-DWI approach. *Magn Reson Imaging, 24*(4), 425-431.

Sachdev, Perminder S., Chen, Xiaohua, Joscelyne, Amy, Wen, Wei, & Brodaty, Henry. (2007). Amygdala in stroke/transient ischemic attack patients and its relationship to cognitive impairment and psychopathology: the Sydney Stroke Study. *Am J Geriatr Psychiatry, 15*(6), 487-496.

Sah, P., Faber, E. S. , Lopez De Armentia, M., & Power, J. (2003). The amygdaloid complex: anatomy and physiology. *Physiol Rev, 83*(3), 803-834.

Sander, D., Grafman, J., & Zalla, T. (2003). The human amygdala: an evolved system for relevance detection. *Rev Neurosci, 14*(4), 303-316.

Sander, D., Grandjean, D., Pourtois, G., Schwartz, S., Seghier, M. L., Scherer, K. R., et al. (2005). Emotion and attention interactions in social cognition: brain regions involved in processing anger prosody. *Neuroimage, 28*(4), 848-858.

Sander, K., Brechmann, A., & Scheich, H. (2003). Audition of laughing and crying leads to right amygdala activation in a low-noise fMRI setting. *Brain Res Brain Res Protoc, 11*(2), 81-91.

Sander, K., & Scheich, H. (2005). Left auditory cortex and amygdala, but right insula dominance for human laughing and crying. *J Cogn Neurosci, 17*(10), 1519-1531.

Schirmer, A., Escoffier, N., Zysset, S., Koester, D., Striano, T., & Friederici, A. D. (2008). When vocal processing gets emotional: on the role of social orientation in relevance detection by the human amygdala. *Neuroimage, 40*(3), 1402-1410.

Schnabel, R. (1966). Zur mikroskopischen Untersuchung optisch anisotroper Strukturen des Nervensystems mit circular polarisiertem Licht. *Acta Neuropathol, 7*(2), 180-184.

Schwarzbauer, C., Davis, M. H., Rodd, J. M., & Johnsrude, I. (2006). Interleaved silent steady state (ISSS) imaging: a new sparse imaging method applied to auditory fMRI. *Neuroimage, 29*(3), 774-782.

Sharot, Tali, Riccardi, Alison M., Raio, Candace M., & Phelps, Elizabeth A. (2007). Neural mechanisms mediating optimism bias. *Nature, 450*(7166), 102-105.

Shayegan, D. K., & Stahl, S. M. (2005). Emotion processing, the amygdala, and outcome in schizophrenia. *Prog Neuropsychopharmacol Biol Psychiatry, 29*(5), 840-845.

Shi, C.J. , & Cassell, M.D. (1998). Cascade projections from somatosensory cortex to the rat basolateral amygdala via the parietal insular cortex. *J Comp Neurol, 399*(4), 469-491.

Shin, R. M., Tsvetkov, E., & Bolshakov, V. Y. (2006). Spatiotemporal asymmetry of associative synaptic plasticity in fear conditioning pathways. *Neuron, 52*(5), 883-896.

Shurcliff, W.H., & Ballard, S.S. (1964). *Polarized Light*. New York: Van Nostrand.

Simon, D., Craig, K. D., Miltner, W. H., & Rainville, P. (2006). Brain responses to dynamic facial expressions of pain. *Pain, 126*(1-3), 309-318.

Smith, Stephen M., Jenkinson, Mark, Woolrich, Mark W., Beckmann, Christian F., Behrens, Timothy E. J., Johansen-Berg, Heidi, et al. (2004). Advances in functional and structural MR image analysis and implementation as FSL. *Neuroimage, 23 Suppl 1*, S208-219.

Solano-Castiella, E., Anwander, A., Lohmann, G., Weiss, M., Docherty, C., Geyer, S., et al. (2010). Diffusion tensor imaging segments the human amygdala in vivo. *Neuroimage, 49*(4), 2958-2965.

Solano-Castiella, E., Lohmann, G., Schäfer, A., Trampel, R., & Turner, R. (2009). Parcellation of the human amygdala using 7T structural MRI. *Neuroimage, 47*(Supplement 1), S72-S72.

Stehling, M.K., Turner, R., & Mansfield, P. (1991). Echo-planar imaging: magnetic resonance imaging in a fraction of a second. *Science, 254*, 43-50.

Talairach, J., & Tournoux, P. (1988). *Co-Planar Stereotaxic Atlas of the Human Brain*. New York: Thieme Medical Publishers.

Tanner, J.E., & Stejskal, E.O. (1968). Restricted Self-Diffusion of Protons in Colloidal Systems by the Pulsed-Gradient, Spin-Echo Method. *J. Chem. Phys., 49*, 1768-1778

Thomas, B.P., Welch, E.B., Niederhauser, B.D., Whetsell, W.O. Jr., Anderson, A.W., Gore, J.C., et al. (2008). High-resolution 7T MRI of the human hippocampus in vivo. *J Magn Reson Imaging, 28*(5), 1266-1272.

Triantafyllou, C., Hoge, R.D., Krueger, G., Wiggins, C.J., Potthast, A., Wiggins, G.C., et al. (2005). Comparison of physiological noise at 1.5 T, 3 T and 7 T and optimization of fMRI acquisition parameters. *Neuroimage, 26*(1), 243-250.

Turner, R., Le Bihan, D., Maier, J., Vavrek, R., Hedges, L.K., & Pekar, J. (1990). Echo-planar imaging of intravoxel incoherent motion. *Radiology, 177*(2), 407-414.

Turner, R., Le Bihan, D., Moonen, C.T., Despres, D., & Frank, J. . (1991). Echo-planar time course MRI of cat brain oxygenation changes. *Magn Reson Med, 22*(1), 159-166.

Van de Moortele, P.F., Akgun, C., Adriany, G. , Moeller, S. , Ritter, J. , Collins, C.M. , et al. (2005). B(1) destructive interferences and spatial phase patterns at 7 T with a head transceiver array coil. *Magn. Reson. Med., 54*(6), 1503-1518.

Vollm, B. A., Taylor, A. N., Richardson, P., Corcoran, R., Stirling, J., McKie, S., et al. (2006). Neuronal correlates of theory of mind and empathy: a functional magnetic resonance imaging study in a nonverbal task. *Neuroimage, 29*(1), 90-98.

Vuilleumier, P. (2009). The Role of the Human Amygdala in Perception and Attention. In P.J. Whalen & E. A. Phelps (Eds.), *The Human Amygdala*. New York: The Guilford Press.

Weiskrantz, L. (1956). Behavioral changes associated with ablation of the amygdaloid complex in monkey. *J. Comp. Physiol. Psychol. , 49*, 381-391.

Wiest, Gerald, Lehner-Baumgartner, Eva, & Baumgartner, Christoph. (2006). Panic attacks in an individual with bilateral selective lesions of the amygdala. *Arch Neurol, 63*(12), 1798-1801.

Wild, B., Rodden, F. A., Grodd, W., & Ruch, W. (2003). Neural correlates of laughter and humour. *Brain, 126*(Pt 10), 2121-2138.

Williams, J. H. (2008). Self-other relations in social development and autism: multiple roles for mirror neurons and other brain bases. *Autism Res, 1*(2), 73-90.

Wolman, M. (1970). On the use of polarized light in pathology. *Pathol Annu, 5*, 381-416.

Wolman, M. (1975). Polarized light microscopy as a tool of diagnostic pathology. *J Histochem Cytochem, 23*(1), 21-50.

Woolrich, M. W., Jbabdi, S., Patenaude, B., Chappell, M., Makni, S., Behrens, T., et al. (2009). Bayesian analysis of neuroimaging data in FSL. *Neuroimage, 45*(1 Suppl), S173-186.

Worsley, K.J. (2001). Statistical analysis of activation images. In P.M. Matthews, P. Jezzard & S.M. Smith (Eds.), *Functional magnetic resonance imaging of the brain: methods for neuroscience*. London: Oxford UP.

Young, B. J., & Leaton, R. N. (1996). Amygdala central nucleus lesions attenuate acoustic startle stimulus-evoked heart rate changes in rats. *Behav Neurosci, 110*(2), 228-237.

Zald, D. H., Lee, J. T., Fluegel, K. W., & Pardo, J. V. (1998). Aversive gustatory stimulation activates limbic circuits in humans. *Brain, 121 (Pt 6)*, 1143-1154.

Zivadinov, R., Stosic, M., Cox, J. L., Ramasamy, D. P., & Dwyer, M. G. (2008). The place of conventional MRI and newly emerging MRI techniques in monitoring different aspects of treatment outcome. *J Neurol, 255 Suppl 1*, 61-74.

Summary

In vivo anatomical segmentation of the human amygdala and parcellation of emotional processing

Eugenia Solano-Castiella

Fakultät für Biowissenschaften, Pharmazie und Psychologie
Universität Leipzig

Introduction

The amygdala is a small structure located deep within the temporal lobes of the brain. The most widely used general description of the amygdala subcomponents is derived from *ex vivo* brain samples (Johnston, 1923). More than half a century later, research exploring the anatomy of the amygdala is still in constant development, and as yet there are no established methods for parcellating the amygdala *in vivo*. As the amygdala lies proximal to the air-filled sinuses, susceptibility artifacts have confounded magnetic resonance imaging (MRI); thus postmortem studies are still necessary to understand the anatomical properties of the amygdala (Amaral & Price, 1984; Amaral, Price, Pitkänen, & Carmichael, 1992; Amunts, et al., 2005; de Olmos, 2004).

The emotional system (commonly known as the limbic system) is highly relevant for the human personality. The amygdala, as a part of this brain system, has been related to a variety of emotional processes identified in different parts of this structure (Ball, et al., 2007; Lanteaume, et al., 2007; K. Sander, et al., 2003; Sharot, et al., 2007; Weiskrantz, 1956). One relationship between emotions and the amygdala was established by identifying the centroid points of the activations associated with a specific emotion within a particular segment (Ball, et al., 2009; Ball, et al., 2007). In order to classify these activations, the study made use of a probabilistic map generated from postmortem samples (Amunts, et al., 2005). This mask, computed using cytoarchitectonic data, was later interpolated to MR resolution. The resulting probabilistic map was used for *in vivo* functional localization within the amygdala (Aylward, et al., 1999). However, several limitations have been reported with respect to the ambiguous borders with the neighbouring regions (Ball, et al., 2009). Therefore, *in vivo*

anatomical segmentation would be remarkably helpful for the successful functional imaging of the amygdala.

Motivated by the known involvement of the amygdala in emotional processing and the tremendous technological advances of non-invasive imaging techniques in the last decade, the goal of this research is to achieve parcellation of the human amygdala for the first time *in vivo,* and to correlate positive and negative emotions with subregions within the amygdala.

Conducted experiments

The experiments conducted within the presented thesis integrate data from multiple MR imaging techniques to elucidate the anatomical properties of the amygdala. We present for the first time a method for robust clustering of the amygdala subcomponents *in vivo,* enabling correlation of amygdala probabilistic maps with emotional processing regions.

Experiment 1. Diffusion tensor imaging (DTI) was used to parcellate the amygdala subregions. This was motivated by the reported extensive connections between amygdaloid nuclei and the rest of the brain (Ghashghaei & Barbas, 2002; J. E. LeDoux, et al., 1990; A. J. McDonald, 1998; A.J. McDonald, 1992; E. A. Phelps, 2004; Pitkänen, 2000; Pitkänen & Amaral, 1994). Although this technique appears promising based on this literature, the use of DTI for analysis of the amygdala is controversial due to the strong dependence of DTI on myelination, and the minimal amount of myelinated fibres in the amygdala. However, after computing the preferential direction-per-voxel, the first striking results revealed robust anisotropic groups within the amygdala. For the first time, this study was able to consistently cluster *in vivo* amygdala components into two main groups (Solano-Castiella, et al., 2010). The probabilistic maps resulting from this data constitute a step towards the *in vivo* study of the subregions of the amygdala, and its specific tissue characteristics.

Experiment 2 employed polarized light imaging (PLI) to verify the DTI-based amygdala parcellation. PLI, an *ex vivo* technique, allows visualization of the direction of myelinated fibres in postmortem tissue (H. Axer, et al., 2002; Dammers, et al., 2010; Larsen, et al., 2007). Therefore PLI is a means for *ex vivo* validation of claims based on MRI data regarding structural anisotropy within grey matter. However, PLI, as an optical technique, has a much higher spatial resolution than DTI. *Experiment 2* results confirmed the presence of anisotropy in the grey area of the amygdala, and

showed directional groups in the 100-µm-thick coronal sections comparable to those found with DTI at an isotropic resolution of (1.72 mm)³.

Experiment 3 was performed to determine whether DTI contrast is possible in a structure with little to no myelin. Myelination is typically associated with anisotropic diffusion in the brain, although the work published by Beaulieu et al. in (1994a) showed that this is not always required. Fetal brain of gestational age of between 15 and 30 weeks were available for study. Such tissues have little or no myelin, although neuronal fibre pathways are already well developed. This extreme case of the non-myelinated fetal brain allows a test of the usefulness of DTI in adult amygdala, where it appears to show robust subdivisions. The investigation of the fetus tissue showed clear anisotropic cortical layers in the complete absence of myelin, and thereby reinforced the argument that organized water diffusion can occur in brain areas with a lack of or small amounts of myelin, such as the amygdala.

These last three experiments have revealed amygdala tissue features using techniques that have found their most popular applications in white matter brain regions. The tissue properties found in the amygdala and the first *in vivo* derived probabilistic maps, encourage the *in vivo* exploration and parcellation of similar brain structures.

Experiment 4 represents a further step toward differentiating components within the amygdala using structural MRI. The variation of relaxation times with tissue type is a major source of MRI contrast. Apparently homogeneous regions may reveal internal structure when improved imaging strategies and better SNR are available. Structural imaging below 3 Tesla shows the amygdala as an undifferentiated grey matter area. Since the contrast at higher field strength (7 Tesla MRI) can be dramatically increased using appropriate MR sequences, we hoped to find tissue contrast differences within the amygdala. This experiment sought further to improve the *in vivo* parcellation of the human amygdala. Combining two different contrasts, and using cutting-edge image analysis, we have been able to provide a robust clustering of three amygdala components *in vivo* using 7 Tesla structural imaging (Solano-Castiella, Lohmann, Schäfer, Trampel, & Turner, 2009). The MR contrast parcellation is similar to the DTI-derived subregions. However, there are differences between these two maps, which may be attributable to the two separate information sources, namely, connectivity (diffusion weighted MRI) and anatomical differences in general (structural MRI).

Experiment 5 integrates the parcellation methods with an fMRI study in an attempt to map the emotional processing centers of the amygdala. We performed an fMRI study at high field strength (7 Tesla MRI) using emotional human non-linguistic sounds in an attempt to identify the anatomical substrate of various emotions. This was assisted by the use of the two different probabilistic maps achieved *in vivo*. Using human emotional vocalizations (laughter, crying, disgust, and surprise) this work identified different regions of the amygdala reacting to specific emotional conditions. Furthermore, the use of the DTI maps provided a useful overview of emotional location tendencies (medial or lateral), while the structural maps confirmed, or in some cases improved, the identification of anatomical substrates underlying a particular emotion.

Conclusions

In conclusion, this thesis presents the first two *in vivo* parcellation methods of the amygdala. It provides, in addition, a deeper look at the amygdaloid tissue itself. The probabilistic maps obtained have allowed a correlation between different emotional valences and the associated anatomical substrates. The results obtained in the course of this thesis thus open new perspectives for the understanding of the amygdala, and ultimately human emotions.

Zusammenfassung

Anatomische Segmentierung der menschlichen Amygdala in vivo und Parzellierung der Verarbeitung von Emotionen

Eugenia Solano-Castiella

Fakultät für Biowissenschaften, Pharmazie und Psychologie

Universität Leipzig

Einführung

Die Amygdala, oder Mandelkern, ist ein Kerngebiet im hinteren Teil des Temporallappens im Gehirn. Die gängigste Darstellung der einzelnen Subkomponenten der Amygdala stammt von ex vivo Gewebeproben (Johnston, 1923). Fast ein Jahrhundert später/Mehr als ein halbes Jahrhundert später wird die Anatomie der Amygdala weiterhin intensiv erforscht, doch gibt es bislang keine anerkannte Methode zur Parzellierung der Amygdala in vivo. Da sich die Amygdala in der Nähe der Stirnhöhlen befindet und daher Suszeptibilitätsartefakte eine Darstellung mithilfe von Magnetresonanztomographie (MRT) erschweren, sind immer noch post mortem Studien erforderlich, um die anatomischen Eigenschaften der Amygdala zu erforschen (Amaral und Price, 1984; Amaral et al., 1992; Amunts et al., 2005; de Olmos, 2004; Heimer et al., 1997).

Das limbische System, auch bekannt als das emotionale Gehirn, ist in hohem Maße für die menschliche Persönlichkeit verantwortlich. Der Mandelkern ist Teil diesen Systems und ist an einer Vielzahl emotionaler Prozesse beteiligt, welche wiederum in verschiedenen Untereinheiten der Amygdala verarbeitet werden (Lanteaume et al., 2007; LeDoux, 2003; LeDoux, 1992; Phelps und LeDoux, 2005; Sharot et al., 2007; Weiskrantz, 1956). Dementsprechend wurde ein Zusammenhang zwischen Emotionen und der Amygdala etabliert, indem der Schwerpunkt einer jeden Aktivierung, welche mit einer bestimmten

Emotion assoziiert war, einer Untereinheit zugeordnet wurde (Ball et al., 2007; Ball et al., 2009). Um die jeweiligen Aktivierungen klassifizieren zu können, wurde eine probabilistische Karte verwendet, welche aus *ex vivo* Proben generiert wurde (Amunts et al., 2005). Diese Karte wurde mit Hilfe von zytoarchitektonischen Methoden angefertigt und nachträglich auf MR-Auflösung extrapoliert. Die daraus gewonnene probabilistische Karte wurde dann, wie oben beschrieben, für die *in vivo* Lokalisierung bestimmter Prozesse in der Amygdala verwendet (Aylward et al., 1999). Jedoch wurde im Rahmen dieser Studien festgestellt, dass es wegen der unklaren Abgrenzungen der Amygdala mit den benachbarten Regionen Einschränkungen in der Auswertbarkeit gab (Ball et al., 2009). Für eine erfolgreiche funktionale Darstellung der Amygdala, wäre daher eine anatomische in vivo Parzellierung der Amygdala sehr hilfreich.

Grundlage für die vorliegende Studie war zum einen, dass die Amygdala eine entscheidende Rolle in der Bearbeitung emotionaler Prozesse spielt und zum anderen, dass der enorme technische Fortschritt der letzten Jahre im Bereich nicht-invasiver Bildgebungstechniken heute eine detailgenauere Darstellung dieser Struktur erlaubt. Ziel der Studie ist es daher, die menschliche Amygdala erstmalig in vivo in ihre einzelnen Subkomponenten einzuteilen und positive und negative Emotionen mit diesen Unterbereichen räumlich zu korrelieren.

Durchgeführte Experimente

Um die anatomischen Eigenschaften der Amygdala zu erforschen, wurden im Rahmen dieser Arbeit verschiedene MR-Techniken eingesetzt. Damit konnte erstmalig eine Methode gefunden werden, um bestimmte Subkomponenten der Amygdala in vivo zuverlässig zu identifizieren. Dies ermöglichte die Herstellung eines Zusammenhangs zwischen den probabilistischen Karten der Amygdala und den Regionen, welche bestimmte Emotionen prozessieren.

Im 1. Experiment wurde mit Hilfe von Diffusion-Tensor-Bildgebung (DTI) die Amygdala in einzelne Subregionen unterteilt. Diese Technik wurde angewendet, da eine umfangreiche Vernetzung der Amygdala mit dem restlichen Gehirn besteht (Ghashghaei und Barbas, 2002; LeDoux et al., 1990; McDonald, 1987, 1998; McDonald and Mascagni, 1997; Pitkänen, 2000; Pitkänen et al., 1997). Da DTI aber von der Existenz myelinisierter Nervenfasern abhängig

ist, erscheint die Anwendung dieser Technik auf die Amygdala, also auf eine Hirnregion mit sehr schwach myelinisierten Fasern, auf den ersten Blick kontrovers. Mit Hilfe der Berechnung der bevorzugten Diffusionsrichtung innerhalb eines jeden Voxels konnten jedoch Voxel-Gruppen mit starker Diffusions-Anisotropie innerhalb der Amygdala identifiziert werden. Zum ersten Mal überhaupt konnten so im Rahmen dieser Studie die Bestandteile der Amygdala *in vivo* in zwei Hauptgruppen unterteilt werden (Solano-Castiella et al., 2010). Die aus diesen Ergebnissen gewonnenen probabilistischen Karten stellen einen signifikanten Fortschritt in der Erforschung der Subkomponenten der Amygdala in vivo und der Eigenschaften ihres Gewebes dar.

Im Rahmen des 2. Experiments wurde mit Hilfe einer Technik, welche auf der Bildgebung mit polarisiertem Licht (Polarized Light Imaging – PLI) basiert, die mit der Diffusions-Tensor-Bildgebung in Experiment 1 gefundene Parzellierung der Amygdala validiert. PLI ist eine Technik, die es erlaubt, die Richtung von myelinierten Fasern in Gewebe *ex vivo* bildlich darzustellen (Axer et al., 2002; Dammers et al., Larsen et al., 2007). Daher dient PLI als Methode, Ergebnisse, die bei der Analyse von MR-Daten bezüglich der strukturellen Anisotropie in der grauen Substanz des Gehirns gewonnen worden sind, zu überprüfen. Jedoch hat PLI, als optische Methode, eine deutlich höhere räumliche Auflösung als DTI. Die Ergebnisse diesen zweiten Experiments haben das Vorliegen von Anisotropie im Bereich der Amygdala bestätigt und gezeigt, dass die gefundenen Gruppierungen von Voxeln ähnlicher Faserrichtung in den koronaren Schnitten (100 µm) mit den Gruppen, die mit Hilfe von DTI bei einer isotropen Auflösung von (1.72 mm)³ ermittelt wurden, vergleichbar sind.

Das 3. Experiment wurde durchgeführt, um zu bestimmen, ob mit DTI in einem Gewebe mit wenig oder gänzlich ohne Myelin Kontrast erzeugt werden kann. Obwohl das Vorhandensein von Myelin typischerweise mit der anisotropen Diffusion im Gehirn assoziiert wird, konnte bereits gezeigt werden, dass Myelin nicht notwendigerweise für das Auftreten von diffusionaler Anisotropie erforderlich ist (Beaulieu et al., 1994), Um dies zu überprüfen, wurden Gehirne von Föten (20. bis 30. Schwangerschaftswoche) *ex vivo* analysiert, da dieses Hirngewebe wenig bis kein Myelin enthält, die neuronalen Faserwege aber bereits ausgeprägt sind. Das Nichtvorhandensein von Myelin in diesen Gehirnen erlaubt es zu testen, ob die Ergebnisse der DTI-Experimente, welche robuste Subdivisionen in der ebenfalls nur wenig myelinisierten Amygdala eines Erwachsenen zeigten, in anderen Geweben reproduzierbar sind. Trotz des Fehlens von Myelin zeigte die Analyse des DTI-Messungen am Fötusgehirn

deutlich anisotrope kortikale Layer. Dadurch konnte bestätigt werden, dass organisierte Wasserdiffusion auch in Gehirnregionen zu finden ist, die, wie die Amygdala, kein bzw. nur wenig Myelin enthalten.

Diese drei Experimente haben Gewebeeigenschaften der Amygdala mit Techniken offengelegt, welche üblicherweise bei der Untersuchung von stark myelinisierten Hirnregionen, wie der weißen Hirnsubstanz eingesetzt werden. Die ermittelten Gewebeeigenschaften der Amygdala und die erstmals in vivo daraus resultierenden probabilistischen Karten zeigen das Potential der entwickelten Methode für die in vivo Untersuchung und Parzellierung von ähnlichen Gehirnstrukturen und sollten als Grundlage weiterer Forschung auf diesem Gebiet fungieren.

Im 4. Experiment konnte durch die Anwendung von struktureller MR-Bildgebung eine weitere Optimierung bei der Identifikation von Substrukturen in der Amygdala erreicht werden. Die hauptsächliche Grundlage für den Bildkontrast sind bei dieser MR-Technik die unterschiedlichen Relaxationszeiten verschiedener Gewebearten. Mit Hilfe von verbesserten Darstellungsmethoden und bei größerem Signal-zu-Rausch Verhältnis zeigen auch sonst scheinbar homogene Regionen eine interne Struktur. Bei einer Feldstärke von 3 Tesla zeigt sich die Amygdala nur als eine homogene graue Hirnregion. Da aber mit der Verwendung einer geeigneten MR-Bildgebungssequenz der Kontrast bei höherer Feldstärken (7 Tesla) erheblich gesteigert werden kann, ist es möglich, Strukturen im Gewebe der Amygdala zu visualisieren. Das Experiment sollte darüber hinaus dazu dienen, die *in vivo* Parzellierung der menschlichen Amygdala weiter zu verbessern. Durch die Kombination von zwei verschiedenen MR-Kontrasten bei 7 Tesla und die Verwendung modernster Bildanalysetechniken konnten *in vivo* drei Subkomponenten der Amygdala identifiziert werden (Solano-Castiella et al., 2009). Die durch diese MR-Technik ermittelte Parzellierung ähnelte der mit Hilfe von DTI gefundenen Kartierung. Allerdings zeigen die Ergebnisse auch Unterschiede. Dies könnte darin begründet sein, dass beide Techniken aus zwei unterschiedlichen Informationsquellen schöpfen, namentlich Konnektivität (DTI) und allgemeine anatomische Unterschiede (strukturelle MR).

Im Rahmen des 5. Experiments wurde versucht, die Verarbeitung von Emotionen innerhalb der Amygdala zu lokalisieren. Dazu wurden die Ergebnisse der beiden Parzellierungsmethoden (DTI und strukturelle MR) in eine fMRI Studie bei 7 Tesla eingebunden. Das Ziel war, unter Verwendung dieser zwei verschiedenen *in vivo* gewonnenen probabilistischen Karten das anatomische Substrat bestimmter Emotionen zu bestimmen. Dazu wurden die Reaktionen verschiedener Regionen der Amygdala auf nicht-sprachliche, menschliche, emotionale Vokalisierungen (Lachen, Weinen, Ekel und Überraschung) gemessen. Mit diesem Paradigma ist es gelungen, verschiedene Regionen der Amygdala zu identifizieren, die auf spezifische emotionale Stimuli unterschiedlich reagieren. Die mit Hilfe von DTI ermittelten Karten dienten hierbei zu Bestimmung der Tendenz, wo Emotionen grundsätzlich verarbeitet werden (medial oder lateral). Die auf der strukturellen MR basierte Parzellierung konnte diese Lokalisierung bestätigen und in einigen Fällen sogar verfeinern, womit die Identifizierung des anatomischen Substrates einer bestimmten Emotion möglich war.

Schlussfolgerung

In der vorliegenden Arbeit wurden erstmals zwei in vivo Methoden für die Parzellierung der Amygdala entwickelt. Darüber hinaus vertieft die Studie das Verständnis für das Gewebe der Amygdala. Die gewonnenen probabilistischen Karten ermöglichten die Etablierungen eines Zusammenhang zwischen der Verarbeitung unterschiedlicher Emotionen und dem entsprechenden anatomischen Substrat. Somit eröffnen die im Zuge dieser Arbeit erzielten Ergebnisse neue Perspektiven für das Verständnis der Amygdala und in Konsequenz auch für das Verstehen der menschlichen Emotionen.

References / Literaturverzeichnis

Amaral, D. G., Price, J. L., 1984. Amygdalo-cortical projections in the monkey (Macaca fascicularis). J Comp Neurol 230, 465-496.

Amaral, D.G., Price, J.L., Pitkänen, A., Carmichael, S.T., 1992. Anatomical organization of the primate amygdaloid complex. In: Aggelton, J.P. (Ed.), The Amygdala: Neurobiological Aspects of Emotion, Memory and Mental Dysfunction. Wiley, New York, pp. 1-66.

Amunts, K., Kedo, O., Kindler, M., Pieperhoff, P., Mohlberg, H., Shah, N. J., Habel, U., Schneider, F., Zilles, K., 2005. Cytoarchitectonic mapping of the human amygdala,

hippocampal region and entorhinal cortex: intersubject variability and probability maps. Anat Embryol (Berl) 210, 343-352.

Axer, H., Leunert, M., Murkoster, M., Grassel, D., Larsen, L., Griffin, L. D., Graf v Keyserlingk, D., 2002. A 3D fiber model of the human brainstem. Comput Med Imaging Graph 26, 439-444.

Aylward, E. H., Minshew, N. J., Goldstein, G., Honeycutt, N. A., Augustine, A. M., Yates, K. O., Barta, P. E., Pearlson, G. D., 1999. MRI volumes of amygdala and hippocampus in non-mentally retarded autistic adolescents and adults. Neurology 53, 2145-2150.

Ball, T., Rahm, B., Eickhoff, S. B., Schulze-Bonhage, A., Speck, O., Mutschler, I., 2007. Response properties of human amygdala subregions: evidence based on functional MRI combined with probabilistic anatomical maps. PLoS One 2, e307.

Ball, T., Derix, J., Wentlandt, J., Wieckhorst, B., Speck, O., Schulze-Bonhage, A., Mutschler, I., 2009. Anatomical specificity of functional amygdala imaging of responses to stimuli with positive and negative emotional valence. J Neurosci Methods 180, 57-70.

Beaulieu C, Allen PS. 1994. Determinants of anisotropic water diffusion in nerves. Magn Reson Med. 31, 394-400

Dammers, J., Axer, M., Grassel, D., Palm, C., Zilles, K., Amunts, K., Pietrzyk, U., 2010. Signal enhancement in polarized light imaging by means of independent component analysis. Neuroimage 49, 1241-1248.

de Olmos, J.S, 2004. The Amygdala. In: Paxinos, G., Mai, J.K. (Eds.), The Human Nervous System. Elsevier Academic Press, San Diego, pp. 739-868.

Ghashghaei, H. T., Barbas, H., 2002. Pathways for emotion: interactions of prefrontal and anterior temporal pathways in the amygdala of the rhesus monkey. Neuroscience 115, 1261-1279.

Heimer, L., Harlan, R.E., Alheid, G.F., Garcia, M.M., DeOlmos, J., 1997. Substantia innominata: A notion which impedes clinical-anatomical correlations in neuropsychiatric disorders. Neuroscience 76, 957-1006.

Johnston, JB, 1923. Further contributions to the study of the evolution of the forebrain. J Comp Neurol 35, 337-481.

Lanteaume, Laura, Khalfa, Stéphanie, Régis, Jean, Marquis, Patrick, Chauvel, Patrick, Bartolomei, Fabrice, 2007. Emotion induction after direct intracerebral stimulations of human amygdala. Cereb Cortex 17, 1307-1313.

Larsen, L., Griffin, L. D., Grassel, D., Witte, O. W., Axer, H., 2007. Polarized light imaging of white matter architecture. Microsc Res Tech 70, 851-863.

LeDoux, J., 2003. The emotional brain, fear, and the amygdala. Cell Mol Neurobiol 23, 727-

738.

LeDoux, J. E., 1992. Brain mechanisms of emotion and emotional learning. Curr Opin Neurobiol 2, 191-197.

LeDoux, J. E., Farb, C., Ruggiero, D. A., 1990. Topographic organization of neurons in the acoustic thalamus that project to the amygdala. J Neurosci 10, 1043-1054.

McDonald, A. J., 1987. Organization of amygdaloid projections to the mediodorsal thalamus and prefrontal cortex: a fluorescence retrograde transport study in the rat. J Comp Neurol 262, 46-58.

McDonald, A. J., 1998. Cortical pathways to the mammalian amygdala. Prog Neurobiol 55, 257-332.

McDonald, A. J., Mascagni, F., 1997. Projections of the lateral entorhinal cortex to the amygdala: a Phaseolus vulgaris leucoagglutinin study in the rat. Neuroscience 77, 445-459.

Phelps, Elizabeth A., LeDoux, Joseph E., 2005. Contributions of the Amygdala to Emotion Processing: From Animal Models to Human Behavior. Neuron 48, 175-187.

Pitkänen, A., 2000. Connectivity of the rat amygdaloid complex. In: Aggelton, J.P. (Ed.), The amygdala: A Functional Analysis. Oxford Univ. Press, Oxford, pp. 31-115.

Pitkänen, A., Savander, V., LeDoux, J. E., 1997. Organization of intra-amygdaloid circuitries in the rat: an emerging framework for understanding functions of the amygdala. Trends Neurosci 20, 517-523.

Sharot, Tali, Riccardi, Alison M., Raio, Candace M., Phelps, Elizabeth A., 2007. Neural mechanisms mediating optimism bias. Nature 450, 102-105.

Solano-Castiella, E., Anwander, A., Lohmann, G., Weiss, M., Docherty, C., Geyer, S., Reimer, E., Friederici, A. D., Turner, R., 2010. Diffusion tensor imaging segments the human amygdala in vivo. Neuroimage 49, 2958-2965.

Solano-Castiella, E., Lohmann, G., Schäfer, A., Trampel, R., Turner, R., 2009. Parcellation of the human amygdala using 7T structural MRI. Neuroimage 47, S72-S72.

Weiskrantz, L., 1956. Behavioral changes associated with ablation of the amygdaloid complex in monkey. J. Comp. Physiol. Psychol. 49, 381-391.

CURRICULUM VITAE
Eugenia Solano-Castiella
(Date of birth: 12.29.1981)

PERSONAL INFORMATION

Current Address	**Permanent Address**
Gottschedstrasse 15	Avd. de Neguri 16, 2drch
04109 Leipzig, Germany	48992 Vizcaya, Spain
Mobile: +49 (0)178 557 2912	Mobile: +34 (0)609 78 44 04
Phone: +49 (0)341 9940 2422	Phone: +34 (0)94 460 61 49
Email: solano@cbs.mpg.com	Email: eugesol@hotmail.com

LANGUAGE AND COMPUTER SKILLS

Languages	**Spanish:** Mother tongue	**German:** Basic knowledge
	English: Fluent	**Italian:** Fluent

Computer skills: Excellent skills in using Microsoft, Macintosh, Linux, Open Office, Lipsia package, FSL (basic knowledge), SPM (basic knowledge), SYNGO (Siemens scanner software), graphics and multimedia programs

WORK EXPERIENCE

Since 02-2007 MAX PLANCK INSTITUTE for Human Cognitive and Brain Sciences, Leipzig (Germany)

PhD student Neurophysics Department

> Worked with Diffusion Tensor Imaging (DTI) at 3 and 7 Tesla Magnetic Resonance Imaging (MRI)
> Segmented the human amygdala using DTI data at a 3 Tesla MRI http://dx.doi.org/10.1016/j.neuroimage.2009.11.027
> Segmented the human amygdala using high resolution structural Imaging (T2, T2*) at a 7 Tesla MRI
> Analyzed birefringence at the amygdaloid grey matter by employing polarized light imaging for DTI data validation purposes
> 7 Tesla MR imaging of postmortem fetal and adult brain
> fMRI at the amygdaloid body region with a 7 Tesla MRI employing auditory human emotional vocalizations

2005-2006 MAX PLANCK INSTITUTE for Human Cognitive and Brain Sciences, Leipzig (Germany)

Internship Baby Laboratory. Neuropsychology Department

> Worked with infants using electroencephalography (EEG)

	➢ Assisted in the research of infant imitation, biological motion and congruent actions
	➢ Prepared EEG stimuli, compiled and analyze EEG data
6 months 2004	**UNIVERSITA DEGLI STUDENTI DI PADOVA, Padova (Italia)** EEG Laboratory. Neuropsychology Department
Internship	➢ Assisted the investigation of cerebral frequency spectrum of the sleeping cycle employing EEG
2002 to 2003 *Internship*	**NEUROLOGICAL CLINIC "LAS ARENAS", Bilbao (Spain)** Neuropsychology group
	➢ Trained on therapy for brain neurodegenerative illnesses and ischemia
1999 to 2002 *Internship*	**RED CROSS, Bilbao (Spain)**
	➢ Worked as licensed sanitary assistant for first aid and highway emergencies
1999 to 2001 *Internship*	**APNABI ASSOCIATION, Bilbao (Spain)**
	➢ Neuropsychological support for patients with schizophrenia, autism and psychosis
	➢ Assisted on cognitive therapy and family care
1999 to 2003	**DEUSTO SOCIAL ASSISTANCE, Bilbao (Spain)**
	➢ Assisted handicapped students

PUBLICATIONS, TEACHING, ANNUAL REPORTS AND CONFERENCES

➢ Solano-Castiella E, Anwander A, Lohmann G, Weiss M, Docherty C, Geyer S, Reimer E, Friederici A.D, Turner R, 2010. Diffusion tensor imaging segments the human Amygdala *in vivo*, Neuroimage. 49:4, 2958-2965

➢ Solano-Castiella E, Schäfer A, Lohmann G, Prueger T, Reimer E, Trampel R, Turner R, 2010. Parcellation of human amygdala *in vivo* using high field MRI (submitted)

➢ Invited guest. Solano-Castiella E. "Segmentation of the amygdala based on multiple MR techniques". Freie Universität Berlin, Berlin (Germany), May 2010

➢ Invited guest. Solano-Castiella E, "United States of Amygdala – How to define borders", Université de Lausanne, CISA Institute, Geneva (Switzerland), Sep. 2009

➢ Lecture on neuroanatomy. Solano-Castiella E. The amygdala development, anatomy, connectivity and function. Feb. 2008. Max Planck Institute, Leipzig

➢ Lecture on neuroanatomy. Solano-Castiella E. The amygdala development, anatomy, connectivity and function. Dec. 2008. Max Planck Institute, Leipzig

➢ Annual report 2007/2008, Max Planck Institute for human cognitive and brain sciences. Solano-Castiella E, Anwander A, Weiss M, Docherty C, Turner R. MRI anatomical segmentation and connectivity of human amygdala.

➢ Solano-Castiella E, Axer H, Turner R, "Polarized light imaging (PLI) of the human amygdala", In: Proc 16th OHBM Scientific Meeting, Barcelona, 2010. 836

➢ Solano-Castiella E, Schäfer A, Lohmann G, Prueger T, Reimer E, Trampel R, Turner R, "Reliable amygdala segmentation using clustering of multimodal data at 7 Tesla", In: Proc 18th ISMRM Scientific Meeting, Stockholm, 2010. 4439 M-PM

➢ Bullmann T, Trampel R, Dhital B, Solano-Castiella E, Ogunlade V, Turner R, Arendt T, "Regulation of the Microtubule Cytoskeleton in Growing Fiber Tracts of the Developing Human Brain", In: Proc 8th Riken CDB Symposium, Kobe (Japan), 2010. P06 W-PM

➤ Solano-Castiella E, Lohmann G, Schäfer A, Trampel R, Turner R, "Parcellation of human amygdala *in vivo* using high field MRI", In: Proc 22nd ECR Scientific Meeting, Vienna, 2010. 594Solano-Castiella E, Lohmann G, Schäfer A, Trampel R, Turner R, "Parcellation of the human Amygdala using structural 7 Tesla MRI", In: Proc 15th OHBM Scientific Meeting, San Francisco, 2009 238 F-PM

➤ Solano-Castiella E, Lohmann G, Schäfer A, Trampel R, Turner R, "Parcellation of the human Amygdala using structural 7 Tesla MRI", In: Proc 26th ESMRMB Scientific Meeting, Antalya, 2009. 594 F-PM

➤ Solano-Castiella E, "United States of the Amygdala – How to define borders", In: Proc 4th Interdisciplinary Max Planck workshop "Science and Fiction", Leipzig, 2009

➤ Solano-Castiella E, Lohmann G, Schäfer A, Trampel R, Turner R, "Parcellation of the human amygdala using structural 7 T MRI", In: Proc ISMRM High Field Workshop, Rome, 2008

➤ Solano-Castiella E, Anwander A, Weiss M, Docherty C, Geyer S, Reimer E, Friederici A.D, Turner R, "Diffusion Tensor Magnetic Resonance Imaging segments human Amygdala *in Vivo*", In: Proc 14th OHBM Scientific Meeting, Melbourne, 2008. 641 TH-AM

➤ Solano-Castiella E, Anwander A, Weiss M, Docherty C, Geyer S, Reimer E, Friederici A.D, Turner R, "Diffusion Tensor Magnetic Resonance Imaging segments human Amygdala *in Vivo*", In: Proc 16th ISMRM Scientific Meeting, Canada, 2008. 1835 T-AM

EDUCATION

2003 to 2004	Università degli studenti di Padova, Erasmus Program Padova, Italy
2001 to 2004	Speciality in Neuropsychology, University of Deusto, Bilbao, Spain
1999 to 2004	Graduated in Psychology at the University of Deusto, Bilbao, Spain
1999	Member of a selected group doing research on Classical and Operant conditioning, University of Deusto, Bilbao, Spain
1999	License on sanitary assistance for first aid and highway emergencies

ADITIONAL CONFERENCES

2009	High Field Workshop, Leipzig, Germany
2009	Symposium "New Frontiers in Science" and "Art and Science" ,Munich, Germany
2007	OHBM Conference, Chicago, USA
2007	ISMRM Conference, Berlin, Germany
2005	Course of "Evolution of Language", Max Planck Institute for Human Cognitive and Brain Sciences, Leipzig, Germany
2004	Intensive course in "Neuropsychology and Schizophrenia", University of Deusto, Bilbao, Spain
2003	Congress of Multiple Sclerosis, Euskalduna. E.M Association. Bilbao, Spain

2002	Seminar on social reintegration, Basque Country Government, Bilbao, Spain
2002	Convention "The Grief", A.E.C.C Association, Bilbao, Spain
2000	Seminar "The Human Genome", University of Deusto, Bilbao, Spain

MEMBERSHIPS

Since 2009	Student member of ESMRMB
Since 2007	Student member of OHBM
Since 2007	Student member of ISMRM

ACADEMIC RESEARCH

2002 to 2005	Neuropsychological research on Schizophrenia
	Research training in Alzheimer: Comparison of dementias
	Small project on child development, behaviour and maltreatment; Analysis of their drawings

Erklärung gemäß §8 (1.9) der Promotionsordnung

Hiermit erkläre ich,

Eugenia Solano-Castiella, geboren am 29. Dezember 1981 in Bilbao, Spanien,

wohnhaft Gottschedstr. 15, 04109, Leipzig,

dass mir die Promotionsordnung der Fakultät für Biowissenschaften, Pharmazie und Psychologie der Universität Leipzig in der Fassung vom 20. Januar 2010 bekannt ist und von mir anerkannt wird. Ich verpflichte mich zur Einhaltung der darin aufgeführten Prinzipien guter wissenschaftlicher Praxis.

Eugenia Solano-Castiella

Leipzig, den 19.10.2010

MPI Series in Human Cognitive and Brain Sciences: